# Resource-efficient shadow tomography using equatorial measurements

Guedong Park<sup>1</sup>, Yong Siah Teo<sup>1\*</sup>, Hyunseok Jeong<sup>1\*</sup>

<sup>1\*</sup>Department of Physics and Astronomy, Seoul National University, Seoul, 08826, Republic of Korea.

\*Corresponding author(s). E-mail(s): ys\_teo@snu.ac.kr; jeongh@snu.ac.kr;

#### Abstract

We propose a resource-efficient shadow-tomography scheme using equatorial-stabilizer measurements generated from subsets of Clifford unitaries. For n-qubit systems, equatorial-stabilizer-based shadow-tomography schemes can estimate M observables (up to an additive error  $\varepsilon$ ) using  $\mathcal{O}(\log(M), \operatorname{poly}(n), 1/\varepsilon^2)$  sampling copies for a large class of observables, including those with traceless parts possessing polynomially-bounded Frobenius norms. For arbitrary quantum-state observables, sampling complexity becomes n-independent— $\mathcal{O}(\log(M), 1/\varepsilon^2)$ . Our scheme only requires an n-depth controlled-Z (CZ) circuit [ $\mathcal{O}(n^2)$  CZ gates] and Pauli measurements per sampling copy, exhibiting a smaller maximal gate count relative to previously-known randomized-Clifford-based proposals. Implementation-wise, the maximal circuit depth is reduced to  $\frac{n}{2} + \mathcal{O}(\log(n))$  with controlled-NOT (CNOT) gates. Alternatively, our scheme is realizable with 2n-depth circuits comprising  $O(n^2)$  nearest-neighboring CNOT gates, with possible further gate-count improvements. We numerically confirm our theoretically-derived shadow-tomographic sampling complexities with random pure states and multiqubit graph states. Finally, we numerically demonstrate that equatorial-stabilizer-based shadow tomography is more noise-tolerant than randomized-Clifford-based schemes in terms of average gate fidelity and state verification for GHZ and W states.

**Keywords:** shadow tomography, quantum tomography, stabilizer states, Clifford gates, circuit depth and gate count, equatorial stabilizer states (ESPOVM), informational completeness

#### 1 Introduction

Quantum algorithms, which are algorithms based on quantum-mechanical principles, have been shown to outperform classical algorithms for many computational tasks [1, 2]. For these purposes, certifying the quality of the prepared (noisy) quantum state is an important prerequisite. Quantum tomography [3–7] is a general method to reconstruct a typically unknown noisy n-qubit quantum state  $\rho$  (or a channel). This, however, requires exponentially many copies of  $\rho$  in n for an accurate reconstruction.

On the other hand, if we are to estimate certain classes of physical properties of unknown states, shadow tomography [8] enables us to do so with a polynomially-large number of samples. The well-known randomized Pauli tomography, or "six-Paulis" tomography [9, 10], is useful for estimating the expectation values of Hamiltonians with low locality, learning quantum channels [11] and measuring non-stabilizerness (or magic) [12, 13]. This procedure uses a simple single-layer circuit structure, and is therefore ineffective in estimating highly-entangled properties of large quantum systems [9]. The second protocol, randomized-Clifford shadow tomography [9], is better for estimating the fidelity between the unknown input and entangled target states for large qubit number n. This advantage originates from the fact that Clifford operations are unitary 3-designs [14–17]. However, for large n, this protocol utilizes at most  $\frac{7n^2}{2}$  neighboring CNOT gates [18, 19] and even if one invokes the unitary 3-design approximation, it still needs  $\mathcal{O}(3^{10}n^2)$  two-qubit gates [20] to execute. Therefore, shadow tomography with arbitrary

Clifford gates could lead to noisy measurement results in real experiments as the large number of noisy gates accumulate physical noise.

Typically, entanglement in target observables with good shadow norms shrinks as the number of sampled neighboring gates decreases [21]. However, it is uncertain whether randomized Clifford tomography is indeed most optimal for pure-state observables from the perspective of low gate number, circuit depth, and input-state copy number to achieve a given estimation accuracy. Although generalized measurements [10, 22, 23] can be used to optimize the gate count or sampling complexity, fault-tolerant implementation of such non-Clifford measurements is believed to be challenging [24, 25]. There exist alternatives with reduced Clifford gate resources [26–28], but the applicable input states and target observables are more restrictive. Hence, a complete analysis of an optimal tomography scheme for broad classes of observables remains an open problem.

In this work, we introduce resource-efficient schemes for shadow tomography, catered to observable-expectation-value estimations, that offer a lower gate count and circuit depth while still being applicable to a large observable class. The key point is that it is not necessary to utilize the entire set of stabilizer states [29, 30] comprising all Clifford-rotated bases. Instead, our proposed schemes employ a smaller stabilizer subset, namely the equatorial stabilizer positive operator-valued measure (ESPOVM) [31] together with the computational basis. Additionally, it is sufficient to perform shadow tomography with an even smaller subset, namely the real ESPOVM or RESPOVM, when the target observable is real with respect to the computational basis.

With rigorous theorems, we demonstrate shadow-tomographic capabilities for our (R)ESPOVM schemes by deriving upper bounds for the observable-expectation-value estimation variance, which is directly related to the shadow norm [9, 21] and sampling-copy-number requirement. Specifically, we note that a sampling complexity of  $\mathcal{O}(\log(M), \operatorname{poly}(n), 1/\varepsilon^2)$  suffices to simultaneously estimate (up to an additive error  $\varepsilon$ ) M complex observables belonging to a broad class, which sufficiently include observables possessing polynomially-bounded Frobenius norms for their traceless parts. For arbitrary quantum-state observables, the sampling complexity is reduced to simply  $\mathcal{O}(\log(M), 1/\varepsilon^2)$ , which is constant in n and on par with randomized-Clifford tomography [9]. In fidelity estimation of real pure-state observables (also known as pure-state verification [32, 33]), RESPOVM gives a smaller multiplicative factor in the averaged sampling-complexity order than ESPOVM, where the average is taken over uniformly-distributed pure-state inputs and observables. As a side, we argue that  $\mathcal{O}(\operatorname{poly}(n))$  single-layer Pauli measurement copies suffice to estimate expectation values of  $\mathcal{O}(\operatorname{poly}(n))$ -Pauli-term Heisenberg Hamiltonians [34, 35].

Furthermore, we shall show that the (R)ESPOVM shadow tomography algorithm requires a simpler circuit structure than that of randomized-Clifford shadow tomography, involving a uniform sampling of commuting CZ gates as the only two-qubit gate resources. A recent result [28] shows that smaller subsets of CZ-circuit-based measurements than our (R)ESPOVM schemes, consisting of mutually-unbiased bases (MUB) [36], may be used to estimate observable expectation values. However, the proposal does not guarantee poly(n)-scaling in sampling complexity for arbitrary target states. According to Ref. [37], our algorithm requires a shorter circuit depth and fewer CZ-gate counts than randomized-Clifford tomography. Furthermore, for larger systems, it follows that our scheme can be implemented with at most 2n-depth, and thus  $n^2 < \frac{7n^2}{2}$  nearest-neighboring (NN) CNOT gates [38]. Having a lower gate count as one reason, we provide numerical evidence in the context of average gate fidelity and state verification showing that (R)ESPOVM shadow tomography possesses a higher circuit-noise tolerance over randomized-Clifford shadow tomography, with Greenburger-Horne-Zeillinger (GHZ) states [39] and W states [40] as prominent examples.

### 2 Results

#### 2.1 Preliminaries

Before presenting our main results, we define and explain several concepts and terminologies that shall be used throughout the article. We consider a source that allows one to prepare multiple copies of an n-qubit quantum state  $\rho$ . The corresponding observable O shall be a Hermitian operator, and is therefore symmetric whenever its matrix elements in the computational basis are all real, at which we call O is real. We define the Clifford group  $Cl_n$  as the set of operators [29, 41],

$$\operatorname{Cl}_n = \{ U \mid \forall E \in \mathcal{P}_n, UEU^{\dagger} \in \mathcal{P}_n \},$$
 (1)

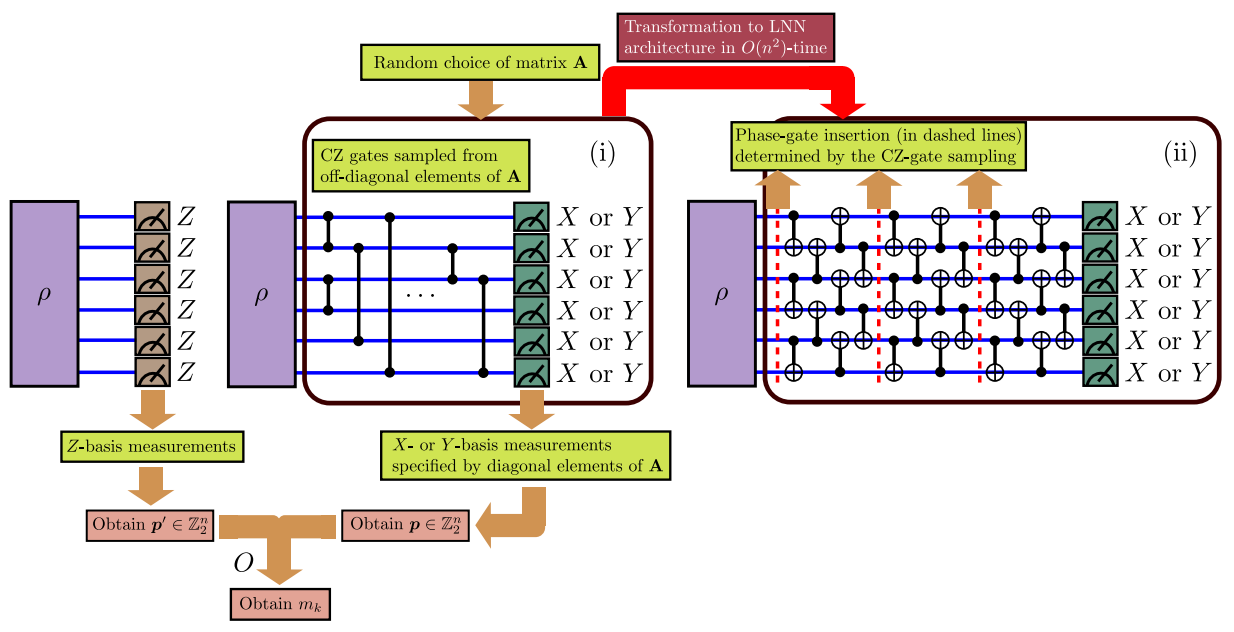


Figure 1 Schematic for 6-qubit (R)ESPOVM shadow tomography to estimate  $\langle O \rangle = \operatorname{tr}(\rho O)$  of an unknown state  $\rho$  and target observable O. Sampled CZ circuits can be transformed to a linear nearest-neighboring (LNN) architecture [38] [circuit (ii)]. Also in (ii), the inserted phase gates are single-qubit gates and the measurement is done in the same manner as in (i). Any one of the two architectures (i) and (ii) can be executed to obtain the measurement bit-string column  $p \in \mathbb{Z}_2^n$ . Together with the bit-string column p' acquired from the computational-basis measurement, the observable expectation value can be reconstructed after repeating N rounds of (p, p') collection.

where  $\mathcal{P}_n$  is the *Pauli group* generated by tensor products of the standard Pauli operators X, Y, Z and the identity I. Next, we define the *pure stabilizer state set*  $\mathcal{S}_n$  as the following set of quantum states:

$$S_n = \{ |\psi\rangle \, | \, |\psi\rangle = U \, |0^{\otimes n}\rangle \text{ for some } U \in \mathrm{Cl}_n \} \,,. \tag{2}$$

Then we say the element  $|\psi\rangle \in \mathcal{S}_n$  as (pure) stabilizer state.

We are now ready to look into subclasses of the stabilizer set  $S_n$ . Specifically, the complex pure equatorial stabilizer state set [31]  $S_n^{\text{eq}}$  and its real counterpart  $S_n^{\text{req}}$  are respectively given by

$$S_n^{\text{eq}} = \left\{ |\phi_{\mathbf{A}}^{\text{eq}}\rangle \equiv \frac{1}{\sqrt{2^n}} \sum_{\boldsymbol{x} \in \mathbb{Z}_2^N} i^{\boldsymbol{x}^\top \mathbf{A} \boldsymbol{x}} |\boldsymbol{x}\rangle \, \middle| \, \mathbf{A} = (a_{ij})_{i,j \in [N]} \text{ where } a_{ij} = a_{ji}, \, a_{ij} \in \left\{ \mathbb{Z}_4 & \text{if } i = j \\ \mathbb{Z}_2 & \text{if } i > j \right\},$$
(3)

$$S_N^{\text{req}} = \left\{ |\phi_{\mathbf{A}}^{\text{req}}\rangle \equiv \frac{1}{\sqrt{2^n}} \sum_{\boldsymbol{x} \in \mathbb{Z}_2^N} (-1)^{\boldsymbol{x}^{\top} \mathbf{A} \boldsymbol{x}} |\boldsymbol{x}\rangle \, \middle| \, \mathbf{A} = (a_{ij})_{i,j \in [N]} \text{ where } a_{ij} \in \left\{ \begin{bmatrix} \mathbb{Z}_2 & \text{if } i \leq j \\ \{0\} & \text{if } i > j \end{bmatrix} \right\}.$$
(4)

We may define *(real) equatorial stabilizer states* in the same manner based on  $\mathcal{S}_n^{\text{eq}}$  and  $\mathcal{S}_n^{\text{req}}$ . From Eqs. (3) and (4), we know that the number of complex equatorial stabilizer states is  $|\mathcal{S}_n^{\text{eq}}| = 2^{\frac{n^2+3n}{2}}$ , and that of real equatorial stabilizer states is  $|\mathcal{S}_n^{\text{req}}| = 2^{\frac{n^2+n}{2}}$ . As the names suggest, these are subsets of  $\mathcal{S}_n$ . The  $\mathcal{S}_n^{\text{eq}}$  was originally used for a faster classical simulation [30, 31]; more explicitly, a faster norm estimation of a given state with a large stabilizer rank.

In this work, we shall turn these two stabilizer subclasses into POVMs for shadow tomography, and consequently reveal the key advantages that are related to the exploitation of their smaller set sizes relative to  $S_n$ . That  $S_n^{\rm eq}$  and  $S_n^{\rm req}$  may be readily transformed into POVMs is straightforward [42], as the corresponding sets of positive operators  $\left\{\frac{2^n}{|S_n^{\rm eq}|}|\phi_{\mathbf{A}}^{\rm eq}\rangle\langle\phi_{\mathbf{A}}^{\rm eq}|\right\}$  and  $\left\{\frac{2^n}{|S_n^{\rm req}|}|\phi_{\mathbf{A}}^{\rm req}\rangle\langle\phi_{\mathbf{A}}^{\rm eq}|\right\}$  house elements that sum to the identity. We coin them *(real) equatorial stabilizer POVMs*, or (R)ESPOVMs for short.

#### 2.2 Equatorial-stabilizer shadow tomography

We now introduce the shadow tomography scheme that uses (real) equatorial stabilizer POVMs. Figure 1 illustrates its schematic implementation, which is used to estimate the expectation value  $tr(\rho O)$  for an

#### Algorithm 1 (R)ESPOVM shadow tomography algorithm

**Require:** n-qubit unknown quantum state  $\rho$ , total input-state copies  $N \in \mathbb{N}$  (even), observable O and the (R)ESPOVM scheme.

```
Ensure: m.
  1: m \leftarrow 0
  2: for k \in [N/2] do
           Prepare \rho as the input state.
  3:
           Randomly choose |\phi_{\mathbf{A}}^{(\mathrm{r})\mathrm{eq}}\rangle uniformly in \mathcal{S}_n^{(\mathrm{r})\mathrm{eq}}. Denote \mathbf{A}=(a_{ij}).
  4:
           for i < j \in [n] do
  5:
                if a_{ij} = 1 then
  6:
                     \rho \leftarrow CZ_{ij} \rho CZ_{ij}, where CZ_{ij} is the CZ unitary operator acting on the i-th and j-th qubits.
  7:
  8.
           end for
  9:
           for i \in [n] do
10:
                if ESPOVM is used then
11:
                     if a_{ii} = 0 \pmod{2} then
12:
                          Perform a Pauli X measurement on the i-th qubit.
13:
14:
                          Perform a Pauli Y measurement on the i-th qubit.
15:
                     end if
16:
17:
                else
                     Perform a Pauli X measurement on the i-th qubit.
18:
                end if
19.
           end for
20:
           Obtain the measurement bit-string outcome p \in \mathbb{Z}_2^n.
21:
22:
           for i \in [n] do
                if ESPOVM is used then
23:
                     a_{ii} \leftarrow a_{ii} + 2p_i \pmod{4}.
24:
                else if RESPOVM is used then
25:
                     a_{ii} \leftarrow a_{ii} + p_i \pmod{2}.
26:
                end if
27:
           end for
28:
           Prepare \rho as an input state.
29:
           Perform a Pauli Z measurement on \rho to obtain the bit-string outcome p' \in \mathbb{Z}_2^n.
30:
           if ESPOVM is used then
31:
                m \leftarrow m + 2^{n} \left\langle \phi_{\mathbf{A}}^{\mathrm{eq}} \right| O \left| \phi_{\mathbf{A}}^{\mathrm{eq}} \right\rangle + \left\langle \mathbf{p}' \right| O \left| \mathbf{p}' \right\rangle - \mathrm{tr}(O).
32:
           else if RESPOVM is used then
33:
                m \leftarrow m + 2^{n-1} \langle \phi_{\mathbf{A}}^{\text{eq}} | O | \phi_{\mathbf{A}}^{\text{eq}} \rangle + \langle \mathbf{p}' | O | \mathbf{p}' \rangle - \frac{1}{2} \text{tr}(O).
34:
           end if
35:
36: end for
37: m \leftarrow \frac{m}{(N/2)}.
```

unknown state  $\rho$  and a known observable O within an additive error  $\varepsilon$ . This is carried out with a given total number of input-state copies N.

The complete systematic procedure for ESPOVM shadow tomography is shown in Algo. 1. For simplicity, here, we summarize the main steps. After preparing the input state  $\rho$ , the observer operates uniformly chosen CZ gates to the input and then measures in Pauli X or Y-basis, to obtain the measurement outcome  $|\phi_{\bf A}^{\rm eq}\rangle\langle\phi_{\bf A}^{\rm eq}|$ . The ESPOVM, all by itself, is *not* informationally complete (IC), whereas the union of the ESPOVM and computational basis is IC [42, 43] and indeed capable of reconstructing an arbitrary  $\rho$  and, thus, general observable expectation values. Therefore, to perform the complete shadow tomography scheme, the observer additionally measures  $\rho$  with the Z-basis measurement. So, two copies of  $\rho$  are required for a single measurement trial, which would give us a bit-string column p from the ESPOVM and another bit-string column p' from the computational basis. However, in Sec. 2.3, we shall see that only a single copy of the input state is necessary for each trial if O is a cluster state. This procedure is repeated for N/2 measurement trials, with a total of N sampling copies (where N should then be even),

and the following estimators (denoted with a caret) are constructed:

$$\widehat{\langle O \rangle} = \begin{cases}
\frac{2^{n}}{(N/2)} \sum_{\substack{\text{sampled } \mathbf{A} \\ \text{over } N/2 \text{ copies}}} \langle \phi_{\mathbf{A}}^{\text{eq}} | O | \phi_{\mathbf{A}}^{\text{eq}} \rangle + \frac{1}{(N/2)} \sum_{\substack{\text{measured } \mathbf{p'} \\ \text{over } N/2 \text{ copies}}} \langle \mathbf{p'} | O | \mathbf{p'} \rangle - \text{tr}(O) \\
(ESPOVM \text{ and comp. basis}),
\end{cases}$$

$$\widehat{\langle O \rangle} = \begin{cases}
\frac{2^{n-1}}{(N/2)} \sum_{\substack{\text{sampled } \mathbf{A} \\ \text{over } N/2 \text{ copies}}} \langle \phi_{\mathbf{A}}^{\text{eq}} | O | \phi_{\mathbf{A}}^{\text{eq}} \rangle + \frac{1}{(N/2)} \sum_{\substack{\text{measured } \mathbf{p'} \\ \text{over } N/2 \text{ copies}}} \langle \mathbf{p'} | O | \mathbf{p'} \rangle - \frac{1}{2} \text{tr}(O) \\
& \underbrace{(N/2) \sum_{\substack{\text{sampled } \mathbf{A} \\ \text{over } N/2 \text{ copies}}} \langle \mathbf{p'} | O | \mathbf{p'} \rangle - \frac{1}{2} \text{tr}(O)
\end{cases}$$
(5)
$$\underbrace{(N/2) \sum_{\substack{\text{sampled } \mathbf{A} \\ \text{over } N/2 \text{ copies}}} \langle \mathbf{p'} | O | \mathbf{p'} \rangle - \frac{1}{2} \text{tr}(O)$$
(7)

Note that these estimators are unbiased by construction, that is the data-average  $\mathbb{E}(\widehat{\langle O \rangle}) = \langle O \rangle$ .

The RESPOVM shadow tomography scheme, which is applicable to estimating expectation values of real target observables, takes on a simpler structure in that the observer does not need to perform the Y-basis measurement. This scheme may be implemented with Algo. 1 with a slight modification in step 4, where in the RESPOVM measurement part the observer now measures only with X-basis to obtain the outcome  $|\phi_{\bf A}^{\rm req}\rangle\langle\phi_{\bf A}^{\rm req}|$  In Sec. 2.3, we shall see that in many cases, the RESPOVM requires much fewer sampling-copy numbers than ESPOVM to achieve the same estimation accuracy.

We summarize the requirements for implementing Algo. 1 for (R)ESPOVM shadow tomography in **Theorem 1.** [(R)ESPOVM implementation] On an n-qubit state  $\rho$ , the implementation of n-qubit ESPOVM shadow tomography requires CZ-gate circuits of depths of at most n by Vizing's theorem [37], and n single-qubit Pauli (X,Y,Z) measurements. For RESPOVM shadow tomography, the Y-basis measurement is not needed.

#### 2.3 Shadow-tomographic properties of equatorial stabilizer POVMs

Shadow tomography aims to estimate state properties with a sampling complexity that grows at most polynomially quickly with the qubit number n. To be more precise, let us specify that a single property estimator is accurate up to a maximal additive error of  $\varepsilon > 0$ . Then, the number of sampling copies should scale as  $\mathcal{O}(\text{poly}(n)/\varepsilon^2)$ . Reference [9] showed that randomized-Clifford tomography achieves  $\varepsilon$ -accurate fidelity estimation between an unknown quantum state and target pure state with the sampling-complexity upper bound  $\mathcal{O}(C/\varepsilon^2)$ , where C is constant. This is derived from the fact that uniformly-random Clifford operations are unitary 3-designs [16, 44]. We shall prove that our (R)ESPOVM algorithms also possess upper bounds with similar scaling behaviors based on the 3-moment properties inherent in (R)ESPOVMs.

For this purpose, we denote the quantities  $\widehat{O}_{\mathbf{A}}^{\mathrm{eq}} \equiv 2^n \langle \phi_{\mathbf{A}}^{\mathrm{eq}} | O | \phi_{\mathbf{A}}^{\mathrm{eq}} \rangle$ ,  $\widehat{O}_{\mathbf{A}}^{\mathrm{req}} \equiv 2^{n-1} \langle \phi_{\mathbf{A}}^{\mathrm{req}} | O | \phi_{\mathbf{A}}^{\mathrm{req}} \rangle$ , and  $\widehat{O}_{\mathbf{x}}^{\mathrm{bin}} \equiv \langle \mathbf{x} | O | \mathbf{x} \rangle$  for one observable O that are measured and obtained in each step of the shadow-tomography procedure, where the matrix  $\mathbf{A}$  and bit string  $\mathbf{x}$  are random in accordance with Algo. 1. The first two random numbers  $\widehat{O}_{\mathbf{A}}^{\mathrm{eq}}$  and  $\widehat{O}_{\mathbf{A}}^{\mathrm{req}}$  refer to the respective outcome estimators for ESPOVM and RESPOVM, and  $\widehat{O}_{\mathbf{x}}^{\mathrm{bin}}$  is the outcome of a Z-basis measurement. Upon defining  $\mathbb{E}(\widehat{O}_{\mathbf{A},\mathbf{x}})$  as the data-average value of  $\widehat{O}_{\mathbf{A},\mathbf{x}}$ , which is defined as

$$\widehat{O}_{\mathbf{A}, \boldsymbol{x}} \equiv \begin{cases} \widehat{O}_{\mathbf{A}}^{\text{eq}} + \widehat{O}_{\boldsymbol{x}}^{\text{bin}} - \text{tr}(O) & (\text{ESPOVM}) \\ \widehat{O}_{\mathbf{A}}^{\text{req}} + \widehat{O}_{\boldsymbol{x}}^{\text{bin}} - \frac{1}{2} \text{tr}(O) & (\text{RESPOVM}), \end{cases}$$
(6)

the estimation variance  $\operatorname{Var}(\widehat{O}_{\mathbf{A},x}) \equiv \mathbb{E}(\widehat{O}_{\mathbf{A},x}^2) - (\mathbb{E}(\widehat{O}_{\mathbf{A},x}))^2$  of our two shadow-tomography schemes is given as,

$$\operatorname{Var}^{(r)\operatorname{eq}}(\widehat{O}_{\mathbf{A},x}) = \operatorname{Var}(\widehat{O}_{\mathbf{A}}^{(r)\operatorname{eq}}) + \operatorname{Var}(\widehat{O}_{x}^{\operatorname{bin}}), \tag{7}$$

because  $\mathbf{A}, \mathbf{x}$  sampling is independent of each other [42]. We remind the Reader of the abbreviated subscripts "eq" and "req" that respectively stand for "equatorial" in "ESPOVM" and "real equatorial" in "RESPOVM". The variance terms on the right side, after maximizing over the input state  $\rho$ , are

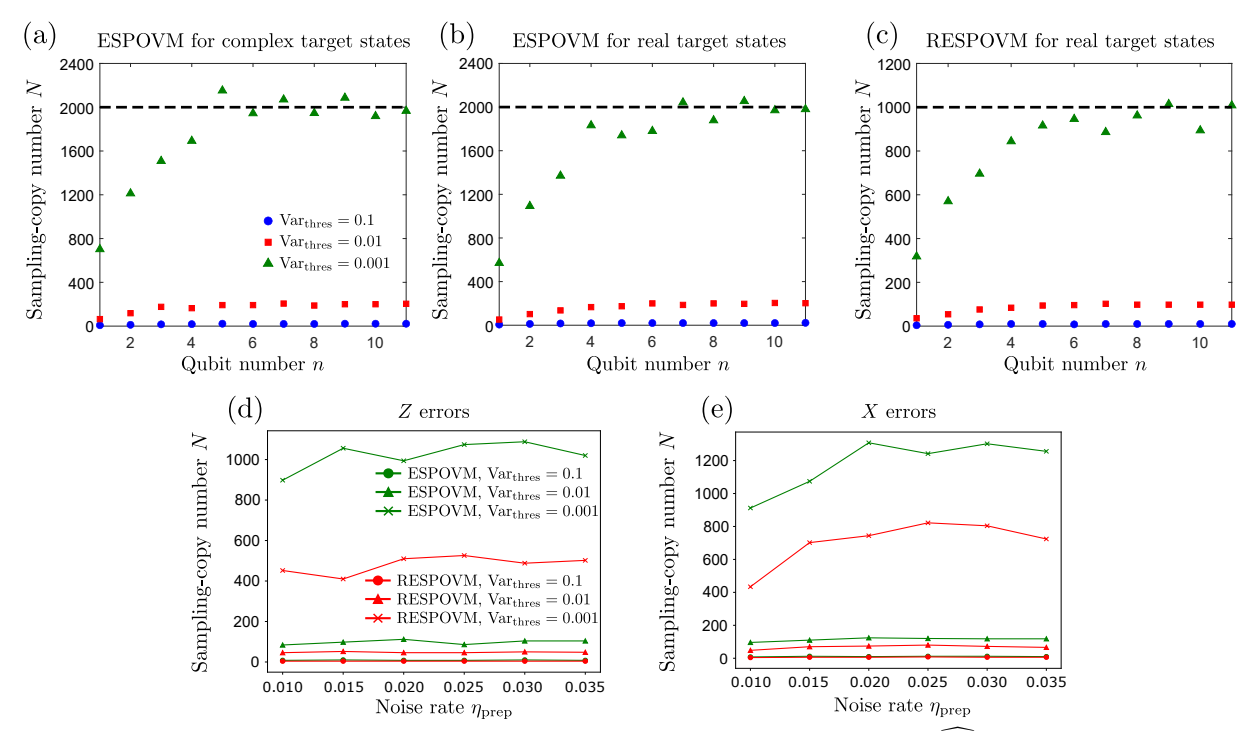


Figure 2 (a–c) Sampling-copy numbers N to achieve a certain threshold variance  $\operatorname{Var}(\slashed{O}) = \operatorname{Var}_{\operatorname{thres}}$  for shadow-tomography state verification on various distributions of n-qubit input and target states. For each N, we averaged the observable variance over 800 experiments per (pure) input  $\rho$  and target O. For (a), we average the variance over uniform distributions of complex input and target states. For (b) and (c), the average is over uniform distributions of complex input and real target states. The horizontal dashed lines represent theoretical asymptotic N values for  $\operatorname{Var}_{\operatorname{thres}} = 0.001$ . (d,e) Sampling-copy numbers N required to achieve the respective variance thresholds (averaged over 400 experiments) for state verification of a 50-qubit noisily-prepared GHZ state. We consider the i.i.d. (d) Z- and (e) X-error channels acting on every qubit with an error probability  $\eta_{\operatorname{prep}}$ .

equivalent to the respective squared shadow norms [9] of the (R)ESPOVM and Z-basis measurement, where each shadow norm is obtained from the following respective classical shadows (inverted channel map  $\mathcal{M}^{-1}$  [9]):

$$\mathcal{M}^{-1}(O) = \begin{cases} 2^{n}O - \operatorname{tr}(O)I & (ESPOVM), \\ 2^{n-1}O - \operatorname{tr}(O)\frac{I}{2} & (RESPOVM), \\ O & (Computational basis). \end{cases}$$
(8)

With Eq. (7), the complete variance of  $\widehat{\langle O \rangle}$  for estimating a single property  $\langle O \rangle$  is given by

$$\operatorname{Var}\left(\widehat{\langle O \rangle}\right) = \begin{cases} \frac{1}{N/2} \operatorname{Var}^{\operatorname{eq}}(\widehat{O}_{\mathbf{A},\boldsymbol{x}}) & (\text{ESPOVM and comp. basis}), \\ \frac{1}{N/2} \operatorname{Var}^{\operatorname{req}}(\widehat{O}_{\mathbf{A},\boldsymbol{x}}) & (\text{RESPOVM and comp. basis}). \end{cases}$$
(9)

Note that since  $\widehat{\langle O \rangle}$  is unbiased,  $\operatorname{Var}\left(\widehat{\langle O \rangle}\right)$  is identical to the *mean-squared error* of  $\widehat{\langle O \rangle}$  that measures the estimation accuracy of  $\widehat{\langle O \rangle}$  with respect to  $\langle O \rangle$ :

$$\operatorname{Var}\left(\widehat{\langle O \rangle}\right) = \mathbb{E}\left(\left(\widehat{\langle O \rangle} - \langle O \rangle\right)^2\right). \tag{10}$$

We state our main result pertaining to the simultaneous shadow tomography of  $M \geq 1$  observables:

Theorem 2. [Sampling-complexity efficiency of (R)ESPOVM shadow tomography] Suppose that one is able to prepare multiple copies of an unknown input quantum state  $\rho$ , and that one is given M observables  $O_1, O_2, \ldots, O_M$  (for RESPOVM shadow tomography, all  $O_j$ s are real).

(i) With (R)ESPOVM shadow-tomography scheme, we can estimate each  $\operatorname{tr}(\rho O_j)$  to within an

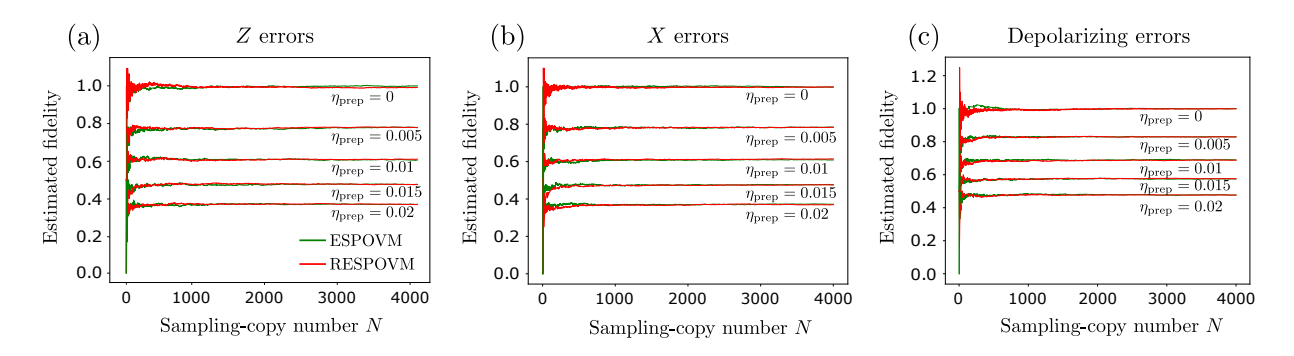


Figure 3 The estimated fidelity with the sampling-copy number N in shadow-tomography state verification of noisilyprepared  $7 \times 7$ -qubit graph states. The (a) Z, (b) X and (c) depolarizing preparation-noise channels are i.i.d. to the individual qubits. Each estimated value of a given N is obtained from the median of all  $\langle |7 \times 7 \text{ graph} \rangle \langle 7 \times 7 \text{ graph} | \rangle$  estimated using the formulas in (5) from over 400 experiments.

additive  $\varepsilon$ -error margin with a success probability  $1-\delta$  if we repeat this scheme over N $\mathcal{O}\left(\frac{\max_{1\leq j\leq M}\left\{\operatorname{Var^{(r)eq}}(\widehat{O_{j}}_{\mathbf{A},\boldsymbol{x}})\right\}}{\varepsilon^{2}}\log\left(\frac{M}{\delta}\right)\right) \ copies, \ such \ that \ for \ all \ 1\leq j\leq M, \ \operatorname{Var^{(r)eq}}(\widehat{O_{j}}_{\mathbf{A},\boldsymbol{x}}) = \operatorname{Var}(\widehat{O_{j}}_{\mathbf{A}}) + \operatorname{Var}(\widehat{O_{j}}_{\boldsymbol{x}}) \ and$ 

$$\operatorname{Var}\left(\widehat{O}_{j\mathbf{A}}^{(r)\operatorname{eq}}\right) \leq \begin{cases} 14 \operatorname{tr}(O_{j0}^{2}) & (\text{for eq}), \\ 13 \operatorname{tr}(O_{j0}^{2}) & (\text{for req}), \end{cases}$$

$$\operatorname{Var}(\widehat{O}_{x}^{\operatorname{bin}}) \leq \operatorname{tr}(O_{j0}^{2}) \qquad (11)$$

where  $O_{j0}$  is the traceless part,  $O_j = \frac{I}{2^n} \mathrm{tr}(O_j)$ .

(ii) If  $2^n \gg 1$ , the averaged value  $\overline{\mathrm{Var}^{(r)\mathrm{eq}}(\hat{\sigma})}^{\rho,\sigma}$  over uniformly-distributed complex pure states  $\rho$  and real pure states  $\sigma$  approaches 1 for eq and  $\frac{1}{2}$  for req. In randomized-Clifford tomography, this average variance approaches 1.

(iii) If  $2^n \gg 1$ , the averaged value  $\overline{\mathrm{Var}^{\mathrm{eq}}(\hat{\sigma})}^{\rho,\sigma}$  over uniformly-distributed complex pure states  $\rho$  and  $\sigma$ approaches 1. In randomized-Clifford tomography, this average variance approaches 1.

Theorem 2 (i) suggests that the estimation variance grows at most polynomially with the qubit number n in many cases. Most notably, if O is also a quantum state  $\sigma$ , then the right side of (11) becomes constant, hence the required sampling-copy number N is independent of n. Note that the variance upper bound and average offered by RESPOVM shadow tomography are lower than those supplied by ESPOVM shadow tomography. Since only an upper bound for  $Var(\langle O \rangle)$  is known, its exact value may be much lower than this bound. Indeed, Theorem 2 (ii) and (iii) imply that one can observe a much lower variance for many cases in state-fidelity estimation. This is especially so when the target state is real, in which case RESPOVM gives a better average variance than both ESPOVM and even randomized-Clifford POVM. Hence, we can expect RESPOVM shadow tomography to be more useful for real observable estimation. This is because even though RESPOVM requires two copies of input states for a single sampling trial, the total number of gates used with the same number of sampling copies is, on average, smaller than half of what is required in randomized-Clifford shadow tomography.

To showcase the performance of (R)ESPOVM shadow tomography, we examine scenarios in state verification, that is fidelity estimation between arbitrary quantum states. Figure 2(a-c) illustrate three exemplifying cases: ESPOVM shadow tomography for uniformly-chosen random complex input and target states. ESPOVM shadow tomography for uniformly-chosen complex input and real target states, and RESPOVM shadow tomography for the same types of random states as in the second case. We observe that the sampling-copy number N to achieve a threshold  $Var(\langle O \rangle)$  saturates beyond a certain qubit number n. These results are consistent with the point of Thm. 2 (i). Moreover, for real target states, the saturated value of N for RESPOVM is half of that for ESPOVM, which is the another message of Thm. 2 (ii). Figure 2(d,e) demonstrates the success of (R)ESPOVM shadow tomography in estimating the fidelity between 50-qubit noisily-prepared GHZ states [45] and pure GHZ state with reasonable N values, where one also observes that RESPOVM needs significantly fewer sampling copies than ESPOVM to achieve the same accuracy. Figure 3 brings (R)ESPOVM shadow tomography to the test through fidelity estimation of noisy 7×7 graph states [46] that has CZ-gate connections to all neighboring qubits. Here,

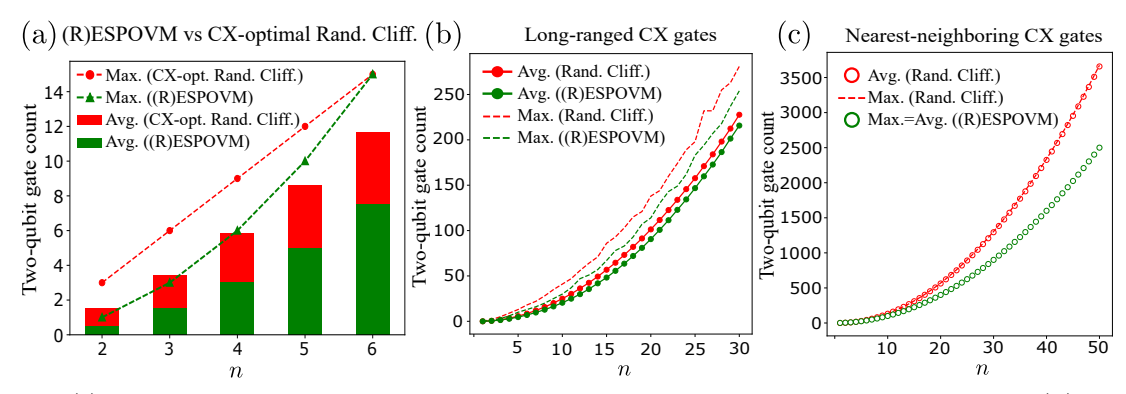


Figure 4 (a) The optimal analytical maximum and average number of long-ranged CNOT gates to implement (R)ESPOVM and randomized-Clifford circuit for low-qubit systems. The latter one is obtained via Tab. 6. of Ref. [51], and is the average gate count over all equivalence classes(This value is nearly equal to the true average). (b) The average number of CNOT gates (over 4000 gate samples) to implement intermediate-sized (R)ESPOVMs and single Hadamard-free (HF) sections of randomized-Clifford circuits [19]. For (R)ESPOVMs, we further contracted the gate count *via* the Patel–Markov–Hayes construction [52]. (c) The maximum and average numbers of NN CNOT gates (over 4000 gate samples) to implement a 2n-depth large-qubit (R)ESPOVM and 3n-depth neighboring implementation of randomized-Clifford circuits [18]. Refer to Sec. 4.3 in "Methods" for a detailed elaboration of these graphs.

N is also the number of measurement trials because every binary measurement outcome gives the same  $\widehat{O}_{\boldsymbol{x}}^{\text{bin}} \equiv \langle \boldsymbol{x} | \, O \, | \boldsymbol{x} \rangle = \frac{1}{2^n}$ , so that binary measurements may be omitted. Note that as the preparation error rate  $\eta_{\text{prep}} \to 0$ , all estimated fidelities approach the desired value of unity. Even when the observable is approximately a cluster state in the sense that  $|\langle \boldsymbol{x} | \, O \, | \boldsymbol{x} \rangle| < \frac{1}{2^{\alpha n}}$  for  $\forall \boldsymbol{x} \in \mathbb{Z}_2^n$ ,  $\alpha > 0$  and a large  $n \in \mathbb{N}$ , if our objective is to reduce the additive error precision, the binary measurement part may also be neglected.

Alternatively, fidelity estimations of stabilizer states may be carried out using simpler specialized quantum circuits reported in Ref. [26]. Nevertheless, we emphasize that all target states achieve the same asymptotic sampling-complexity bound that is constant in n with (R)ESPOVM shadow-tomography. This means that our technique clearly applies to many other interesting states, including the Dicke states [47], for which  $N = \mathcal{O}(n^{2k})$  using the method in Ref. [26].

Another important class of physical observables are n-qubit Heisenberg-type Hamiltonians taking the general form  $O = \sum_{p} J_{p} Z^{p} + \sum_{q} J'_{q} X^{q} + \sum_{k} J''_{k} Y^{k}$  for all real  $J_{p}$ ,  $J'_{q}$  and  $J''_{k}$ , where every summation has  $\mathcal{O}(\text{poly}(n))$  terms. They are crucial to the study of spin systems and many other aspects of condensed-matter physics [34, 35]. While more elaborative discussions shall be presented in Sec. 4.2 of "Methods", we remark here that expectation values of any such Hamiltonian can be estimated with poly(n) sampling complexities via only Pauli measurements.

# 2.4 Low gate count and depth for implementing (R)ESPOVM shadow tomography

For both the ESPOVM and RESPOVM shadow-tomography algorithms, we note that the intermediate Clifford operation requires only CZ gates and hence the implementation of randomly chosen CZ gates needs at most  $\mathcal{O}(n^2)$ -time. In the language of quantum circuits, Vizing's theorem [37, 48, 49] states that an arbitrary CZ circuit requires a circuit depth of at most n when only CZ gates are employed.

With the aid of CNOT gates, we can reduce the depth to  $\frac{n}{2} + \mathcal{O}(\log(n))$  [37]. Furthermore, with just NN two-qubit gates, only a circuit depth of 2n is needed [42, 50] with CNOT and S gates, which is lower than the worst-case circuit depth of 7n for the implementation of randomized-Clifford tomography [9, 18, 19, 42]. In Sec. 4.3 of the "Methods" section, we further reduced the depth of randomized Clifford tomography to 3n. This is possible since we are using only non-adaptive Clifford circuits. These arguments are gathered into the following statements:

Theorem 3. [Gate-count efficiency of (R)ESPOVM shadow tomography] [37, 38] Both ES-POVM and RESPOVM shadow-tomography algorithms can be implemented by circuits of depth  $\frac{n}{2} + \mathcal{O}(\log(n))$  (for  $n \geq 39$ ) comprising long-ranged Clifford gates, or those of depth of at most 2n using neighboring Clifford gates, while randomized Clifford needs at most 3n neighboring Clifford gates. The implementation of linear nearest-neighboring (LNN) architecture takes  $\mathcal{O}(n^2)$ -time for each sampling copy.

The essence of this theorem is an improvement in gate count with (R)ESPOVM shadow tomography. From the graphical illustration of this theorem, in Fig. 4 (a,b), we can observe that even before the  $\frac{n}{2}$ -depth contraction, randomized CZ-circuit implementation requires a lower gate count than what is

required in randomized-Clifford tomography. In particular, Fig. 4(c) shows that the gate counts between LNN architectures differ with a more significant multiplicative factor. Although more optimistic proposals to realize unitary 2-designs with log-depth Clifford circuits exist [9, 53], it is not known how many the sampling-copy number is needed and what the actual feasible gate count would be when these proposals are transformed into LNN architectures.

The CZ-circuit-based architecture of our (R)ESPOVM schemes also presents an attractive feature for experimental implementation, especially with the soaring entangling-gate fidelities recently achieved in various quantum-computing platforms. While a more comprehensive survey shall be given in Sec. 4.5 of "Methods", we quote some recent experimental fidelities achieved in some of these platforms: 99.5% two-qubit gate fidelity in Rydberg-atom quantum computing [54], over 99.5% for semiconductor-spin-based systems [55], and up to 99.93% with superconducting qubits [56].

#### 2.5 Noise tolerance of (R)ESPOVM shadow tomography

The presence of multiple two-qubit gates in a circuit-based quantum-algorithm implementation, be it randomized-Clifford or (R)ESPOVM shadow tomography, enforces a restriction on the individual gatenoise threshold if one is to achieve a given total error rate of the output state before the observable measurement is performed. From Fig. 4(a,b), we observed that our (R)ESPOVM scheme requires a lower long-ranged gate count than randomized-Clifford sampling. Therefore, we note that the required noise threshold for each two-qubit gate is affordably larger for (R)ESPOVMs. Figure. 4(c) shows that in an LNN architecture, the required number of CNOT gates is reduced more effectively and better noise improvements can be expected.

As a testament to the higher noise tolerances (R)ESPOVM shadow-tomography protocols can achieve, we firstly compare the average gate fidelity [57] of the low-qubit random CZ-based RESPOVM circuits and random Clifford circuits. The significant gap between Rand. Cliff. 1 and Rand. Cliff. 2 is derived by the fact that in Rand. Cliff. 1, we can only give the noise to the lower half of CNOT gates, while we could not in Rand. Cliff. 2. The expression and computation of the average gate fidelity are presented in Sec. 4.4 of "Methods". Fig. 5 (a,b) manifest that gate fidelity estimation yields higher rates than one of random Clifford sampling, closer to 1 which is the desired value for pure circuits. Second, we investigate their performances on fidelity estimations for GHZ  $[|GHZ_n\rangle \equiv \frac{1}{\sqrt{2}}(|0\rangle^{\otimes n} + |1\rangle^{\otimes n})]$  [39] and W states  $[|W_n\rangle \equiv \frac{1}{\sqrt{n}}(|0\rangle^{\otimes (n-1)}|1\rangle + |0\rangle^{\otimes (n-2)}|1,0\rangle + \ldots + |1\rangle|0\rangle^{\otimes (n-1)})]$  for n=3,4 and 8 in the presence of depolarizing-noise channels. Clearly, a good estimated value should be close to unity. From the graphs presented in Fig. 5, for the same depolarizing error rates, we can observe that RESPOVM shadow tomography provides larger fidelity estimates than randomized-Clifford methods. It should be noted that the gap is much larger than the gap between previously obtained average gate fidelities. We expect that this resource-efficient shadow tomography will offer similar estimation-accuracy advantages in many other cases, such as the state verification of large non-stabilizer quantum states, at which available schemes are more restrictive. Furthermore, since we did not use any circuit contraction technique for RESPOVM and neighboring architecture here, further gap improvement throughout Fig. 5 after the modifications is in the prospect.

#### 3 Discussion

In this article, we propose resource-efficient methods to carry out quantum shadow tomography using equatorial-stabilizer measurements that are derived from smaller subsets of the full set of stabilizer states. We first prove that these equatorial-stabilizer measurements, together with the computational-basis measurements are indeed informationally complete and possess desirable sampling complexity that grows, in many cases, at most polynomially in the number of qubits n and reciprocally in the square of the target additive estimation error. In typical scenarios, such as state verification tasks, the sampling complexity of equatorial-stabilizer shadow tomography is independent of n.

Furthermore, we showed that these economic shadow-tomography algorithms utilize long-ranged Clifford bases with circuit depths of  $\frac{n}{2} + \mathcal{O}(\log(n))$ . When restricted to only LNN architectures, our algorithms are considerably efficient to implement, requiring only 2n-depth NN CNOT gates, owing to their simpler circuit geometry. We demonstrated that our methods require fewer Clifford basis count than randomized-Clifford tomography for both long-ranged and LNN implementations, while still preserving the classes of applicable observables for many cases in terms of the shadow-norm or estimation variance criterion. Our depth- (or gate-)efficient shadow-tomography schemes become practically important for performing realistic quantum-computation tasks as they permit larger gate-error thresholds. This is also crucial to

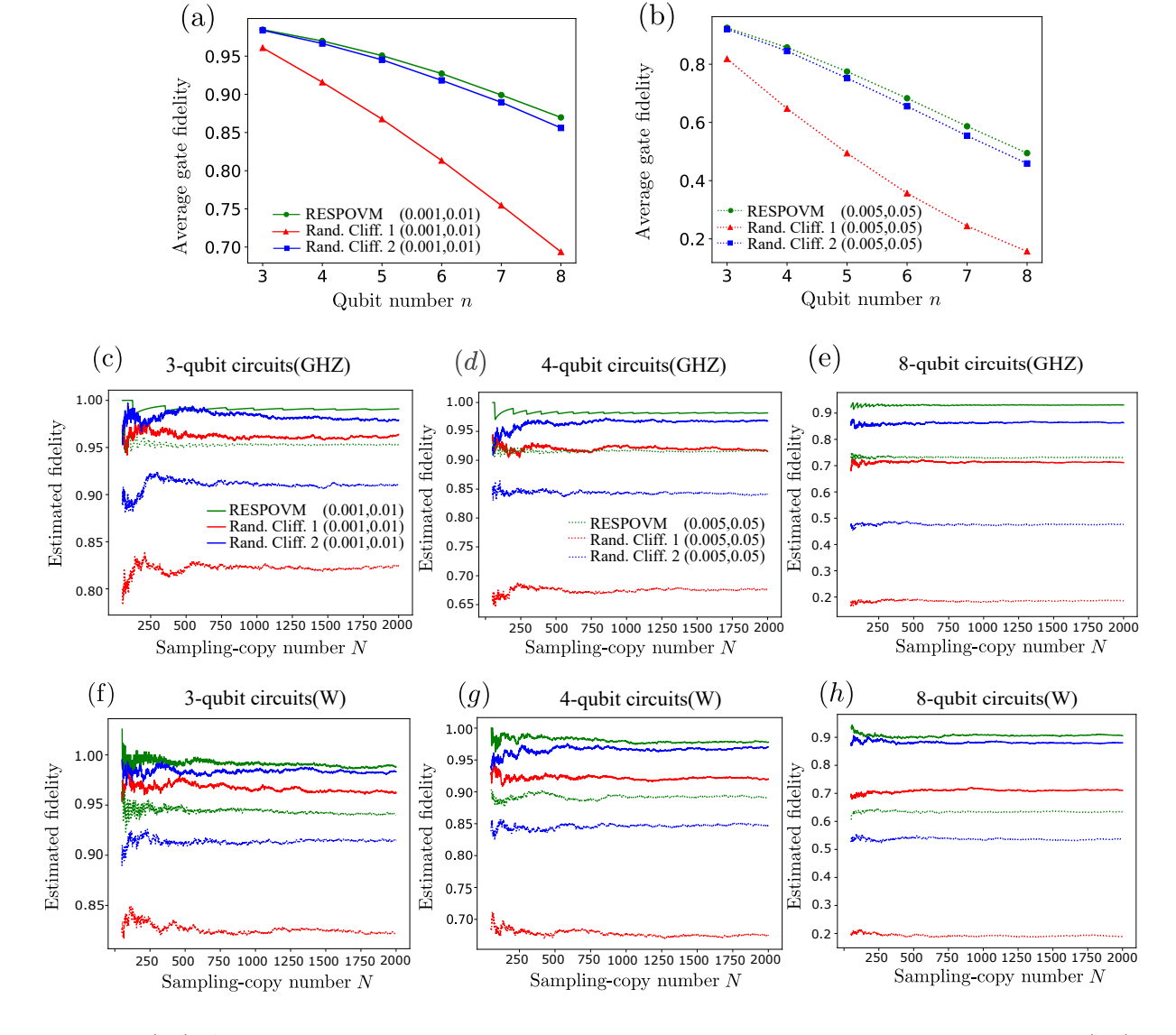


Figure 5 (a,b): Averaged gate fidelity comparison between noisy RESPOVM and randomized-Clifford circuit. (c-h): ESPOVM shadow-tomography performances in state verification of (c-e) GHZ and (f-h) W states with increasing number of input-state copies N. For (a-h), two randomized-Clifford circuits are considered here: Rand. Cliff. 1 indicates the sampling and decomposition scheme via Ref. [29] (or [51] for 3-qubit circuits), and Rand. Cliff. 2 refers to the sampling method in Ref. [19] in which noise is attributed only to the single HF-section. RESPOVM is implemented with arbitrary CZ gates. We added depolarization noise to each gate with given error rates. The legends  $(\eta_1, \eta_2)$  indicate the respective depolarizing error rates for  $(\eta_1)$  single-qubit (H, S, Pauli) and  $(\eta_2)$  two-qubit gates (CNOT,CZ). Note that if a noisy CNOT gate is positioned in the circuit such that it corresponds to some linear transformation of the measurement outcomes right a perfect CNOT gate, then we need not assign noise for this gate in principle. This is because classically post-processing of the measurement outcomes is sufficient to implement such a gate operation. For (a,b), averaged gate fidelity is computed via the Monte Carlo method with 300 random pure states input and 2000 random circuit samples. For (c-h), The estimated fidelity is obtained by taking the median of 200 estimated values for a given number of input states.

certain auxiliary quantum tasks, such as those in quantum error mitigation for instance, where it is recently known [58] that such tasks would require sampling-copy numbers that increase exponentially with the circuit depth.

Thus far, the (R)ESPOVM schemes we have found to have good shadow-tomographic properties require both computational-basis and CZ-circuit measurements that involve very different circuit depths, with the former being single-layered while the latter grows linearly with n in depth. One possible future work would be to investigate if there exist other such pairs of measurement circuits of comparable depths that can reduce the maximum circuit depth employed whilst maintaining the same estimation quality. Reference [28] proposes to use MUB subsets of the CZ-circuit measurements for observable expectation-value estimation. It does not show poly(n)-scaled variance for arbitrary states, but could still serve as an instructive starting point. Yet another desirable observation is the rather large error-threshold advantages in using equatorial-stabilizer shadow tomography on GHZ state-verification tasks in contrast

to randomized-Clifford shadow tomography, as shown in Fig. 5. This is beyond what we expected from the average-gate-fidelity comparison. The underlying reason behind the significant estimation-quality gap has to do with the sparsity of the input GHZ state in the computational basis that results in a large room for obtaining a very good estimated fidelity so long as the bit strings measured by (R)ESPOVM are of the correct parity. One may also expect W states to behave similarly. This readily sets another research direction on identifying important classes of target quantum states that could lead to highly-effective gate-error threshold improvements.

Clifford circuits are well-known quantum circuits [59, 60] whose noise-tolerant properties could be realizable in the near future. Therefore, we expect our work to establish practical research directions on gate-efficient observable-expectation-value estimations for noisy intermediate-scale quantum computation.

#### 4 Methods

In this section, we elaborate on our key results with discussions concerning the (R)ESPOVM shadow-tomography algorithm, calculations leading to the estimation accuracies and systematic approaches to counting the gate complexities needed to implement (R)ESPOVM schemes. Along the way, we shall sketch the proofs for Theorems 1 to 3 and include their details that are appropriate and coherent to the general discussions in this section without diving into other required technical lemmas and miscellaneous statements to complete the proofs. The reader is invited to refer to the Supplementary Information for all remaining arguments not covered here. Further, we introduce the notion of average gate fidelity and detailed expression of the recent status of Clifford gates implementation in reality.

#### 4.1 Procedures and algorithm for equatorial-stabilizer shadow tomography

Before we present the details of (R)ESPOVM shadow tomography, we first introduce the notation  $\mathbb{E}_{\sigma \in \mathcal{D}(A)} f(\sigma)$  that refers to the expected value of the function  $f(\sigma)$  of a random variable  $\sigma \in A$  that follows a uniformly random distribution  $\mathcal{D}(A)$  with domain A. In particular, we call  $\mathbb{E}_{\sigma \in \mathcal{D}(A)} \sigma^{\otimes t}$  as the t-th moment of A. With this, we have the following lemma [42].

**Lemma 1.** For the n-qubit system,

(i) 
$$[31] \mathbb{E}_{|\phi_{\mathbf{A}}^{\text{eq}}\rangle \in \mathcal{D}(\mathcal{S}_n^{\text{eq}})} |\phi_{\mathbf{A}}^{\text{eq}}\rangle \langle \phi_{\mathbf{A}}^{\text{eq}}| = \mathbb{E}_{|\phi_{\mathbf{A}}^{\text{req}}\rangle \in \mathcal{D}(\mathcal{S}_n^{\text{req}})} |\phi_{\mathbf{A}}^{\text{req}}\rangle \langle \phi_{\mathbf{A}}^{\text{req}}| = \frac{I}{2^n},$$
 (12)

(ii) [31] 
$$\mathbb{E}_{|\phi_{\mathbf{A}}^{\mathrm{eq}}\rangle \in \mathcal{D}(\mathcal{S}_{n}^{\mathrm{eq}})} |\phi_{\mathbf{A}}^{\mathrm{eq}}\rangle \langle \phi_{\mathbf{A}}^{\mathrm{eq}}|^{\otimes 2} = \frac{1}{4^{n}} \left( I + \sum_{\boldsymbol{x}, \boldsymbol{y} \in \mathbb{Z}_{2}^{n}} |\boldsymbol{x}\boldsymbol{y}\rangle \langle \boldsymbol{y}\boldsymbol{x}| - \sum_{\boldsymbol{x} \in \mathbb{Z}_{2}^{n}} |\boldsymbol{x}\boldsymbol{x}\rangle \langle \boldsymbol{x}\boldsymbol{x}| \right),$$
 (13)

(iii) 
$$\mathbb{E}_{|\phi_{\mathbf{A}}^{\text{req}}\rangle\in\mathcal{D}(\mathcal{S}_{n}^{\text{req}})} |\phi_{\mathbf{A}}^{\text{req}}\rangle \langle \phi_{\mathbf{A}}^{\text{req}}|^{\otimes 2} = \frac{1}{4^{n}} \left( I + \sum_{\boldsymbol{x},\boldsymbol{y}\in\mathbb{Z}_{2}^{n}} |\boldsymbol{x}\boldsymbol{y}\rangle \langle \boldsymbol{y}\boldsymbol{x}| + \sum_{\boldsymbol{x},\boldsymbol{y}\in\mathbb{Z}_{2}^{n}} |\boldsymbol{x}\boldsymbol{x}\rangle \langle \boldsymbol{y}\boldsymbol{y}| - 2\sum_{\boldsymbol{x}\in\mathbb{Z}_{2}^{n}} |\boldsymbol{x}\boldsymbol{x}\rangle \langle \boldsymbol{x}\boldsymbol{x}| \right).$$
(14)

We note that from Lem. 1 (i), all elements from the respective sets  $\left\{\frac{2^n}{|S_n^{\text{req}}|} |\phi_{\mathbf{A}}^{\text{eq}}\rangle \langle \phi_{\mathbf{A}}^{\text{eq}}|\right\}$  and  $\left\{\frac{2^n}{|S_n^{\text{req}}|} |\phi_{\mathbf{A}}^{\text{req}}\rangle \langle \phi_{\mathbf{A}}^{\text{req}}|\right\}$  form a POVM. Using Lem. 1 (ii) and (iii), we can obtain the following formulas which are directly related to our tomography schemes [42]:

**Lemma 2.** For an unknown n-qubit quantum state  $\rho$  and Hermitian operator O,

$$\operatorname{tr}(\rho \, O) = \sum_{|\phi_{\mathbf{A}}^{\text{eq}}\rangle \in \mathcal{S}_{n}^{\text{eq}}} \frac{2^{2n}}{|\mathcal{S}_{n}^{\text{eq}}|} \left\langle \phi_{\mathbf{A}}^{\text{eq}} \right| \rho \left| \phi_{\mathbf{A}}^{\text{eq}} \right\rangle \left\langle \phi_{\mathbf{A}}^{\text{eq}} \right| O \left| \phi_{\mathbf{A}}^{\text{eq}} \right\rangle + \sum_{\boldsymbol{x} \in \mathbb{Z}_{2}^{n}} \left\langle \boldsymbol{x} \right| \rho \left| \boldsymbol{x} \right\rangle \left\langle \boldsymbol{x} \right| O \left| \boldsymbol{x} \right\rangle - \operatorname{tr}(O) \,. \tag{15}$$

If O is a real matrix with respect to the computational basis,

$$\operatorname{tr}(\rho O) = \sum_{|\phi_{\mathbf{A}}^{\text{req}}\rangle \in \mathcal{S}_{n}^{\text{req}}} \frac{2^{2n-1}}{|\mathcal{S}_{n}^{\text{req}}|} \left\langle \phi_{\mathbf{A}}^{\text{req}} | \rho |\phi_{\mathbf{A}}^{\text{req}}\rangle \left\langle \phi_{\mathbf{A}}^{\text{req}} | O |\phi_{\mathbf{A}}^{\text{req}}\rangle + \sum_{\boldsymbol{x} \in \mathbb{Z}_{2}^{n}} \left\langle \boldsymbol{x} | \rho | \boldsymbol{x}\rangle \left\langle \boldsymbol{x} | O | \boldsymbol{x}\rangle - \frac{1}{2} \operatorname{tr}(O).$$
 (16)

We are ready to provide more details concerning the (R)ESPOVM shadow-tomography procedure, thereby explaining the validity of Algo. 1. We shall only discuss matters related to the ESPOVM, as the dissertation for RESPOVM follows similarly. Let us assume an input state  $\rho = \sum_{z,w \in \mathbb{Z}_2^n} |z\rangle \langle w| \langle z| \rho |w\rangle$ .

The procedure begins by a random selection of  $|\phi_{\mathbf{A}}^{\mathrm{eq}}\rangle \in \mathcal{S}_{n}^{\mathrm{eq}}$ , that is the matrix **A** from uniformly distributed elements in the set

$$\mathcal{A} \equiv \left\{ \mathbf{A} \middle| \mathbf{A} = (a_{ij})_{i,j \in [n]} \text{ where } a_{ij} = a_{ji}, a_{ii} \in \mathbb{Z}_4, a_{ij} \in \mathbb{Z}_2 \text{ if } i \neq j \right\}.$$
 (17)

Operationally, this is akin to flipping a coin  $\frac{n^2-n}{2}$  times to determine all symmetric off-diagonal elements and flipping a uniform 4-sided die n times to determine all diagonal elements of  $\mathbf{A}$ . Now, given a single-qubit (two-qubit resp.) operation K, we define  $K_i$  ( $K_{ij}$ ) as K acting on the i-th (i-th and j-th) qubit. After choosing a random  $\mathbf{A}$ , we perform  $\operatorname{CZ}_{ij}$  gate operations whenever  $a_{ij}=1$  and i< j, followed by single-qubit operations  $U_i$  such that

$$U_{i} \equiv \begin{cases} I_{i} & \text{if } a_{ii} = 0, \\ S^{\dagger} & \text{if } a_{ii} = 1, \\ Z_{i} & \text{if } a_{ii} = 2, \\ S_{i} & \text{if } a_{ii} = 3, \end{cases}$$
 or simply,  $U_{i} \equiv (S^{\dagger})^{i}$ . (18)

Next, we apply Hadamard gates  $H \equiv \bigotimes_{i=1}^n H_i$ . The subsequent evolved state  $\rho'$  is written as

$$\rho \leftarrow \rho' = \frac{1}{2^n} \sum_{\boldsymbol{z}, \boldsymbol{w}, \boldsymbol{s}, \boldsymbol{t} \in \mathbb{Z}_2^n} i^{3\boldsymbol{z} \cdot \mathbf{A} \boldsymbol{z}^\top + \boldsymbol{w} \cdot \mathbf{A} \boldsymbol{w}^\top} (-1)^{\boldsymbol{z} \cdot \boldsymbol{s} + \boldsymbol{w} \cdot \boldsymbol{t}} |\boldsymbol{s}\rangle \langle \boldsymbol{t}| \langle \boldsymbol{z}| \rho |\boldsymbol{w}\rangle.$$
(19)

Here,  $a \cdot b$  refers to the binary inner product between a and b. We shall now perform the Pauli Z-basis measurement independently on all the qubits. The probability  $\operatorname{prob}(p \mid A)$  to obtain a specific binary string  $p \in \mathbb{Z}_2^n$  is

$$\operatorname{prob}(\boldsymbol{p} \mid \mathbf{A}) \equiv \langle \boldsymbol{p} \mid \boldsymbol{\rho}' \mid \boldsymbol{p} \rangle = \frac{1}{2^{n}} \sum_{\boldsymbol{z}, \boldsymbol{w}, \boldsymbol{s}, \boldsymbol{t} \in \mathbb{Z}_{2}^{n}} i^{3\boldsymbol{z} \mathbf{A} \boldsymbol{z}^{\top} + \boldsymbol{w} \mathbf{A} \boldsymbol{w}^{\top}} (-1)^{\boldsymbol{z} \cdot \boldsymbol{s} + \boldsymbol{w} \cdot \boldsymbol{t}} \langle \boldsymbol{p} \mid \boldsymbol{s} \rangle \langle \boldsymbol{t} \mid \boldsymbol{p} \rangle \langle \boldsymbol{z} \mid \boldsymbol{\sigma} \mid \boldsymbol{w} \rangle,$$

$$= \frac{1}{2^{n}} \sum_{\boldsymbol{z}, \boldsymbol{w} \in \mathbb{Z}_{2}^{n}} i^{3\boldsymbol{z} \mathbf{A} \boldsymbol{z}^{\top} + \boldsymbol{w} \mathbf{A} \boldsymbol{w}^{\top}} (-1)^{\boldsymbol{z} \cdot \boldsymbol{p} + \boldsymbol{w} \cdot \boldsymbol{p}} \langle \boldsymbol{z} \mid \boldsymbol{\sigma} \mid \boldsymbol{w} \rangle,$$

$$= \frac{1}{2^{n}} \sum_{\boldsymbol{z}, \boldsymbol{w} \in \mathbb{Z}_{2}^{n}} (-i)^{\boldsymbol{z} \mathbf{A} \boldsymbol{z}^{\top} - 2\boldsymbol{z} \cdot \boldsymbol{p}} i^{\boldsymbol{w} \mathbf{A} \boldsymbol{w}^{\top} - 2\boldsymbol{w} \cdot \boldsymbol{p}} \langle \boldsymbol{z} \mid \boldsymbol{\sigma} \mid \boldsymbol{w} \rangle,$$

$$= \langle \boldsymbol{\phi}_{\mathbf{A}'}^{eq} \rangle \rho | \boldsymbol{\phi}_{\mathbf{A}'}^{eq} \rangle, \qquad (20)$$

where  $\mathbf{A}'$  is an  $n \times n$  matrix such that  $a'_{ij} = a_{ij}$  for  $i \neq j$ , and  $a'_{ii} = a_{ii} + 2p_i \pmod{4}$ . The last equation can be obtained by following the definition of Eq. (3). Now, we define  $\mathbf{D}(\mathbf{p})$  as the  $n \times n$  diagonal matrix whose *i*-th diagonal element is equal to  $p_i$ , and also note, from Eq. (3), that

$$\frac{2^{n}}{|\mathcal{S}_{n}^{\text{eq}}|} \left\langle \phi_{\mathbf{A}}^{\text{eq}} \right| \rho \left| \phi_{\mathbf{A}}^{\text{eq}} \right\rangle = \frac{1}{|\mathcal{S}_{n}^{\text{eq}}|} \sum_{\boldsymbol{z}, \boldsymbol{w} \in \mathbb{Z}_{2}^{n}} (-\mathrm{i})^{\boldsymbol{z} \mathbf{A} \boldsymbol{z}^{\top}} \mathrm{i}^{\boldsymbol{w} \mathbf{A} \boldsymbol{w}^{\top}} \left\langle \boldsymbol{z} \right| \rho \left| \boldsymbol{w} \right\rangle = \sum_{\boldsymbol{p} \in \mathbb{Z}_{2}^{n}} \frac{1}{|\mathcal{S}_{n}^{\text{eq}}|} \mathrm{prob}(\boldsymbol{p} \mid \mathbf{A} - 2\mathbf{D}(\boldsymbol{p})), \quad (22)$$

where the final equality is a result of Eq. (20).

The left-hand side of Eq. (22) corresponds to the probability distribution of  $\mathbf{A}$  we want to sample from. Also, given a  $\mathbf{p} \in \mathbb{Z}_2^n$ , the probability to sample the matrix  $\mathbf{A} - 2\mathbf{D}(\mathbf{p})$  is constant  $\left(\frac{1}{|\mathcal{S}_n^{\text{eq}}|}\right)$ . Hence, we can interpret the right-most side of Eq. (22) as the probability to get the matrix  $\mathbf{A}$  after we uniformly sampled the matrix  $\mathbf{A}'$  and add  $2\mathbf{D}(\mathbf{p})$  (see steps 22 through 28 in Algo. 1). In this way, the desired sample of  $\mathbf{A}$  is obtained.

Furthermore, we note that one can propagate the measurement section to the left-over Hadamard gates and phase gates. In that case, the CZ gates are the only remaining intermediate gates, and Vizing's theorem states that only at most n layers of CZ gates are needed to realize an arbitrary n-qubit CZ circuit, which settles part of Thm. 1. One must still carry out either the Pauli X or Y measurement depending on the phase gate acting on that qubit. However, the phase gate implementation is unnecessary and we simply perform an X or Y-basis measurement. The reason is that Z (S resp.) just flips the measurement outcome of X (Y) measurement. For example, implementing Z and obtaining the X-measurement outcome 0 is equivalent to just measuring in the X-basis, obtaining the outcome 1, which gives the same diagonal

value of the sampled **A**. That is why we can transform above procedure to take X or Y-measurement depending on only the mod 2 features of sampled  $a_{ii}$  ( $i \in [n]$ ), not using single qubit phase gates, and add  $2\mathbf{D}(p)$  to  $\mathbf{A}'$ . This closes the proof of Thm. 1 for the ESPOVM scheme, and also justifies steps 22 through 28 in Algo. 1.

Harking back to Eq. (2), in order to complete the shadow tomography protocol, one also acquires  $p' \in \mathbb{Z}_2^n$  following the distribution  $\langle p' | \rho | p' \rangle$ , which can be done easily by measuring  $\rho$  in the Pauli Z basis. Hence, the algorithm for an unbiased estimation of  $\operatorname{tr}(O\rho)$  can be summarized as follows:

- 1. Measure one copy of  $\rho$  with the POVM  $\{\frac{2^n}{|S_n^{\rm eq}|}|\phi_{\mathbf{A}}^{\rm eq}\rangle\langle\phi_{\mathbf{A}}^{\rm eq}|\}$  defined by a uniformly-chosen  $\mathbf{A}$  from the set  $\mathcal{A}$  in (17). This is done by (i) uniformly choosing an  $\mathbf{A}'\in\mathcal{A}$ , (ii) obtain a  $\mathbf{p}\in\mathbb{Z}_2^n$  from measuring the rotated output copy  $U_{\mathbf{A}'}^{\dagger}\rho U_{\mathbf{A}'}$ , where  $U_{\mathbf{A}'}|0^{\otimes n}\rangle=|\phi_{\mathbf{A}'}^{\rm eq}\rangle$ , (iii) and take  $\mathbf{A}=\mathbf{A}'+2\mathbf{D}(\mathbf{p})$ . The measurement outcome  $\mathbf{p}$  would then follow the distribution  $\frac{2^n}{|S_n^{\rm eq}|}\langle\phi_{\mathbf{A}}^{\rm eq}|\rho|\phi_{\mathbf{A}}^{\rm eq}\rangle$ .
- 2. Measure one copy of  $\rho$  in Z-basis and obtain  $p' \in \mathbb{Z}_2^n$  following the distribution  $\langle p' | \rho | p' \rangle$ .
- 3. Calculate  $\widehat{O}_{\mathbf{A}.\boldsymbol{x}} \equiv 2^n \langle \phi_{\mathbf{A}}^{\text{eq}} | O | \phi_{\mathbf{A}}^{\text{eq}} \rangle + \langle \boldsymbol{p}' | O | \boldsymbol{p}' \rangle \text{tr}(\widehat{O}).$

Algorithm 1 is the pseudocode encapsulation of all the arguments we made thus far.

#### 4.2 Estimation-variance analysis of equatorial-stabilizer shadow tomography

We shall now sketch the proof of Thm. 2 (i). The proofs of (ii) and (iii) contain more technical elements that are more suitably located in Supplementary Information.

We note that

$$\operatorname{Var}(\widehat{O}_{\mathbf{A}}^{\operatorname{eq}}) = \mathbb{E}\left(\left\{2^{n} \left\langle \phi_{\mathbf{A}}^{\operatorname{eq}} \right| O \left| \phi_{\mathbf{A}}^{\operatorname{eq}} \right\rangle - \mathbb{E}\left(2^{n} \left\langle \phi_{\mathbf{A}}^{\operatorname{eq}} \right| O \left| \phi_{\mathbf{A}}^{\operatorname{eq}} \right\rangle\right)\right\}^{2}\right)$$

$$= \mathbb{E}\left(\left\{2^{n} \left\langle \phi_{\mathbf{A}}^{\operatorname{eq}} \right| \left(O_{0} + \frac{I}{2^{n}} \operatorname{tr}(O)\right) \left| \phi_{\mathbf{A}}^{\operatorname{eq}} \right\rangle - \mathbb{E}\left(2^{n} \left\langle \phi_{\mathbf{A}}^{\operatorname{eq}} \right| \left(O_{0} + \frac{I}{2^{n}} \operatorname{tr}(O)\right) \left| \phi_{\mathbf{A}}^{\operatorname{eq}} \right\rangle\right)\right\}^{2}\right)$$

$$= \mathbb{E}\left(\left\{2^{n} \left\langle \phi_{\mathbf{A}}^{\operatorname{eq}} \right| O_{0} \left| \phi_{\mathbf{A}}^{\operatorname{eq}} \right\rangle - \mathbb{E}\left(2^{n} \left\langle \phi_{\mathbf{A}}^{\operatorname{eq}} \right| O_{0} \left| \phi_{\mathbf{A}}^{\operatorname{eq}} \right\rangle\right)\right\}^{2}\right)$$

$$= \operatorname{Var}(\widehat{O}_{0}^{\operatorname{eq}})$$

$$(23)$$

where the second line is easily derived noting that  $O_0$  is traceless part,  $O - \frac{I}{2^n} \operatorname{tr}(O)$ , hence  $\operatorname{tr}(O_0) = 0$ . Since we can follow the same reasoning to  $\operatorname{Var}(\widehat{O}_{\mathbf{A}}^{\operatorname{eq}})$  and  $\operatorname{Var}(\widehat{O}_{\mathbf{x}}^{\operatorname{bin}})$ , we only need to consider the variance of the  $O_0$ .

Now, we scrutinize the variance.

$$\operatorname{Var}^{(r)\operatorname{eq}}(\widehat{O}_{0\mathbf{A}}^{(r)\operatorname{eq}}) = \mathbb{E}((\widehat{O}_{0\mathbf{A}}^{(r)\operatorname{eq}})^{2}) - \mathbb{E}(\widehat{O}_{0\mathbf{A}}^{(r)\operatorname{eq}})^{2} \leq \mathbb{E}((\widehat{O}_{0\mathbf{A}}^{(r)\operatorname{eq}})^{2}), \tag{24}$$

where  $\mathbb{E}$  is the expected value of  $\widehat{O}_{0\mathbf{A}} \equiv 2^n \langle \phi_{\mathbf{A}}^{(\mathrm{r})\mathrm{eq}} | O_0 | \phi_{\mathbf{A}}^{(\mathrm{r})\mathrm{eq}} \rangle$ . Hence, to obtain the upper bound of the estimation variance of  $\widehat{O}_{0\mathbf{A}}^{(\mathrm{r})\mathrm{eq}}$ , all we need to do is bound  $\mathbb{E}((\widehat{O}_{0\mathbf{A}}^{(\mathrm{r})\mathrm{eq}})^2)$  from above. Let us first rewrite

$$\mathbb{E}((\widehat{O}_{0\mathbf{A}}^{(r)eq})^{2}) = \frac{2^{\gamma}}{\left|\mathcal{S}_{n}^{(r)eq}\right|} \sum_{\left|\phi_{\mathbf{A}}^{(r)eq}\right| \in \mathcal{S}_{n}^{(r)eq}} \left\langle \phi_{\mathbf{A}}^{(r)eq} \right| \rho \left|\phi_{\mathbf{A}}^{(r)eq}\right| \left\langle \phi_{\mathbf{A}}^{(r)eq} \right| O_{0} \left|\phi_{\mathbf{A}}^{(r)eq}\right| \left\langle \phi_{\mathbf{A}}^{(r)eq} \right| O_{0} \left|\phi_{\mathbf{A}}^{(r)eq}\right| \left\langle \phi_{\mathbf{A}}^{(r)eq} \right| \left\langle \phi_{\mathbf{A}}^{(r)$$

Therefore, we need the third moment  $\mathbb{E}_{|\phi_{\mathbf{A}}^{(r)eq}\rangle\in\mathcal{D}\left(\mathcal{S}_{n}^{(r)eq}\right)}|\phi_{\mathbf{A}}^{(r)eq}\rangle\langle\phi_{\mathbf{A}}^{(r)eq}|^{\otimes 3}$ , and for this, let us first define the following two sets:

$$\mathcal{K}_1(\mathbb{Z}_2^n) \equiv \{ \boldsymbol{P} = (\boldsymbol{x}, \boldsymbol{y}, \boldsymbol{z}, \boldsymbol{w}, \boldsymbol{s}, \boldsymbol{t}) | \boldsymbol{x}, \boldsymbol{y}, \boldsymbol{z}, \boldsymbol{w}, \boldsymbol{s}, \boldsymbol{t} \in \mathbb{Z}_2^n, \text{ all } p_i \text{'s are pairwise equal} \}, \tag{26}$$

$$\mathcal{K}_2(\mathbb{Z}_2^n) \equiv \{ \boldsymbol{P} = (\boldsymbol{x}, \boldsymbol{y}, \boldsymbol{z}, \boldsymbol{w}, \boldsymbol{s}, \boldsymbol{t}) | \boldsymbol{P} \in \mathcal{K}_1(\mathbb{Z}_2^n) \text{ and if } \{\boldsymbol{x}, \boldsymbol{y}, \boldsymbol{z}\} \text{ and } \{\boldsymbol{w}, \boldsymbol{s}, \boldsymbol{t}\} \text{ have a same common element,}$$
say  $\boldsymbol{v}$ , and the other 2 variables in  $\{\boldsymbol{x}, \boldsymbol{y}, \boldsymbol{z}\} \setminus \{\boldsymbol{v}\}$  or  $\{\boldsymbol{w}, \boldsymbol{s}, \boldsymbol{t}\} \setminus \{\boldsymbol{v}\}$  are equal, say  $\boldsymbol{v}'$ , remaining 2

variables must be equal to v'. (27)

For example,  $\{(1,0,0,1,0,0),(1,1,0,1,1,0),(1,0,0,1,1,1)\}\subset \mathcal{K}_1(\mathbb{Z}_2)$ , and  $\{(1,0,0,1,0,0),(1,1,0,1,1,0)\}\subset \mathcal{K}_2(\mathbb{Z}_2)$  but  $(1,0,0,1,1,1)\notin \mathcal{K}_2(\mathbb{Z}_2)$ . With these notations, we obtain another lemma [42]:

Lemma 3.

(i) 
$$\mathbb{E}_{|\phi_{\mathbf{A}}^{\text{req}}\rangle\in\mathcal{D}(\mathcal{S}_{n}^{\text{req}})} |\phi_{\mathbf{A}}^{\text{req}}\rangle \langle \phi_{\mathbf{A}}^{\text{req}}|^{\otimes 3} = \frac{1}{8^{n}} \sum_{(\boldsymbol{x},\boldsymbol{y},\boldsymbol{z},\boldsymbol{w},\boldsymbol{s},\boldsymbol{t})\in\mathcal{K}_{1}(\mathbb{Z}_{2}^{n})} |\boldsymbol{x}\boldsymbol{y}\boldsymbol{z}\rangle \langle \boldsymbol{w}\boldsymbol{s}\boldsymbol{t}|.$$
 (28)

(ii) 
$$\mathbb{E}_{|\phi_{\mathbf{A}}^{\mathrm{eq}}\rangle \in \mathcal{D}(\mathcal{S}_{n}^{\mathrm{eq}})} |\phi_{\mathbf{A}}^{\mathrm{eq}}\rangle \langle \phi_{\mathbf{A}}^{\mathrm{eq}}|^{\otimes 3} = \frac{1}{8^{n}} \sum_{(\boldsymbol{x}, \boldsymbol{y}, \boldsymbol{z}, \boldsymbol{w}, \boldsymbol{s}, \boldsymbol{t}) \in \mathcal{K}_{2}(\mathbb{Z}_{2}^{n})} |\boldsymbol{x}\boldsymbol{y}\boldsymbol{z}\rangle \langle \boldsymbol{w}\boldsymbol{s}\boldsymbol{t}|.$$
 (29)

Now, we define five more finite series,

$$C^{(i)} \equiv \sum_{\boldsymbol{x} \in \mathbb{Z}_2^n} |\boldsymbol{x} \boldsymbol{x} \boldsymbol{x}\rangle \langle \boldsymbol{x} \boldsymbol{x} \boldsymbol{x}|, \qquad (30)$$

$$\mathcal{C}^{(\mathrm{ii})} \equiv \sum_{\boldsymbol{x},\boldsymbol{y} \in \mathbb{Z}_2^n} \left( \left| \boldsymbol{y} \boldsymbol{x} \boldsymbol{x} \right\rangle \left\langle \boldsymbol{y} \boldsymbol{x} \boldsymbol{x} \right| + \left| \boldsymbol{x} \boldsymbol{y} \boldsymbol{x} \right\rangle \left\langle \boldsymbol{y} \boldsymbol{x} \boldsymbol{x} \right| + \left| \boldsymbol{x} \boldsymbol{x} \boldsymbol{y} \right\rangle \left\langle \boldsymbol{y} \boldsymbol{x} \boldsymbol{x} \right| + \left| \boldsymbol{y} \boldsymbol{x} \boldsymbol{x} \right\rangle \left\langle \boldsymbol{x} \boldsymbol{y} \boldsymbol{x} \right| + \left| \boldsymbol{x} \boldsymbol{y} \boldsymbol{x} \right\rangle \left\langle \boldsymbol{x} \boldsymbol{y} \boldsymbol{x} \right| + \left| \boldsymbol{x} \boldsymbol{x} \boldsymbol{y} \right\rangle \left\langle \boldsymbol{x} \boldsymbol{y} \boldsymbol{x} \right|$$

$$+\left|yxx\right\rangle\left\langle xxy\right|+\left|xyx\right\rangle\left\langle xxy\right|+\left|xxy\right\rangle\left\langle xxy\right|\right),$$
 (31)

$$\mathcal{C}^{( ext{iii})} \equiv \sum_{oldsymbol{x},oldsymbol{y} \in \mathbb{Z}_2^n} \left( |oldsymbol{y}oldsymbol{x}oldsymbol{y}| + |oldsymbol{x}oldsymbol{y}oldsymbol{y}| + |oldsymbol{x}oldsymbol{y}oldsymbol{y}| + |oldsymbol{y}oldsymbol{y}oldsymbol{y}| + |oldsymbol{y}oldsymbol{y}oldsymbol{y}| + |oldsymbol{y}oldsymbol{y}oldsymbol{y}| + |oldsymbol{y}oldsymbol{y}oldsymbol{y}| + |oldsymbol{y}oldsymbol{y}oldsymbol{y}| + |oldsymbol{y}oldsymbol{y}oldsymbol{y}oldsymbol{y}| + |oldsymbol{y}oldsymbol{y}oldsymbol{y}| + |oldsymbol{y}oldsymbol{y}oldsymbol{y}oldsymbol{y}| + |oldsymbol{y}oldsymbol{y}oldsymbol{y}oldsymbol{y}| + |oldsymbol{y}oldsymbol{y}oldsymbol{y}oldsymbol{y}| + |oldsymbol{y}oldsymbol{y}oldsymbol{y}oldsymbol{y}| + |oldsymbol{y}oldsymbol{y}oldsymbol{y}oldsymbol{y}| + |oldsymbol{y}oldsymbol{y}oldsymbol{y}oldsymbol{y}| + |oldsymbol{y}oldsymbol{y}oldsymbol{y}oldsymbol{y}oldsymbol{y}| + |oldsymbol{y}oldsymbol{y}oldsymbol{y}oldsymbol{y}| + |oldsymbol{y}oldsymbol{y}oldsymbol{y}oldsymbol{y}oldsymbol{y}| + |oldsymbol{y}oldsymbol{y}oldsymbol{y}oldsymbol{y}| + |oldsymbol{y}oldsymbol{y}oldsymbol{y}oldsymbol{y}| + |oldsymbol{y}oldsymbol{y}oldsymbol{y}oldsymbol{y} + |oldsymbol{y}oldsymbol{y}oldsymbol{y}oldsymbol{y} + |oldsymbol{y}oldsymbol{y}oldsymbol{y} + |oldsymbol{y}oldsymbol{y}oldsymbol{y} + |oldsymbol{y}oldsymbol{y}oldsymbol{y} + |oldsymbol{y}oldsymbol{y}oldsymbol{y} + |oldsymbol{y}oldsymbol{y}oldsymbol{y} + |oldsymbol{y}oldsymbol{y}oldsymbol{y} + |oldsymbol{y}oldsymbol{y} + |oldsymbol{y} + |old$$

$$C^{(\text{iv})} \equiv \sum_{\boldsymbol{x}, \boldsymbol{y}, \boldsymbol{z} \in \mathbb{Z}_{2}^{n}} \left( \left| \boldsymbol{x} \boldsymbol{y} \boldsymbol{z} \right\rangle \left\langle \boldsymbol{x} \boldsymbol{y} \boldsymbol{z} \right| + \left| \boldsymbol{x} \boldsymbol{y} \boldsymbol{z} \right\rangle \left\langle \boldsymbol{z} \boldsymbol{x} \boldsymbol{y} \right| + \left| \boldsymbol{x} \boldsymbol{y} \boldsymbol{z} \right\rangle \left\langle \boldsymbol{y} \boldsymbol{z} \boldsymbol{x} \right| + \left| \boldsymbol{x} \boldsymbol{y} \boldsymbol{z} \right\rangle \left\langle \boldsymbol{y} \boldsymbol{x} \boldsymbol{z} \right| + \left| \boldsymbol{x} \boldsymbol{y} \boldsymbol{z} \right\rangle \left\langle \boldsymbol{x} \boldsymbol{z} \boldsymbol{y} \right| + \left| \boldsymbol{x} \boldsymbol{y} \boldsymbol{z} \right\rangle \left\langle \boldsymbol{z} \boldsymbol{y} \boldsymbol{x} \right|,$$

$$(33)$$

$$C^{(v)} \equiv \sum_{x,y,z \in \mathbb{Z}_{2}^{n}} (|xxz\rangle \langle yyz| + |xxz\rangle \langle yzy| + |xxz\rangle \langle zyy| + |xzx\rangle \langle yyz| + |xzx\rangle \langle yyz| + |xzx\rangle \langle yzy| + |xzx\rangle \langle zyy| + |zxx\rangle \langle zyy| + |zxx\rangle \langle zyy|).$$

$$(34)$$

Then, the result for ESPOVMs can be rewritten as

$$\mathbb{E}_{|\phi_{\mathbf{A}}^{\text{eq}}\rangle \in \mathcal{D}(\mathcal{S}_{n}^{\text{eq}})} |\phi_{\mathbf{A}}^{\text{eq}}\rangle \langle \phi_{\mathbf{A}}^{\text{eq}}|^{\otimes 3} = \frac{1}{8^{n}} \sum_{(\boldsymbol{x}, \boldsymbol{y}, \boldsymbol{z}, \boldsymbol{w}, \boldsymbol{s}, \boldsymbol{t}) \in \mathcal{K}_{2}(\mathbb{Z}_{2}^{n})} |\boldsymbol{x}\boldsymbol{y}\boldsymbol{z}\rangle \langle \boldsymbol{w}\boldsymbol{s}\boldsymbol{t}| 
= \frac{1}{8^{n}} \left\{ \mathcal{C}^{i} + (\mathcal{C}^{(\text{ii})} - 9\mathcal{C}^{(\text{i})}) + [\mathcal{C}^{(\text{iv})} - 6\mathcal{C}^{(\text{i})} - 2(\mathcal{C}^{(\text{ii})} - 9\mathcal{C}^{(\text{i})})] \right\} 
= \frac{1}{8^{n}} (4\mathcal{C}^{(\text{i})} - \mathcal{C}^{(\text{ii})} + \mathcal{C}^{(\text{iv})}).$$
(35)

Also, for RESPOVMs,

$$\mathbb{E}_{|\phi_{\mathbf{A}}^{\text{req}}\rangle\in\mathcal{D}(\mathcal{S}_{n}^{\text{req}})}|\phi_{\mathbf{A}}^{\text{req}}\rangle\langle\phi_{\mathbf{A}}^{\text{req}}|^{\otimes 3} = \frac{1}{8^{n}} \sum_{(\boldsymbol{x},\boldsymbol{y},\boldsymbol{z},\boldsymbol{w},\boldsymbol{s},\boldsymbol{t})\in\mathcal{K}_{1}(\mathbb{Z}_{2}^{n})} |\boldsymbol{x}\boldsymbol{y}\boldsymbol{z}\rangle\langle\boldsymbol{w}\boldsymbol{s}\boldsymbol{t}|$$

$$= \frac{1}{8^{n}} \left\{ \mathcal{C}^{(i)} + (\mathcal{C}^{(\text{ii})} - 9\mathcal{C}^{(\text{i})}) + (\mathcal{C}^{(\text{iii})} - 6\mathcal{C}^{(\text{i})}) + [\mathcal{C}^{(\text{iv})} - 6\mathcal{C}^{(\text{i})} - 2(\mathcal{C}^{(\text{ii})} - 9\mathcal{C}^{(\text{i})})] \right\}$$

$$+ [\mathcal{C}^{(\text{v})} - 9\mathcal{C}^{(\text{i})} - 3(\mathcal{C}^{(\text{iii})} - 6\mathcal{C}^{(\text{i})}) - (\mathcal{C}^{(\text{ii})} - 9\mathcal{C}^{(\text{i})})] \right\}$$

$$= \frac{1}{8^{n}} (16\mathcal{C}^{(\text{i})} - 2\mathcal{C}^{(\text{ii})} - 2\mathcal{C}^{(\text{iii})} + \mathcal{C}^{(\text{iv})} + \mathcal{C}^{(\text{v})}). \tag{36}$$

Upon recalling Eq. (25),

$$\mathbb{E}((\widehat{O}_{0\mathbf{A}}^{\text{eq}})^{2}) = 2^{3n} \operatorname{tr}\left(\mathbb{E}_{|\phi_{\mathbf{A}}^{\text{eq}}\rangle \in \mathcal{D}(\mathcal{S}_{n}^{\text{eq}})} |\phi_{\mathbf{A}}^{\text{eq}}\rangle \langle \phi_{\mathbf{A}}^{\text{eq}}|^{\otimes 3} \left(\rho \otimes O_{0} \otimes O_{0}\right)\right). \tag{37}$$

For ESPOVMs, by Eq. (35), we can rewrite this as

$$\mathbb{E}((\widehat{O_0}_{\mathbf{A}}^{\mathrm{eq}})^2) = \mathrm{tr}\left((4\mathcal{C}^{(\mathrm{i})} - \mathcal{C}^{(\mathrm{ii})} + \mathcal{C}^{(\mathrm{iv})})(\rho \otimes O_0 \otimes O_0)\right). \tag{38}$$

Similarly, we can show that from Eqs. (25) and (36),

$$\mathbb{E}((\widehat{O_0}_{\mathbf{A}}^{\mathrm{req}})^2) = \frac{1}{4} \mathrm{tr} \left( (16\mathcal{C}^{(\mathrm{i})} - 2\mathcal{C}^{(\mathrm{iii})} - 2\mathcal{C}^{(\mathrm{iii})} + \mathcal{C}^{(\mathrm{iv})} + \mathcal{C}^{(\mathrm{v})}) (\rho \otimes O_0 \otimes O_0) \right). \tag{39}$$

We are now ready to provide an upper bound for  $\mathbb{E}((\widehat{O_0}_{\mathbf{A}}^{\mathrm{req}})^2)$  by utilizing **Lemma 4.** [42] Given the above definitions, for arbitrary state  $\rho$  and hermitian operator  $O_0$ ,

$$\left| \operatorname{tr} \left( \mathcal{C}^{(i)}(\rho \otimes O_0 \otimes O_0) \right) \right| \le \operatorname{tr} \left( O_0^2 \right) , \tag{40}$$

$$\left| \operatorname{tr} \left( \mathcal{C}^{(ii)}(\rho \otimes O_0 \otimes O_0) \right) \right| \le 7 \operatorname{tr} \left( O_0^2 \right) , \tag{41}$$

$$\left| \operatorname{tr} \left( \mathcal{C}^{(iii)} (\rho \otimes O_0 \otimes O_0) \right) \right| \le 6 \operatorname{tr} \left( O_0^2 \right) , \tag{42}$$

$$\left| \operatorname{tr} \left( \mathcal{C}^{(\mathrm{iv})} (\rho \otimes O_0 \otimes O_0) \right) \right| \le 3 \operatorname{tr} \left( O_0^2 \right) , \tag{43}$$

$$\left| \operatorname{tr} \left( \mathcal{C}^{(v)}(\rho \otimes O_0 \otimes O_0) \right) \right| \le 7 \operatorname{tr} \left( O_0^2 \right) , \tag{44}$$

Therefore,

$$\mathbb{E}((\widehat{O_0}_{\mathbf{A}}^{\text{eq}})^2) \le 4 \left| \operatorname{tr} \left( \mathcal{C}^{(i)}(\rho \otimes O_0 \otimes O_0) \right) \right| + \left| \operatorname{tr} \left( \mathcal{C}^{(ii)}(\rho \otimes O_0 \otimes O_0) \right) \right| + \left| \operatorname{tr} \left( \mathcal{C}^{(iv)}(\rho \otimes O_0 \otimes O_0) \right) \right| \le 14 \operatorname{tr}(O_0^2). \tag{45}$$

Similarly, we can show that  $E_{\rho}((\widehat{O_0}_{\mathbf{A}}^{\text{req}})^2) \leq 13 \text{tr}(O_0^2)$ .

Furthermore, for  $\mathbb{E}((\widehat{O_0}_{\mathbf{A}}^{\mathrm{bin}})^2)$ 

$$\mathbb{E}((\widehat{O_0}_{\mathbf{A}}^{\mathrm{bin}})^2) = \sum_{\boldsymbol{x} \in \mathbb{Z}_2^n} \langle \boldsymbol{x} | \rho | \boldsymbol{x} \rangle \langle \boldsymbol{x} | O_0 | \boldsymbol{x} \rangle \langle \boldsymbol{x} | O_0 | \boldsymbol{x} \rangle \leq \sum_{\boldsymbol{x}, \boldsymbol{y} \in \mathbb{Z}_2^n} \langle \boldsymbol{x} | \rho | \boldsymbol{x} \rangle \langle \boldsymbol{x} | O_0 | \boldsymbol{y} \rangle \langle \boldsymbol{y} | O_0 | \boldsymbol{x} \rangle \leq \operatorname{tr}(O_0^2). \quad (46)$$

With this, and the arguments leading to Eq. (23) and Eq. (7), Thm. 2 (i) is proven. The upper bound of the sampling-copy number, that is  $\mathcal{O}\left(\frac{\operatorname{Var}_{\rho}^{(r)\operatorname{eq}}(\widehat{O}_{0}\mathbf{A},j)}{\varepsilon^2}\log\left(\frac{M}{\delta}\right)\right)$  for M observables, follows from the statistical benefits of using the median-of-means estimation method [61–63].

Suppose that the single observable O of interest is a quantum state  $\sigma$ . Then  $\operatorname{tr}(O_0^2) = \operatorname{tr}\left(\left(\sigma - \frac{I}{2^n}\right)^2\right) = \operatorname{tr}\left(\sigma^2\right) - \frac{\operatorname{tr}(\sigma)}{2^{n-1}} + \frac{1}{2^n} \leq \operatorname{tr}(\sigma^2) \leq 1$ . Hence, any quantum-state observable  $\sigma$  possesses a constant estimation variance and demonstrates shadow-tomographic advantage with (R)ESPOVM, provided that the trace inner-product between  $\sigma$  and equatorial stabilizer state is computable efficiently.

We shall next consider the scenario in which O is a Hamiltonian. Let A, B and C be subsets of  $\mathbb{Z}_2^n \setminus \{\mathbf{0}\}$ , each of  $\operatorname{poly}(n)$  size. We restrict the form of the Hamiltonian to  $O = \sum_{p \in A} J_p Z^p + \sum_{q \in B} J_q' X^q + \sum_{k \in C} J_k'' Y^k$  in terms of the Pauli operators P = X, Y and Z, where  $P^k$  for  $k \in \mathbb{Z}_2^n$  means  $\bigotimes_{i=1}^n P^{k_i}$ , and  $J_p$ ,  $J_q$ , and  $J_k$  are real-valued functions. Such a Heisenberg model is a sufficiently representative model for explaining popular strongly-correlated systems in statistical mechanics [34, 35]. First, observe that the expectation value of the first term,  $\sum_{p \in A} J_p Z^p$ , can be rewritten as

$$\operatorname{tr}\left(\rho \sum_{\boldsymbol{p} \in A} J_{\boldsymbol{p}} Z^{\boldsymbol{p}}\right) = \sum_{\substack{\boldsymbol{p} \in A \\ x, y \in \mathbb{Z}_{2}^{n}}} J_{\boldsymbol{p}} \langle \boldsymbol{x} | \rho | \boldsymbol{y} \rangle \langle \boldsymbol{y} | Z^{\boldsymbol{p}} | \boldsymbol{x} \rangle = \sum_{\substack{\boldsymbol{p} \in A \\ x, y \in \mathbb{Z}_{2}^{n}}} J_{\boldsymbol{p}} \langle \boldsymbol{x} | \rho | \boldsymbol{y} \rangle (-1)^{\boldsymbol{p} \cdot \boldsymbol{x}} \delta_{\boldsymbol{x}, \boldsymbol{y}}$$

$$= \sum_{\substack{\boldsymbol{p} \in A \\ x \in \mathbb{Z}_{2}^{n}}} \langle \boldsymbol{x} | \rho | \boldsymbol{x} \rangle (-1)^{\boldsymbol{p} \cdot \boldsymbol{x}} J_{\boldsymbol{p}}. \tag{47}$$

From the above result, the corresponding estimation algorithm is straightforward. We first measure the input  $\rho$  with the Z basis, obtain the binary outcome  $x \in \mathbb{Z}_2^n$ , and then take the estimator to be  $\sum_{p \in A} (-1)^{p \cdot x} J_p$ . Since A has  $\operatorname{poly}(n)$  size, we can calculate this efficiently. Moreover, we easily note that the estimation variance of this estimator is bounded by  $\operatorname{poly}(n)$ , hence by the Hoeffding inequality, it only takes  $N = \mathcal{O}(\operatorname{poly}(n)/\varepsilon^2)$  sampling copies within  $\varepsilon$  additive precision. The other terms,  $\sum_{q \in B} J'_q X^q$  and  $\sum_{k \in C} J''_k Y^k$ , can be estimated in a similar manner but with an additional rotation of the input with  $H^{\otimes n}$  or  $S^{\dagger \otimes n}$  gates before the binary measurement. Even when the Hamiltonian has a general form,  $O = \sum_{P \in \mathcal{P}} \alpha(P)P$ , where  $\mathcal{P}$  is a poly-sized subset of the n-qubit Pauli group and  $\alpha$  is a real-valued function, we can assert that similar scale of the sampling-copy number is needed, by rotating via single qubit gates for each Pauli term. With this, we may now conclude that our tomography methods serve as efficient hybrid-circuit platforms for both state verification and Heisenberg-type Hamiltonian estimation, in the sense that one may flexibly turn the (R)ESPOVM section on or off and employ suitable single-qubit Clifford gates before the binary-measurement section depending on the observable types measured. Therefore, this opens an avenue for more applications of our scheme in variational quantum algorithms (VQA) [64, 65].

#### 4.3 Gate, depth, and time complexity for circuit implementation

We now discuss the architectural requirements of (R)ESPOVM shadow tomography, which cover the main ideas of the proof for Thm. 3. In particular, this discussion also considers the implementation of an (LNN) architecture for (R)ESPOVM tomography and compares its circuit-depth and time-complexity resources with those of randomized-Clifford shadow tomography.

The typical methods for fidelity estimation (with pure target states) are Flammia's direct fidelity-estimation scheme [26] and randomized-Clifford shadow tomography [9]. While Flammia's method has the lower gate count and circuit depth than our schemes, its estimable region of observables is much more restricted than both the randomized-Clifford and our (R)ESPOVM schemes. As such, only the latter two schemes shall be of interest here.

The randomized-Clifford scheme uses only one input state for one sampling copy. Before analyzing the time complexity, we briefly explain how the scheme may be used to estimate  $\widehat{\langle O \rangle} = \operatorname{tr}(\rho \, O)$  (see Ref. [9] for details).

- 1. Take  $\rho$  as an input and uniformly choose a Clifford unitary U from  $\mathrm{Cl}_n$ .
- 2. Take  $\rho \leftarrow U \rho U^{\dagger}$ .
- 3. Measure in the Z basis and obtain the outcome  $p \in \mathbb{Z}_2^n$ .
- 4. Compute  $\widehat{O} = (2^n + 1) \langle \boldsymbol{p} | O | \boldsymbol{p} \rangle \operatorname{tr}(O)$ .
- 5. Repeat all previous steps and take the average of N  $\widehat{O}$ 's to obtain the estimator  $\widehat{\langle O \rangle}$  for  $\langle O \rangle$ .

For an arbitrary observable O, the randomized-Clifford shadow tomography estimation variance  $\operatorname{Var}_{\rho}^{\operatorname{randCl}}(\widehat{O})$  is bounded from above by  $\operatorname{3tr}(O^2)$  [9]. Therefore, this scheme is efficient for state verification of arbitrary target states, albeit with the assumption that every  $\widehat{O}$  is efficiently computable.

Reference [19] showed that we can efficiently sample a Clifford unitary U from  $Cl_n$  in  $\mathcal{O}(n^2)$ -time. In addition, the sampled form contains the HF'—SW—H—HF sections (where small uppercase letters here refer to gate layers as opposed to regular uppercase ones that denote gate labels, and HF and HF' are Hadamard-free sections) where HF-section is CNOT<sup>↓</sup>—CZ—S—PAULI layered circuit. Here, H, SW, CNOT<sup>↓</sup>, CZ and S respectively refer to pure layers of Hadamard gates, SWAP gates, CNOT gates with control qubits higher than the target ones when visualized in a standard circuit diagram, CZ gates and S gates, where SW naturally contains CNOT. We note that the HF'—SW sections are not needed for randomized-Clifford shadow tomography. The reason is that the measurement outcome of a uniform-Clifford measurement can be obtained from the following procedure: One first uniformly samples a Clifford unitary operator and takes its inverse, which possesses the form HF<sup>-1</sup>—H—sw<sup>-1</sup>—HF'<sup>-1</sup>. Then one just measures in the Z basis after the  $\mathrm{HF}^{-1}$ —H sections and linearly transform this intermediate bitstring outcome with the subsequent CNOT and Pauli transformations in sw<sup>-1</sup>—HF'<sup>-1</sup> to arrive at the final bitstring outcome. In  $\mathcal{O}(n^3)$ -time, one can optimize the maximal depth of HF<sup>-1</sup>—H sections with longrange gates to  $n + \mathcal{O}(\log(n))$  if  $n \geq 70$  [37]. Even though the corresponding asymptotic upper bound of depth is  $\mathcal{O}(\frac{n}{\log(n)})$  [66, 67], it has a large constant factor [37] and hence will not improve the former limit for circuits holding hundreds of qubits. If only NN gates are available, we can express the CNOT gate layers inside the HF-section in terms of a northwestern matrix [68] and SWAP gates. Here, we do not need to implement the swapping operations, since one can simply propagate all swapping operations out of the circuit. The CNOT circuit of a northwestern-matrix form after the CZ circuits can be further

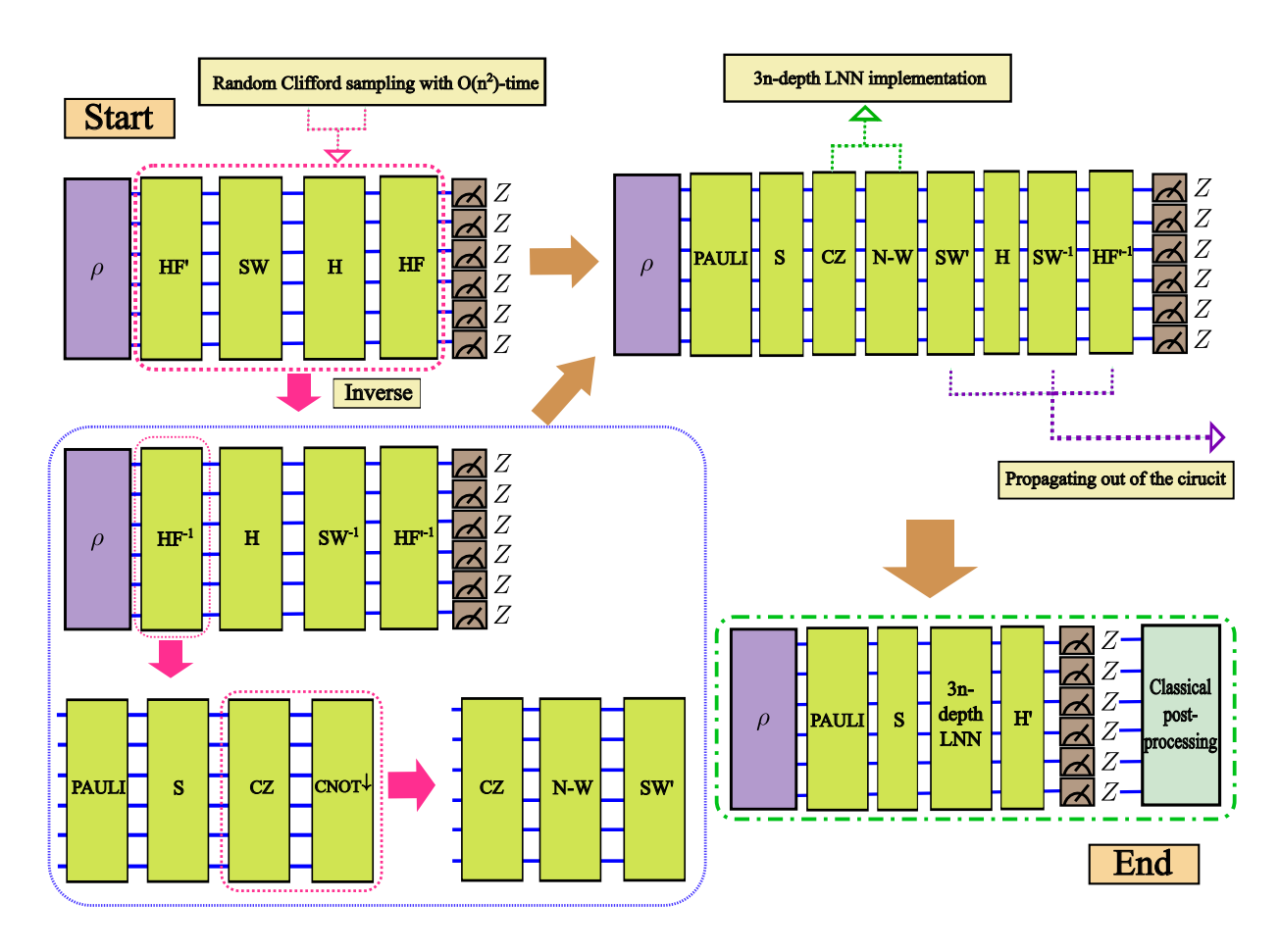


Figure 6 The schematic diagram of uniform sampling of a 3n-depth Clifford-circuit measurement in the LNN-architecture. Here, the N-W section is a CNOT circuit expressing the  $n \times n$  north-western matrix [18] for the binary strings. The final classical post-processing step multiplies an  $n \times n$  binary matrix to the measured outcome bit string, which takes  $\mathcal{O}(n^2)$ -time.

decomposed into 3n-depth NN CNOT circuits and phase-gate insertion layers [18, 68] in  $\mathcal{O}(n^3)$ -time. A schematic illustration is presented in Fig. 6.

Having discussed uniform Clifford sampling, starting from random CZ-gate implementation, we shall now discuss how one can further contract the gate count for (R)ESPOVM shadow tomography. For this purpose, we make use of the Patel-Markov-Hayes (PMH) construction [52]. First, we transform Y measurements as X-basis measurements after phase gates and drag all S,  $S^{\dagger}$  and Z gates to the left of all the CZ gates ,i.e very first of the circuit. This is possible because these gates commute with CZ gates. Next, we may decompose the CZ circuit into CNOT—CZ—CNOT [42], where CZ contains only  $\mathcal{O}(n)$  CZ gates. After which, we implement the left CNOT section with  $\mathcal{O}(\frac{n^2}{\log(n)})$  CNOT gates [29, 52]. The right CNOT section can be ignored because we now only measure in the X basis, and so this amounts to only a linear transformation of the measurement outcome. If we return to the randomized-Clifford scheme discussed previously, one may also reduce the gate count if some CNOT gates are simplified to just linear transformations of the measured outcome. For instance, a CNOT gate placed before two X basis measurements can be simplified to just a linear transformation of the measured outcome. In Fig 1(b), we applied each of these two reductions to (R)ESPOVM and random-Clifford respectively, and saw that there is still gate count improvement with (R)ESPOVM.

As we saw in Thm. 1, there is an alternative depth reduction technique for CZ circuits. (R)ESPOVM shadow tomography can be implemented with at most n-depth long-ranged CZ gates (or with CNOT and H gates). This maximal depth can be reduced to  $\frac{n}{2} + \mathcal{O}(\log(n))$  given that  $n \geq 39$  according to Ref. [37], which is half the gate complexity in contrast to randomized-Clifford implementation. Furthermore, with only neighboring CNOT gates and S gates, we can implement (R)ESPOVM with 2n-depth LNN architecture in  $\mathcal{O}(n^2)$ -time. To show this time-complexity bound, we may use the strategy employed in Ref. [38]. We first construct a 2n-depth circuit consisting of NN CNOT gates in advance following the designated rules dictated by Thm. 6 in [38]. With this, the main task for the time-complexity-bound proof is as follows: Given a CZ circuit that performs the map  $|\mathbf{x}\rangle \mapsto (-1)^{Q(\mathbf{x})} |\mathbf{x}\rangle$ , where  $\mathbf{x} \in \mathbb{Z}_2^n$  and Q is a quadratic

binary-valued polynomial, find the values  $u_j, u_{j,k}$  in  $\mathbb{Z}_4$   $(j \in [n], k \in \{j+1, j+2, \ldots, n\})$  such that

$$(-1)^{Q(\mathbf{x})} = i^{\sum_{j=1}^{n} u_j y_j + \sum_{j=1}^{n} \sum_{k=j+1}^{n} u_{j,k} (y_j \oplus y_k)}.$$
 (48)

Here,  $\oplus$  and + respectively refer to modulo-2 and modulo-4 additions. The  $y_i$ 's  $(i \in [n])$  are defined by,

$$y_i = x_1 \oplus x_2 \oplus x_3 \oplus \dots \oplus x_i. \tag{49}$$

After inserting the phase gates  $S^{u_{j,k}}$  and  $S^{u_l}$  following the manual in Ref. [38], we finally realize the LNN architecture of CZ circuit. To analyze the time-complexity, we rewrite (49) as

$$\begin{cases} x_1 = y_1 \\ x_i = y_i \oplus y_{i-1} \ (i \in \{2, 3, \dots, n\}). \end{cases}$$
 (50)

Now, consider one off-diagonal component of  $(-1)^{Q(x)}$ . We have simple identity  $(-1)^{x_{\mu}x_{\nu}} = i^{3x_{\mu}+3x_{\nu}+(x_{\mu}\oplus x_{\nu})}$ . Then by Eq. (50),

$$(-1)^{x_{\mu}x_{\nu}} = i^{3(y_{\mu} \oplus y_{\mu-1}) + 3(y_{\nu} \oplus y_{\nu-1}) + (y_{\mu} \oplus y_{\mu-1} \oplus y_{\nu} \oplus y_{\nu-1})}, \quad y_0 \equiv 0.$$
 (51)

Using the equality  $\mathbf{i}^{a\oplus b\oplus c}=\mathbf{i}^{3a+3b+3c+3(a\oplus b)+3(a\oplus c)+3(b\oplus c)}$   $(a,b,c\in\mathbb{Z}_2)$  and setting  $a=y_\mu,b=y_{\mu-1},c=y_\nu\oplus y_{\nu-1}$ , we can express  $\mathbf{i}^{y_\mu\oplus y_{\mu-1}\oplus y_\nu\oplus y_{\nu-1}}$  as a product of  $\mathbf{i}^{y_\mu},\mathbf{i}^{y_{\mu-1}},\mathbf{i}^{y_\nu\oplus y_{\nu-1}}$  and  $\mathbf{i}^{y_\mu\oplus y_\nu\oplus y_{\nu-1}},\mathbf{i}^{y_\mu\oplus y_\nu\oplus y_{\nu-1}},\mathbf{i}^{y_{\mu-1}\oplus y_\nu\oplus y_{\nu-1}}$ . Again, in a similar manner, we can decompose  $\mathbf{i}^{y_\mu\oplus y_\nu\oplus y_{\nu-1}}$  and  $\mathbf{i}^{y_{\mu-1}\oplus y_\nu\oplus y_{\nu-1}}$  into a product of powers of  $\mathbf{i}$ , each with an exponent not exceeding 3 variables. In conclusion, there exist *constant-sized* sets  $A,B\subset[n]$  such that

$$(-1)^{x_{\mu}x_{\nu}} = i^{\sum_{a \in A} u'_a y_a + \sum_{a,b \in B} u'_{a,b} (y_a \oplus y_b)}, \tag{52}$$

where  $u'_{\mu}, u'_{\mu,\nu} \in \mathbb{Z}_4$ . Therefore, upon noting that a CZ circuit has at most  $\frac{n^2-n}{2}$  CZ gates, we have the following scheme for implementing any (long-ranged) CZ circuit in an LNN architecture:

- 1. Prepare a 2n-depth NN CNOT circuit based on the prescriptions in Ref. [38].
- 2. For each unitary  $CZ_{j,k}$  acting on the j-th and k-th qubits, find the sets  $A_{j,k}$  and  $B_{j,k}$  such that  $(-1)^{x_a x_b} = i^{\sum_{a \in A_{j,k}} u'_a y_a + \sum_{a,b \in B_{j,k}} u'_{a,b} (y_a \oplus y_b)}$ . Record all  $u'_a$  and  $u'_{a,b}$  corresponding to  $A_{j,k}$  and  $B_{j,k}$ .
- 3. Insert the phase gates  $S^{u'_a}(a \in A_{j,k})$  and  $S^{u'_{a,b}}(a,b \in B_{j,k})$  according to the insertion rules in Ref. [38].
- 4. Repeat steps 2 and 3 for all  $j, k \in [n]$ . If there is already some phase gate acting on the location, we multiply the existing one and the gate we put this time.

The Reader may consult [42] for the precise NN CNOT-circuit prescription and phase-gate insertion rule. For each  $j, k \in [n]$ , we note that steps 2 to 4 each takes constant time to execute. Since there is a total of  $\mathcal{O}(n^2)$  steps to be repeated, the total time-complexity is  $\mathcal{O}(n^2)$ .

#### 4.4 Average gate fidelity

Suppose a circuit described by a unitary operator U is subjected to noise. The resulting operation is a noisy quantum channel  $\mathcal{U}$ . One can then measure the averaged quality of this noisy channel with respect to U over a uniform distribution of pure states, namely with the average gate fidelity defined as [57]

$$F_{avg}(\mathcal{U}) \equiv \int (d\phi) \langle \phi | U^{\dagger} \mathcal{U}(|\phi\rangle \langle \phi|) U | \phi \rangle.$$
 (53)

Here, the integration element  $(d\phi)$  is the Haar measure. This function can be generalized to a circuit unitary ensemble G where each circuit with operation U has the probability measure (dU) to be sampled,

$$F_{avg}(G) \equiv \int_{U \in G} (dU) F_{avg}(\mathcal{U}) = \int (d\phi) \int_{U \in G} (dU) \langle \phi | U^{\dagger} \mathcal{U}(|\phi\rangle \langle \phi|) U | \phi \rangle.$$
 (54)

Terminology-wise, we shall also call this the average gate fidelity of G. If noise is absent, then  $F_{avg}(G) = 1$ , as it should.

In Fig. 5 we endow each gate with depolarization noise. This is equivalent to enacting a Pauli operation that is uniformly chosen from the single-qubit (or two-qubit resp.) Pauli group to each single-qubit (twoqubit) gate of a given error rate. Therefore, we can estimate the average gate fidelity  $F_{avg}(G)$  with the depolarization error rates  $(\eta_1, \eta_2)$  according to the following Monte Carlo procedure for an n-qubit system:

- 1. Set the sufficiently large  $M, N \in \mathbb{N}$ . The M is the number of the Haar random input pure states and N is that of randomly chosen circuit samples for each state input.
- 2. Choose a quantum state  $|\phi\rangle$  according to the Haar measure: generate a  $2^n$ -dimensional complex column with all entries i.i.d. standard Gaussian distribution and normalize it by its norm.
- 3. Randomly choose  $U \in G$  according to the distribution measure dU (in Fig. 5, we take dU to be uniform and discrete).
- 4. For each single-qubit (two-qubit resp.) gate in U, we toss a coin with the biased rate  $(1 \eta_1, \eta_1)$  $[(1-\eta_2,\eta_2)]$ . If a "tail" is obtained, one uniformly chooses a Pauli operator from the single-qubit (twoqubit) Pauli group and enact it after the gate. Doing this for all gates in U, one gets the new circuit
- 5. Calculate  $f_{U,\phi} \equiv \langle \phi | U^{\dagger}U' | \phi \rangle \langle \phi | U'^{\dagger}U | \phi \rangle = \left| \langle \phi | U^{\dagger}U' | \phi \rangle \right|^2$  (this step is efficient for small n). 6. Repeat steps 3 to 5 with the same input state  $|\phi\rangle$  to obtain N such  $f_{U_1,\phi}, f_{U_2,\phi}, \ldots, f_{U_N,\phi}$ . Define
- $g_{\phi,N} = \frac{1}{N} \sum_{j=1}^{N} f_{U_j,\phi}.$ 7. Repeat step 6 with M Haar-distributed input pure states  $|\phi_1\rangle, \ldots, |\phi_M\rangle$  and obtain  $g_{\phi_1,N}, \ldots, g_{\phi_M,N}.$ Then  $\frac{1}{M} \sum_{j=1}^{M} g_{\phi_j,N} \to F_{avg}(G)$  in the limit of large M and N.

# 4.5 Survey of recent CZ-gate implementation schemes

We shall list all recent fidelity values sorted according to some of these platforms. In photonic quantum computing, a fidelity of over 81% has been reported on silicon-nitride photonic chips [69], and over 99% when Zeeman coupling with quantum dots and nitrogen-vacancy centers is exploited in simulations [70]. Spin-based quantum computation allows for more than 99.5% fidelity [55, 71]. On Rydberg-interacting platforms, Ref. [72], [73] and later [54] respectively reported gate fidelities of 89%, 97% and 99.5% using atomic-qubit-array entanglement. Using adiabatic pulses, simulations revealed fidelity values greater than 99.9% [74]. On superconducting platforms, adiabaticity-shortcut techniques allows for over 96% fidelity [75], 97.6% with fluxonium qubits [76] and 99.1% through interfering superconducting qubits with weak anharmonicity [77]. Nonadiabatic CZ gates were also realized with 99.54% fidelity [78]. Furthermore, gmon qubits employed by Google AI Quantum demonstrated gate fidelities as high as 99.81% [79]. The more recent fidelity of 99.93% is possible with intermediate leakage control [56].

# Acknowledgements

This work was supported by the National Research Foundation of Korea (NRF) grants funded by the Korean government (Grant Nos. NRF-2023R1A2C1006115, NRF-2022M3K4A1097117, NRF2022M3E4A1076099 and RS-2023-00237959) via the Institute of Applied Physics at Seoul National University, the Institute of Information & Communications Technology Planning & Evaluation (IITP) grant funded by the Korea government (MSIT) (IITP-2021-0-01059 and IITP-2023-2020-0-01606), and the Brain Korea 21 FOUR Project grant funded by the Korean Ministry of Education.

# 6 Data Availability

Source data that support the plots within this paper and other findings of this study are available from the corresponding author upon reasonable request.

#### References

- [1] Shor, P.W.: Polynomial-Time Algorithms for Prime Factorization and Discrete Logarithms on a Quantum Computer. SIAM J. Comput **26**(5), 1484–1509 (1997) https://doi.org/10.1137/  $\pm 0097539795293172$
- [2] Deutsch, D., Jozsa, R.: Rapid solution of problems by quantum computation. Proc. R. Soc. Lond. A: Math. Phys. Sci. 439(1907), 553–558 (1992) https://doi.org/10.1098/rspa.1992.0167

- [3] D'Ariano, G.M., De Laurentis, M., Paris, M.G., Porzio, A., Solimeno, S.: Quantum tomography as a tool for the characterization of optical devices. J. opt., B Quantum semiclass. opt. 4(3), 127 (2002) https://doi.org/10.1088/1464-4266/4/3/366
- [4] Paris, M.G.A., Řeháček, J. (eds.): Quantum State Estimation. Lect. Not. Phys., vol. 649. Springer, Berlin (2004). https://www.biblio.com/book/quantum-state-estimation-lecture-notes-physics/d/ 1533004714
- [5] Teo, Y.S.: Introduction to Quantum-State Estimation. World Scientific Publishing Co., Singapore (2015). https://www.worldscientific.com/worldscibooks/10.1142/9617#t=aboutBook
- [6] O'Donnell, R., Wright, J.: Efficient quantum tomography. In: Proc. Annu. ACM Symp. Theory Comput., pp. 899–912 (2016). https://doi.org/10.1145/2897518.2897544
- [7] Nielsen, E., Gamble, J.K., Rudinger, K., Scholten, T., Young, K., Blume-Kohout, R.: Gate set tomography. Quantum 5, 557 (2021) https://doi.org/10.22331/q-2021-10-05-557
- [8] Aaronson, S.: Shadow tomography of quantum states. In: Proc. Annu. ACM Symp. Theory Comput., pp. 325–338 (2018). https://doi.org/10.1145/3188745.3188802
- [9] Huang, H.-Y., Kueng, R., Preskill, J.: Predicting many properties of a quantum system from very few measurements. Nat. Phys **16**(10), 1050–1057 (2020) https://doi.org/10.1038/s41567-020-0932-7
- [10] Acharya, A., Saha, S., Sengupta, A.M.: Shadow tomography based on informationally complete positive operator-valued measure. Phys. Rev. A 104(5), 052418 (2021) https://doi.org/10.1103/PhysRevA.104.052418
- [11] Huang, H.-Y., Chen, S., Preskill, J.: Learning to predict arbitrary quantum processes. arXiv:2210.14894 (2023) https://doi.org/10.48550/arXiv.2210.14894
- [12] Leone, L., Oliviero, S.F., Hamma, A.: Stabilizer Rényi entropy. Phys. Rev. Lett. **128**(5), 050402 (2022) https://doi.org/10.1103/PhysRevLett.128.050402
- [13] Oliviero, S.F., Leone, L., Hamma, A., Lloyd, S.: Measuring magic on a quantum processor. npj Quantum Inf. 8(1), 148 (2022) https://doi.org/10.1038/s41534-022-00666-5
- [14] Webb, Z.: The Clifford group forms a unitary 3-design. Quantum Inf. Comput. **16**(15&16), 1379–1400 (2016) https://doi.org/10.26421/QIC16.15-16-8
- [15] Zhu, H.: Multiqubit Clifford groups are unitary 3-designs. Phys. Rev. A  $\bf 96$ , 062336 (2017) https://doi.org/10.1103/PhysRevA.96.062336
- [16] Kueng, R., Gross, D.: Qubit stabilizer states are complex projective 3-designs. arXiv:1510.02767 (2015). https://doi.org/10.48550/ARXIV.1510.02767
- [17] Puchała, Z., Miszczak, J.A.: Symbolic integration with respect to the Haar measure on the unitary groups. B POL ACAD SCI-TECH **65**(1), 21–27 (2017) https://doi.org/10.1515/bpasts-2017-0003
- [18] Maslov, D., Yang, W.: CNOT circuits need little help to implement arbitrary Hadamard-free Clifford transformations they generate. npj Quantum Inf. **9**(1), 96 (2023) https://doi.org/10.1038/s41534-023-00760-2
- [19] Bravyi, S., Maslov, D.: Hadamard-Free Circuits Expose the Structure of the Clifford Group. IEEE Trans. Inf. Theory 67(7), 4546–4563 (2021) https://doi.org/10.1109/TIT.2021.3081415
- [20] Brandão, F.G.S.L., Harrow, A.W., Horodecki, M.: Local Random Quantum Circuits are Approximate Polynomial-Designs. Commun. Math. Phys. **346**(2), 397–434 (2016) https://doi.org/10.1007/s00220-016-2706-8
- [21] Bertoni, C., Haferkamp, J., Hinsche, M., Ioannou, M., Eisert, J., Pashayan, H.: Shallow shadows: Expectation estimation using low-depth random Clifford circuits. arXiv:2209:12924 (2022). https://doi.org/10.48550/ARXIV.2209.12924

- [22] Grier, D., Pashayan, H., Schaeffer, L.: Sample-optimal classical shadows for pure states. arXiv:2211.11810 (2022). https://doi.org/10.48550/ARXIV.2211.11810
- [23] Nguyen, H.C., Bönsel, J.L., Steinberg, J., Gühne, O.: Optimizing Shadow Tomography with Generalized Measurements. Phys. Rev. Lett. **129**, 220502 (2022) https://doi.org/10.1103/PhysRevLett. 129.220502
- [24] Garion, S., Kanazawa, N., Landa, H., McKay, D.C., Sheldon, S., Cross, A.W., Wood, C.J.: Experimental implementation of non-Clifford interleaved randomized benchmarking with a controlled-S gate. Phys. Rev. Res. 3, 013204 (2021) https://doi.org/10.1103/PhysRevResearch.3.013204
- [25] Wang, X., Zhan, X., Li, Y., Xiao, L., Zhu, G., Qu, D., Lin, Q., Yu, Y., Xue, P.: Generalized Quantum Measurements on a Higher-Dimensional System via Quantum Walks. Phys. Rev. Lett. 131, 150803 (2023) https://doi.org/10.1103/PhysRevLett.131.150803
- [26] Flammia, S.T., Liu, Y.-K.: Direct Fidelity Estimation from Few Pauli Measurements. Phys. Rev. Lett. 106, 230501 (2011) https://doi.org/10.1103/PhysRevLett.106.230501
- [27] Silva, M.P., Landon-Cardinal, O., Poulin, D.: Practical Characterization of Quantum Devices without Tomography. Phys. Rev. Lett. 107, 210404 (2011) https://doi.org/10.1103/PhysRevLett.107.210404
- [28] Zhang, Q., Liu, Q., Zhou, Y.: Minimal Clifford Shadow Estimation by Mutually Unbiased Bases. arXiv:2310.18749 (2023) https://doi.org/10.48550/arXiv.2310.18749
- [29] Aaronson, S., Gottesman, D.: Improved simulation of stabilizer circuits. Phys. Rev. A **70**, 052328 (2004) https://doi.org/10.1103/PhysRevA.70.052328
- [30] Bravyi, S., Gosset, D.: Improved classical simulation of quantum circuits dominated by Clifford gates. Phys. Rev. Lett. **116**(25), 250501 (2016) https://doi.org/10.1103/PhysRevLett.116.250501
- [31] Bravyi, S., Browne, D., Calpin, P., Campbell, E., Gosset, D., Howard, M.: Simulation of quantum circuits by low-rank stabilizer decompositions. Quantum 3, 181 (2019) https://doi.org/10.22331/q-2019-09-02-181
- [32] Dangniam, N., Han, Y.-G., Zhu, H.: Optimal verification of stabilizer states. Phys. Rev. Res. 2, 043323 (2020) https://doi.org/10.1103/PhysRevResearch.2.043323
- [33] Zhu, H., Hayashi, M.: Efficient Verification of Hypergraph States. Phys. Rev. Appl. 12, 054047 (2019) https://doi.org/10.1103/PhysRevApplied.12.054047
- [34] Takahashi, M., Suzuki, M.: One-dimensional anisotropic Heisenberg model at finite temperatures. Prog. Theor. Phys 48(6), 2187–2209 (1972) https://doi.org/10.1143/PTP.48.2187
- [35] Bertini, B., Heidrich-Meisner, F., Karrasch, C., Prosen, T., Steinigeweg, R., č, M.: Finite-temperature transport in one-dimensional quantum lattice models. Rev. Mod. Phys. **93**, 025003 (2021) https://doi.org/10.1103/RevModPhys.93.025003
- [36] DURT, T., ENGLERT, B.-G., BENGTSSON, I., ZYCZKOWSKI, K.: On mutually unbiased bases. International Journal of Quantum Information 08(04), 535–640 (2010) https://doi.org/10.1142/ S0219749910006502
- [37] Maslov, D., Zindorf, B.: Depth Optimization of CZ, CNOT, and Clifford Circuits. IEEE Trans. Quantum Eng. 3, 1–8 (2022) https://doi.org/10.1109/TQE.2022.3180900
- [38] Maslov, D., Roetteler, M.: Shorter stabilizer circuits via Bruhat decomposition and quantum circuit transformations. IEEE Transactions on Information Theory **64**(7), 4729–4738 (2018) https://doi.org/10.1109/TIT.2018.2825602
- [39] Greenberger, D.M., Horne, M.A., Zeilinger, A.: Going Beyond Bell's Theorem. arXiv:0712.0921 (2007) https://doi.org/10.48550/arXiv.0712.0921
- [40] Dür, W., Vidal, G., Cirac, J.I.: Three qubits can be entangled in two inequivalent ways. Phys. Rev.

- A 62, 062314 (2000) https://doi.org/10.1103/PhysRevA.62.062314
- [41] Gottesman, D.: The Heisenberg Representation of Quantum Computers. arXiv:quant-ph/9807006 (1998) https://doi.org/10.48550/arXiv.quant-ph/9807006
- [42] See Supplementary Information for additional detailed explanations and proofs of this paper.
- [43] Scott, A.J.: Tight informationally complete quantum measurements. J. Phys. A Math. Theor. **39**(43), 13507 (2006) https://doi.org/10.1088/0305-4470/39/43/009
- [44] Zhu, H., Kueng, R., Grassl, M., Gross, D.: The Clifford group fails gracefully to be a unitary 4-design. arXiv:1609.08172 (2016) https://doi.org/10.48550/arXiv.1609.08172
- [45] Briegel, H.J., Raussendorf, R.: Persistent Entanglement in Arrays of Interacting Particles. Phys. Rev. Lett. 86, 910–913 (2001) https://doi.org/10.1103/PhysRevLett.86.910
- [46] Anders, S., Briegel, H.J.: Fast simulation of stabilizer circuits using a graph-state representation. Phys. Rev. A 73, 022334 (2006) https://doi.org/10.1103/PhysRevA.73.022334
- [47] Bärtschi, A., Eidenbenz, S.: Deterministic Preparation of Dicke States, pp. 126–139. Springer, Denmark (2019). https://doi.org/10.1007/978-3-030-25027-0\_9
- [48] Berge, C., Fournier, J.C.: A short proof for a generalization of Vizing's theorem. J. Graph Theory 15(3), 333–336 (1991) https://doi.org/10.1002/jgt.3190150309
- [49] Misra, J., Gries, D.: A constructive proof of Vizing's theorem. Inf. Process. Lett **41**(3), 131–133 (1992) https://doi.org/10.1016/0020-0190(92)90041-S
- [50] Maslov, D., Roetteler, M.: Shorter Stabilizer Circuits via Bruhat Decomposition and Quantum Circuit Transformations. IEEE Trans. Inf. Theory 64(7), 4729–4738 (2018) https://doi.org/10.1109/TIT.2018.2825602
- [51] Bravyi, S., Latone, J.A., Maslov, D.: 6-qubit optimal Clifford circuits. npj Quantum. Inf. 8(1), 79 (2022) https://doi.org/10.1038/s41534-022-00583-7
- [52] Patel, K.N., Markov, I.L., Hayes, J.P.: Optimal synthesis of linear reversible circuits. arXiv:quant-ph/0302002 (2008) https://doi.org/10.48550/arXiv.quant-ph/0302002
- [53] Cleve, R., Leung, D., Liu, L., Wang, C.: Near-linear constructions of exact unitary 2-designs. arXiv:1501.04592 (2016) https://doi.org/10.48550/arXiv.1501.04592
- [54] Evered, S.J., Bluvstein, D., Kalinowski, M., Ebadi, S., Manovitz, T., Zhou, H., Li, S.H., Geim, A.A., Wang, T.T., Maskara, N., Levine, H., Semeghini, G., Greiner, M., Vuletić, V., Lukin, M.D.: High-fidelity parallel entangling gates on a neutral-atom quantum computer. Nature 622(7982), 268–272 (2023) https://doi.org/10.1038/s41586-023-06481-y
- [55] Xue, X., Russ, M., Samkharadze, N., Undseth, B., Sammak, A., Scappucci, G., Vandersypen, L.M.K.: Quantum logic with spin qubits crossing the surface code threshold. Nature **601**(7893), 343–347 (2022) https://doi.org/10.1038/s41586-021-04273-w
- [56] Negîrneac, V., Ali, H., Muthusubramanian, N., Battistel, F., Sagastizabal, R., Moreira, M.S., Marques, J.F., Vlothuizen, W.J., Beekman, M., Zachariadis, C., Haider, N., Bruno, A., DiCarlo, L.: High-fidelity controlled-z gate with maximal intermediate leakage operating at the speed limit in a superconducting quantum processor. Phys. Rev. Lett. 126, 220502 (2021) https://doi.org/10.1103/PhysRevLett.126.220502
- [57] Leone, L., Oliviero, S.F.E., Hamma, A.: Nonstabilizerness determining the hardness of direct fidelity estimation. Phys. Rev. A **107**, 022429 (2023) https://doi.org/10.1103/PhysRevA.107.022429
- [58] Tsubouchi, K., Sagawa, T., Yoshioka, N.: Universal cost bound of quantum error mitigation based on quantum estimation theory. arXiv:2208.09385 (2023) https://doi.org/10.48550/arXiv.2208.09385

- [59] Shi, S., Xu, B., Zhang, K., Ye, G.-S., Xiang, D.-S., Liu, Y., Wang, J., Su, D., Li, L.: High-fidelity photonic quantum logic gate based on near-optimal Rydberg single-photon source. Nat. Commun. 13(1), 4454 (2022) https://doi.org/10.1038/s41467-022-32083-9
- [60] Xie, T., Zhao, Z., Xu, S., Kong, X., Yang, Z., Wang, M., Wang, Y., Shi, F., Du, J.: 99.92%-Fidelity CNOT Gates in Solids by Noise Filtering. Phys. Rev. Lett. 130(3), 030601 (2023) https://doi.org/ 10.1103/PhysRevLett.130.030601
- [61] Lerasle, M.: Lecture Notes: Selected topics on robust statistical learning theory. arXiv:1908.10761 (2019) https://doi.org/10.48550/arXiv.1908.10761
- [62] Blair, C.: Problem complexity and method efficiency in optimization (a. s. nemirovsky and d. b. yudin). SIAM Rev. **27**(2), 264–265 (1985) https://doi.org/10.1137/1027074
- [63] Jerrum, M.R., Valiant, L.G., Vazirani, V.V.: Random generation of combinatorial structures from a uniform distribution. Theor. Comput. Sci. 43, 169–188 (1986) https://doi.org/10.1016/0304-3975(86)90174-X
- [64] Cerezo, M., Arrasmith, A., Babbush, R., Benjamin, S.C., Endo, S., Fujii, K., McClean, J.R., Mitarai, K., Yuan, X., Cincio, L., et al.: Variational quantum algorithms. Nat. Rev. Phys. 3(9), 625–644 (2021) https://doi.org/10.1038/s42254-021-00348-9
- [65] Cerezo, M., Sharma, K., Arrasmith, A., Coles, P.J.: Variational quantum state eigensolver. npj Quantum Inf. 8(1), 113 (2022) https://doi.org/10.1038/s41534-022-00611-6
- [66] Brugière, T.G.d., Baboulin, M., Valiron, B., Martiel, S., Allouche, C.: Reducing the Depth of Linear Reversible Quantum Circuits. IEEE Trans. Quantum Eng. 2, 1–22 (2021) https://doi.org/10.1109/ TQE.2021.3091648
- [67] Jiang, J., Sun, X., Teng, S.-H., Wu, B., Wu, K., Zhang, J.: Optimal space-depth trade-off of CNOT circuits in quantum logic synthesis. In: Proc. Annu. ACM-SIAM Symp. Discrete Algorithms, pp. 213–229 (2020). https://doi.org/10.1137/1.9781611975994.13
- [68] Kutin, S.A., Moulton, D.P., Smithline, L.M.: Computation at a distance. arXiv:quant-ph/0701194 (2007) https://doi.org/10.48550/arXiv.quant-ph/0701194
- [69] Lee, J.-M., Lee, W.-J., Kim, M.-S., Cho, S., Ju, J.J., Navickaite, G., Fernandez, J.: Controlled-not operation of sin-photonic circuit using photon pairs from silicon-photonic circuit. Opt. Commun. 509, 127863 (2022) https://doi.org/10.1016/j.optcom.2021.127863
- [70] Russo, A., Barnes, E., Economou, S.E.: Photonic graph state generation from quantum dots and color centers for quantum communications. Phys. Rev. B 98, 085303 (2018) https://doi.org/10.1103/ PhysRevB.98.085303
- [71] Rimbach-Russ, M., Philips, S.G.J., Xue, X., Vandersypen, L.M.K.: Simple framework for systematic high-fidelity gate operations. Quantum Sci. Technol. 8(4), 045025 (2023) https://doi.org/10.1088/ 2058-9565/acf786
- [72] Graham, T.M., Kwon, M., Grinkemeyer, B., Marra, Z., Jiang, X., Lichtman, M.T., Sun, Y., Ebert, M., Saffman, M.: Rydberg-mediated entanglement in a two-dimensional neutral atom qubit array. Phys. Rev. Lett. 123, 230501 (2019) https://doi.org/10.1103/PhysRevLett.123.230501
- [73] Levine, H., Keesling, A., Semeghini, G., Omran, A., Wang, T.T., Ebadi, S., Bernien, H., Greiner, M., Vuletić', V., Pichler, H., Lukin, M.D.: Parallel implementation of high-fidelity multiqubit gates with neutral atoms. Phys. Rev. Lett. 123, 170503 (2019) https://doi.org/10.1103/PhysRevLett.123. 170503
- [74] Saffman, M., Beterov, I.I., Dalal, A., Páez, E.J., Sanders, B.C.: Symmetric rydberg controlled-z gates with adiabatic pulses. Phys. Rev. A **101**, 062309 (2020) https://doi.org/10.1103/PhysRevA. 101.062309

- [75] Wang, T., Zhang, Z., Xiang, L., Jia, Z., Duan, P., Zong, Z., Sun, Z., Dong, Z., Wu, J., Yin, Y., Guo, G.: Experimental realization of a fast controlled- z gate via a shortcut to adiabaticity. Phys. Rev. Appl. 11, 034030 (2018) https://doi.org/10.1103/PhysRevApplied.11.034030
- [76] Simakov, I.A., Mazhorin, G.S., Moskalenko, I.N., Abramov, N.N., Grigorev, A.A., Moskalev, D.O., Pishchimova, A.A., Smirnov, N.S., Zikiy, E.V., Rodionov, I.A., Besedin, I.S.: Coupler microwaveactivated controlled phase gate on fluxonium qubits. arXiv:2302.09819 (2023) https://doi.org/10. 48550/arXiv.2302.09819
- [77] Rol, M.A., Battistel, F., Malinowski, F.K., Bultink, C.C., Tarasinski, B.M., Vollmer, R., Haider, N., Muthusubramanian, N., Bruno, A., Terhal, B.M., DiCarlo, L.: Fast, high-fidelity conditional-phase gate exploiting leakage interference in weakly anharmonic superconducting qubits. Phys. Rev. Lett. 123, 120502 (2019) https://doi.org/10.1103/PhysRevLett.123.120502
- [78] Li, S., Castellano, A.D., Wang, S., Wu, Y., Gong, M., Yan, Z., Rong, H., Deng, H., Zha, C., Guo, C., Sun, L., Peng, C., Zhu, X., Pan, J.-W.: Realisation of high-fidelity nonadiabatic cz gates with superconducting qubits. npj Quantum Inf. 5(1), 84 (2019) https://doi.org/10.1038/s41534-019-0202-7
- [79] Foxen, B., Neill, C., Dunsworth, A., Roushan, P., Chiaro, B., Megrant, A., Kelly, J., Chen, Z., Satzinger, K., Barends, R., Arute, F., Arya, K., Babbush, R., Bacon, D., Bardin, J.C., Boixo, S., Buell, D., Burkett, B., Chen, Y., Collins, R., Farhi, E., Fowler, A., Gidney, C., Giustina, M., Graff, R., Harrigan, M., Huang, T., Isakov, S.V., Jeffrey, E., Jiang, Z., Kafri, D., Kechedzhi, K., Klimov, P., Korotkov, A., Kostritsa, F., Landhuis, D., Lucero, E., McClean, J., McEwen, M., Mi, X., Mohseni, M., Mutus, J.Y., Naaman, O., Neeley, M., Niu, M., Petukhov, A., Quintana, C., Rubin, N., Sank, D., Smelyanskiy, V., Vainsencher, A., White, T.C., Yao, Z., Yeh, P., Zalcman, A., Neven, H., Martinis, J.M.: Demonstrating a continuous set of two-qubit gates for near-term quantum algorithms. Phys. Rev. Lett. 125, 120504 (2020) https://doi.org/10.1103/PhysRevLett.125.120504
- [80] Horn RA, J.C. (ed.): Matrix Analysis vol. 561. Cambridge University Press, Cambridge (1985). https://www.cambridge.org/core/books/matrix-analysis/9CF2CB491C9E97948B15FAD835EF9A8B# fndtn-contents

# **Supplementary Information**

# Variance of sum of independent estimators

Here, we prove Eq. (7) by considering a more general case. Suppose p(x) and q(y) are independent probability distributions for the data bit strings x and y over domains A and B respectively, and that the estimators are  $\hat{a}(x)$  and  $\hat{b}(y)$  respectively. Now, let us define a new estimator  $\hat{a}(x) + \hat{b}(y)$ . We calculate its variance, which is expressed as

Var

$$= \sum_{\boldsymbol{x} \in A, \boldsymbol{y} \in B} p(\boldsymbol{x}) q(\boldsymbol{y}) \left\{ \left( (\widehat{a}(\boldsymbol{x}) + \widehat{b}(\boldsymbol{y})) - \sum_{\boldsymbol{x}' \in A, \boldsymbol{y}' \in B} \left\{ p(\boldsymbol{x}') q(\boldsymbol{y}') \left( \widehat{a}(\boldsymbol{x}') + \widehat{b}(\boldsymbol{y}') \right) \right\} \right\}^{2} \right\}$$

$$= \sum_{\boldsymbol{x} \in A, \boldsymbol{y} \in B} p(\boldsymbol{x}) q(\boldsymbol{y}) \left[ \widehat{a}(\boldsymbol{x})^{2} + \widehat{b}(\boldsymbol{y})^{2} + 2\widehat{a}(\boldsymbol{x}) \widehat{b}(\boldsymbol{y}) \right]$$

$$- 2 \left( \widehat{a}(\boldsymbol{x}) + \widehat{b}(\boldsymbol{y}) \right) \sum_{\boldsymbol{x}' \in A, \boldsymbol{y}' \in B} \left\{ p(\boldsymbol{x}') q(\boldsymbol{y}') (\widehat{a}(\boldsymbol{x}') + \widehat{b}(\boldsymbol{y}')) \right\} \right] + \left\{ \sum_{\boldsymbol{x}' \in A, \boldsymbol{y}' \in B} \left\{ p(\boldsymbol{x}') q(\boldsymbol{y}') (\widehat{a}(\boldsymbol{x}') + \widehat{b}(\boldsymbol{y}')) \right\} \right\}^{2}$$

$$= \sum_{\boldsymbol{x} \in A, \boldsymbol{y} \in B} p(\boldsymbol{x}) q(\boldsymbol{y}) \left[ \widehat{a}(\boldsymbol{x})^{2} + \widehat{b}(\boldsymbol{y})^{2} + 2\widehat{a}(\boldsymbol{x}) \widehat{b}(\boldsymbol{y}) \right]$$

$$- 2 \left( \widehat{a}(\boldsymbol{x}) + \widehat{b}(\boldsymbol{y}) \right) \sum_{\boldsymbol{x}' \in A, \boldsymbol{y}' \in B} \left\{ p(\boldsymbol{x}') q(\boldsymbol{y}') (\widehat{a}(\boldsymbol{x}') + \widehat{b}(\boldsymbol{y}')) \right\} \right\}$$

$$\left\{ \sum_{\boldsymbol{x} \in A, \boldsymbol{y} \in B} \left\{ p(\boldsymbol{x}) q(\boldsymbol{y}) (\widehat{a}(\boldsymbol{x}) + \widehat{b}(\boldsymbol{y})) \right\} \right\} \left\{ \sum_{\boldsymbol{x}' \in A, \boldsymbol{y}' \in B} \left\{ p(\boldsymbol{x}') q(\boldsymbol{y}') (\widehat{a}(\boldsymbol{x}') + \widehat{b}(\boldsymbol{y}')) \right\} \right\}$$

$$= \sum_{\boldsymbol{x} \in A} p(\boldsymbol{x}) \left\{ \widehat{a}(\boldsymbol{x})^{2} - \left\{ \sum_{\boldsymbol{x} \in A} p(\boldsymbol{x}) \widehat{a}(\boldsymbol{x}) \right\}^{2} \right\} + \sum_{\boldsymbol{y} \in A} q(\boldsymbol{y}) \left\{ \widehat{b}(\boldsymbol{y})^{2} - \left\{ \sum_{\boldsymbol{y} \in A} q(\boldsymbol{y}) \widehat{b}(\boldsymbol{y}) \right\}^{2} \right\},$$

$$(58)$$

where the last expression is the sum of variances of each independent estimator  $\widehat{a}$  and  $\widehat{b}$ . (R)ESPOVM and computational basis measurement are done independently and we take the estimator  $\widehat{O}_{\mathbf{A},x} \equiv \widehat{O}_{\mathbf{A}}^{(\mathbf{r})\mathrm{eq}} + \widehat{O}_{x}^{\mathrm{bin}} - \mathrm{tr}(O)$ . By ignoring the constant  $\mathrm{tr}(O)$  that does not contribute to the variance analysis, we easily note that Eq. (7) is just a special case of the above general argument. More explicitly, A is a (R)ESPOVM, B is the computational basis, a is  $O_{\mathbf{A}}^{(\mathbf{r})\mathrm{eq}}$ , and b is  $\widehat{O}_{x}^{\mathrm{bin}}$ .

# The proof of Lemma 1

The first and second moments of the equatorial-stabilizer set are shown in Ref. [31]. So, we only consider the RESPOVM case and adopt similar strategies for ESPOVMs. Note that for  $\forall p \in \mathbb{Z}_n^2$ ,

$$Z^{p}\mathbb{E}_{|\phi_{\mathbf{A}}^{\text{req}}\rangle\in\mathcal{D}(\mathcal{S}_{n}^{\text{req}})}|\phi_{\mathbf{A}}^{\text{req}}\rangle\langle\phi_{\mathbf{A}}^{\text{req}}|Z^{p} = \mathbb{E}_{|\phi_{\mathbf{A}}^{\text{req}}\rangle\in\mathcal{D}(\mathcal{S}_{n}^{\text{req}})}\frac{1}{2^{n}}\sum_{\boldsymbol{x},\boldsymbol{y}\in\mathbb{Z}_{2}^{n}}(-1)^{\boldsymbol{x}\mathbf{A}\boldsymbol{x}^{T}+\boldsymbol{y}\mathbf{A}\boldsymbol{y}^{T}+\boldsymbol{p}\cdot(\boldsymbol{x}+\boldsymbol{y})}|\boldsymbol{x}\rangle\langle\boldsymbol{y}|,$$

$$=\mathbb{E}_{|\phi_{\mathbf{A}}^{\text{req}}\rangle\in\mathcal{D}(\mathcal{S}_{n}^{\text{req}})}\frac{1}{2^{n}}\sum_{\boldsymbol{x},\boldsymbol{y}\in\mathbb{Z}_{2}^{n}}(-1)^{\boldsymbol{x}\mathbf{A}'\boldsymbol{x}^{T}+\boldsymbol{y}\mathbf{A}'\boldsymbol{y}^{T}}|\boldsymbol{x}\rangle\langle\boldsymbol{y}|,$$

$$=\mathbb{E}_{|\phi_{\mathbf{A}}^{\text{req}}\rangle\in\mathcal{D}(\mathcal{S}_{n}^{\text{req}})}|\phi_{\mathbf{A}'}\rangle\langle\phi_{\mathbf{A}'}|,$$

$$=\mathbb{E}_{|\phi_{\mathbf{A}}^{\text{req}}\rangle\in\mathcal{D}(\mathcal{S}_{n}^{\text{req}})}|\phi_{\mathbf{A}}\rangle\langle\phi_{\mathbf{A}}|,$$

$$(59)$$

where for  $\forall i, j \in [n], A'_{ii} = A_{ii} + p_i \pmod{2}$  otherwise  $A'_{ij} = A_{ij}$ . The fourth equality holds because the reparametrization of **A** does not affect its uniform-distribution first moment. Thus

 $\mathbb{E}_{|\phi_{\mathbf{A}}^{\mathrm{req}}\rangle\in\mathcal{D}(\mathcal{S}_{n}^{\mathrm{req}})}|\phi_{\mathbf{A}}^{\mathrm{req}}\rangle\langle\phi_{\mathbf{A}}^{\mathrm{req}}|$  commutes with all Pauli Z-operators and is diagonal in the computational basis. Notice that all diagonal elements are  $\frac{1}{2^{n}}$ . Therefore  $\mathbb{E}_{|\phi_{\mathbf{A}}^{\mathrm{req}}\rangle\in\mathcal{D}(\mathcal{S}_{n}^{\mathrm{req}})}|\phi_{\mathbf{A}}\rangle\langle\phi_{\mathbf{A}}|=\frac{\mathbb{I}}{2^{n}}$ , which is Lem. 1 (i).

Next, note that

$$\mathbb{E}_{|\phi_{\mathbf{A}}^{\text{req}}\rangle\in\mathcal{D}(\mathcal{S}_{n}^{\text{req}})} |\phi_{\mathbf{A}}^{\text{req}}\rangle \langle \phi_{\mathbf{A}}^{\text{req}}|^{\otimes 2} = \mathbb{E}_{|\phi_{\mathbf{A}}^{\text{req}}\rangle\in\mathcal{D}(\mathcal{S}_{n}^{\text{req}})} \frac{1}{4^{n}} \sum_{\boldsymbol{x},\boldsymbol{y},\boldsymbol{z},\boldsymbol{w}\in\mathbb{Z}_{n}^{n}} (-1)^{\boldsymbol{x}\boldsymbol{A}\boldsymbol{x}^{T} + \boldsymbol{y}\boldsymbol{A}\boldsymbol{y}^{T} + \boldsymbol{z}\boldsymbol{A}\boldsymbol{z}^{T} + \boldsymbol{w}\boldsymbol{A}\boldsymbol{w}^{T}} |\boldsymbol{x}\boldsymbol{y}\rangle \langle \boldsymbol{z}\boldsymbol{w}|,$$

$$= \frac{1}{4^{n}} \sum_{\boldsymbol{x},\boldsymbol{y},\boldsymbol{z},\boldsymbol{w}\in\mathbb{Z}_{n}^{n}} \mathbb{E}_{|\phi_{\mathbf{A}}^{\text{req}}\rangle\in\mathcal{D}(\mathcal{S}_{n}^{\text{req}})} \left\{ (-1)^{\boldsymbol{x}\boldsymbol{A}\boldsymbol{x}^{T} + \boldsymbol{y}\boldsymbol{A}\boldsymbol{y}^{T} + \boldsymbol{z}\boldsymbol{A}\boldsymbol{z}^{T} + \boldsymbol{w}\boldsymbol{A}\boldsymbol{w}^{T}} \right\} |\boldsymbol{x}\boldsymbol{y}\rangle \langle \boldsymbol{z}\boldsymbol{w}|.$$
(60)

Now, we focus on terms in the curly brackets. Since the elements of **A** oscillate between 0 and 1, the nonzero coefficients of  $|x,y\rangle\langle z,w|$  must satisfy the following equations for all  $p,q\in [n](p< q)$ ,

$$\begin{cases} x_p + y_p + z_p = w_p, \\ x_p x_q + y_p y_q + z_p z_q + w_p w_q = 0. \end{cases}$$
 (61)

Now, substitute the upper equation to lower one. We obtain that

$$x_p(y_q + z_q) + y_p(z_q + x_q) + z_p(x_q + y_q) = 0. (62)$$

If x = y = z, the above equation must hold. Suppose x, y, z are not all the same. Then there exists  $p' \in [n]$  such that two of  $x_{p'}, y_{p'}, z_{p'}$  are equal but the rest are not. Also,  $x_i = y_i = z_i$  for  $i \le p'$ . WLOG, we may assume  $x_{p'} = y_{p'} \ne z_{p'}$ , then for  $\forall q > p'$ ,

$$(x_q + y_q)(x_{p'} + z_{p'}) = 0 \rightarrow x_q = y_q : x_{p'} \neq z_{p'}.$$
 (63)

It follows that nonzero coefficients of  $|x,y\rangle\langle z,w|$  must be such that two of x,y,z are equal. Based on this observation, (61) implies several cases: (i) x=y,z=w, (ii) x=z,y=w, and (iii) x=w,y=z. In all these cases  $\mathbb{E}_{|\phi_{\mathbf{A}}^{\mathrm{req}}\rangle\in\mathcal{D}(\mathcal{S}_n^{\mathrm{req}})}\left\{(-1)^{x\mathbf{A}x^T+y\mathbf{A}y^T+z\mathbf{A}z^T+w\mathbf{A}w^T}\right\}=1$ . Hence, we obtain the following results.

$$\mathbb{E}_{|\phi_{\mathbf{A}}^{\text{req}}\rangle \in \mathcal{D}(\mathcal{S}_{n}^{\text{req}})} |\phi_{\mathbf{A}}^{\text{req}}\rangle \langle \phi_{\mathbf{A}}^{\text{req}}|^{\otimes 2} = \frac{1}{4^{n}} \left( I + \sum_{\boldsymbol{x}, \boldsymbol{y} \in \mathbb{Z}_{2}^{n}} |\boldsymbol{x}\boldsymbol{y}\rangle \langle \boldsymbol{y}\boldsymbol{x}| + \sum_{\boldsymbol{x}\boldsymbol{y} \in \mathbb{Z}_{2}^{n}} |\boldsymbol{x}\boldsymbol{x}\rangle \langle \boldsymbol{y}\boldsymbol{y}| - 2\sum_{\boldsymbol{x} \in \mathbb{Z}_{2}^{n}} |\boldsymbol{x}\boldsymbol{x}\rangle \langle \boldsymbol{x}\boldsymbol{x}| \right), \quad (64)$$

which is the result of Lem. 1 (iii) and completes the proof.

# The proof of Lemma 2

First, we consider ESPOVMs. By Lem. 1,

$$\mathbb{E}_{|\phi_{\mathbf{A}}^{\text{eq}}\rangle \in \mathcal{S}_{n}^{\text{eq}}} \left( \left\langle \phi_{\mathbf{A}}^{\text{eq}} \right| \sigma \left| \phi_{\mathbf{A}}^{\text{eq}} \right\rangle \left\langle \phi_{\mathbf{A}}^{\text{eq}} \right| O \left| \phi_{\mathbf{A}}^{\text{eq}} \right\rangle \right) = \text{tr} \left\{ \left( \mathbb{E}_{|\phi_{\mathbf{A}}^{\text{eq}}\rangle \in \mathcal{D}(\mathcal{S}_{n}^{\text{eq}})} \left| \phi_{\mathbf{A}}^{\text{eq}} \right\rangle \left\langle \phi_{\mathbf{A}}^{\text{eq}} \right|^{\otimes 2} \right) (\sigma \otimes O) \right\} 
= \frac{1}{4^{n}} \text{tr} \left\{ \left( I + \sum_{\boldsymbol{x}, \boldsymbol{y} \in \mathbb{Z}_{2}^{n}} \left| \boldsymbol{x} \boldsymbol{y} \right\rangle \left\langle \boldsymbol{y} \boldsymbol{x} \right| - \sum_{\boldsymbol{x} \in \mathbb{Z}_{2}^{n}} \left| \boldsymbol{x} \boldsymbol{x} \right\rangle \left\langle \boldsymbol{x} \boldsymbol{x} \right| \right) (\sigma \otimes O) \right\}, 
= \frac{1}{4^{n}} \left\{ \text{tr}(O) + \sum_{\boldsymbol{x}, \boldsymbol{y} \in \mathbb{Z}_{2}^{n}} \left\langle \boldsymbol{y} \right| \sigma \left| \boldsymbol{x} \right\rangle \left\langle \boldsymbol{x} \right| O \left| \boldsymbol{y} \right\rangle - \sum_{\boldsymbol{x} \in \mathbb{Z}_{2}^{n}} \left\langle \boldsymbol{x} \right| \sigma \left| \boldsymbol{x} \right\rangle \left\langle \boldsymbol{x} \right| O \left| \boldsymbol{x} \right\rangle \right\}, 
= \frac{1}{4^{n}} \left\{ \text{tr}(O) + \text{tr}(O\sigma) - \sum_{\boldsymbol{x} \in \mathbb{Z}_{2}^{n}} \left\langle \boldsymbol{x} \right| \sigma \left| \boldsymbol{x} \right\rangle \left\langle \boldsymbol{x} \right| O \left| \boldsymbol{x} \right\rangle \right\}.$$
(66)

Hence, we obtain the following result,

$$\sum_{|\phi_{\mathbf{A}}^{\text{eq}}\rangle \in \mathcal{S}_{n}^{\text{eq}}} \frac{2^{2n}}{|\mathcal{S}_{n}^{\text{eq}}|} \langle \phi_{\mathbf{A}}^{\text{eq}} | \rho | \phi_{\mathbf{A}}^{\text{eq}} \rangle \langle \phi_{\mathbf{A}}^{\text{eq}} | O | \phi_{\mathbf{A}}^{\text{eq}} \rangle + \sum_{\boldsymbol{x} \in \mathbb{Z}_{2}^{n}} \langle \boldsymbol{x} | \rho | \boldsymbol{x} \rangle \langle \boldsymbol{x} | O | \boldsymbol{x} \rangle - \text{tr}(O) = \text{tr}(O\rho).$$
 (67)

Next, we consider RESPOVMs and also assume O to be a real observable, that is  $\langle \boldsymbol{a} | O | \boldsymbol{b} \rangle \in \mathbb{R}$  for  $\forall \boldsymbol{a}, \boldsymbol{b} \in \mathbb{Z}_2^n$ . Then,

$$\mathbb{E}_{|\phi_{\mathbf{A}}^{\text{req}}\rangle \in \mathcal{S}_{n}^{\text{req}}} \left( \left\langle \phi_{\mathbf{A}}^{\text{req}} \middle| \sigma \middle| \phi_{\mathbf{A}}^{\text{req}} \right\rangle \left\langle \phi_{\mathbf{A}}^{\text{Req}} \middle| O \middle| \phi_{\mathbf{A}}^{\text{req}} \right\rangle \right) = \text{tr} \left\{ \left( \mathbb{E}_{|\phi_{\mathbf{A}}^{\text{eq}}\rangle \in \mathcal{D}(\mathcal{S}_{n}^{\text{eq}})} \middle| \phi_{\mathbf{A}}^{\text{eq}} \right\rangle \left\langle \phi_{\mathbf{A}}^{\text{eq}} \middle| ^{\otimes 2} \right) (\sigma \otimes O) \right\}$$

$$= \frac{1}{4^{N}} \text{tr} \left\{ \left( I + \sum_{\mathbf{x}, \mathbf{y} \in \mathbb{Z}_{2}^{n}} |\mathbf{x}\mathbf{y}\rangle \left\langle \mathbf{y}\mathbf{x} \middle| + \sum_{\mathbf{x}, \mathbf{y} \in \mathbb{Z}_{2}^{n}} |\mathbf{x}\mathbf{x}\rangle \left\langle \mathbf{y}\mathbf{y} \middle| - 2 \sum_{\mathbf{x} \in \mathbb{Z}_{2}^{n}} |\mathbf{x}\mathbf{x}\rangle \left\langle \mathbf{x}\mathbf{x} \middle| \right) (\sigma \otimes O) \right\}$$

$$= \frac{1}{4^{N}} \left\{ \text{tr}(O) + \sum_{\mathbf{x}, \mathbf{y} \in \mathbb{Z}_{2}^{n}} \left\langle \mathbf{y} \middle| \sigma \middle| \mathbf{x}\rangle \left\langle \mathbf{x} \middle| O \middle| \mathbf{y} \right\rangle + \sum_{\mathbf{x}, \mathbf{y} \in \mathbb{Z}_{2}^{n}} \left\langle \mathbf{y} \middle| \sigma \middle| \mathbf{x}\rangle \left\langle \mathbf{y} \middle| O \middle| \mathbf{x} \right\rangle - 2 \sum_{\mathbf{x} \in \mathbb{Z}_{2}^{n}} \left\langle \mathbf{x} \middle| \sigma \middle| \mathbf{x}\rangle \left\langle \mathbf{x} \middle| O \middle| \mathbf{x} \right\rangle \right\}$$

$$= \frac{1}{4^{N}} \left\{ \text{tr}(O) + 2 \sum_{\mathbf{x}, \mathbf{y} \in \mathbb{Z}_{2}^{n}} \left\langle \mathbf{y} \middle| \sigma \middle| \mathbf{x}\rangle \left\langle \mathbf{x} \middle| O \middle| \mathbf{y} \right\rangle - 2 \sum_{\mathbf{x} \in \mathbb{Z}_{2}^{n}} \left\langle \mathbf{x} \middle| \sigma \middle| \mathbf{x}\rangle \left\langle \mathbf{x} \middle| O \middle| \mathbf{x} \right\rangle \right\}$$

$$= \frac{1}{4^{N}} \left\{ \text{tr}(O) + 2 \text{tr}(O\sigma) - 2 \sum_{\mathbf{x} \in \mathbb{Z}_{2}^{n}} \left\langle \mathbf{x} \middle| \sigma \middle| \mathbf{x}\rangle \left\langle \mathbf{x} \middle| O \middle| \mathbf{x} \right\rangle \right\}.$$
(68)

This is equivalent to,

$$\sum_{|\phi_{\mathbf{A}}^{\text{req}}\rangle \in \mathcal{S}_{n}^{\text{req}}} \frac{2^{2n-1}}{|\mathcal{S}_{n}^{\text{req}}|} \left\langle \phi_{\mathbf{A}}^{\text{req}} \right| \rho \left| \phi_{\mathbf{A}}^{\text{req}} \right\rangle \left\langle \phi_{\mathbf{A}}^{\text{req}} \right| O \left| \phi_{\mathbf{A}}^{\text{req}} \right\rangle + \sum_{\boldsymbol{x} \in \mathbb{Z}_{n}^{n}} \left\langle \boldsymbol{x} \right| \rho \left| \boldsymbol{x} \right\rangle \left\langle \boldsymbol{x} \right| O \left| \boldsymbol{x} \right\rangle - \frac{1}{2} \text{tr}(O) = \text{tr}(O\rho).$$
 (70)

Equation (68) is valid when O is real. This proves Lem. 2. In Eq. (7), we ignore the tr(O) term since it is constant and, hence, does not affect the variance.

# The proof of Lemma 3

We start with  $S_n^{\text{req}}$ . Similar to Eq. (60),

$$\mathbb{E}_{|\phi_{\mathbf{A}}^{\text{req}}\rangle \in \mathcal{D}(\mathcal{S}_{n}^{\text{req}})} |\phi_{\mathbf{A}}^{\text{req}}\rangle \langle \phi_{\mathbf{A}}^{\text{req}}|^{\otimes 3}$$

$$= \mathbb{E}_{|\phi_{\mathbf{A}}^{\text{req}}\rangle \in \mathcal{D}(\mathcal{S}_{n}^{\text{req}})} \frac{1}{8^{n}} \sum_{\boldsymbol{x}, \boldsymbol{y}, \boldsymbol{z}, \boldsymbol{w}, \boldsymbol{s}, \boldsymbol{t} \in \mathbb{Z}_{2}^{n}} (-1)^{\boldsymbol{x} \mathbf{A} \boldsymbol{x}^{T} + \boldsymbol{y} \mathbf{A} \boldsymbol{y}^{T} + \boldsymbol{z} \mathbf{A} \boldsymbol{z}^{T} + \boldsymbol{w} \mathbf{A} \boldsymbol{w}^{T} + \boldsymbol{s} \mathbf{A} \boldsymbol{s}^{T} + \boldsymbol{t} \mathbf{A} \boldsymbol{t}^{T}} |\boldsymbol{x}, \boldsymbol{y}, \boldsymbol{z}\rangle \langle \boldsymbol{w}, \boldsymbol{s}, \boldsymbol{t}|$$

$$= \frac{1}{8^{n}} \sum_{\boldsymbol{x}, \boldsymbol{y}, \boldsymbol{z}, \boldsymbol{w}, \boldsymbol{s}, \boldsymbol{t} \in \mathbb{Z}_{2}^{n}} \mathbb{E}_{|\phi_{\mathbf{A}}^{\text{req}}\rangle \in \mathcal{D}(\mathcal{S}_{n}^{\text{req}})} \left\{ (-1)^{\boldsymbol{x} \mathbf{A} \boldsymbol{x}^{T} + \boldsymbol{y} \mathbf{A} \boldsymbol{y}^{T} + \boldsymbol{z} \mathbf{A} \boldsymbol{z}^{T} + \boldsymbol{w} \mathbf{A} \boldsymbol{w}^{T} + \boldsymbol{s} \mathbf{A} \boldsymbol{s}^{T} + \boldsymbol{t} \mathbf{A} \boldsymbol{t}^{T}} \right\} |\boldsymbol{x}, \boldsymbol{y}, \boldsymbol{z}\rangle \langle \boldsymbol{w}, \boldsymbol{s}, \boldsymbol{t}|. \quad (71)$$

By the same token, for nonzero coefficients in the summand, the following equations must hold for all  $p, q \in [n]$ :

$$\begin{cases} x_p + y_p + z_p + w_p + s_p = t_p \pmod{2}, \\ x_p x_q + y_p y_q + z_p z_q + w_p w_q + s_p s_q + t_p t_q = 0 \pmod{2}. \end{cases}$$
 (72)

Substituting the upper equation into the lower one, we obtain,

$$x_p(y_q + z_q + w_q + s_q) + y_p(z_q + x_q + w_q + s_q) + z_p(x_q + y_q + w_q + s_q) + w_p(x_q + y_q + z_q + s_q) + s_p(x_q + y_q + z_q + w_q) = 0.$$
 (73)

If x = y = z = w = s, the above equation clearly holds. Otherwise, we have two cases:

(i) There exists  $p' \in [n]$  such that two of  $x_{p'}, y_{p'}, z_{p'}, w_{p'}, s_{p'}$  are 0 (1 resp.) and the rest are 1 (0), and  $x_i = y_i = z_i = w_i = s_i$  for i < p'.

(ii) There exists  $p' \in [n]$  such that four of  $x_{p'}, y_{p'}, z_{p'}, w_{p'}, s_{p'}$  are 0 (1 resp.) and the other is 1 (0), and  $x_i = y_i = z_i = w_i = s_i$  for i < p'.

First, suppose case (i). WLOG, when  $x_{p'} = y_{p'}$  (\*), then  $z_{p'} = w_{p'} = s_{p'} = x_{p'} + 1$ , which together with Eq. (73), implies that

$$x_{p'}y_q + x_qy_{p'} + (x_{p'} + 1)(x_q + y_q) = x_q + y_q = 0 \pmod{2} :: x_{p'} = y_{p'}. \tag{74}$$

So, we obtain x = y. Substituting this back to Eq. (72),

$$\begin{cases} z_p + w_p + s_p = t_p \pmod{2}, \\ z_p z_q + w_p w_q + s_p s_q + t_p t_q = 0 \pmod{2}. \end{cases}$$
 (75)

This is exactly what we have obtained during the calculation of the second moment. Hence we conclude the same statement, two of z, w, s are equal. By the first equation of Eq. (75), the remaining one equals t. Therefore, we conclude that each two of x, y, z, w, s, t must be equal. Note that even if we chose two other variables, not x and y in assumption(\*), we arrive at the same conclusion.

Next, let us suppose case (ii). By the first equation of Eq. (72),  $x_i = y_i = z_i = w_i = s_i = t_i$  for i < p'. WLOG, assume that  $x_{p'} = y_{p'} = z_{p'} = w_{p'} \neq s_{p'}$ . Then, we obtain  $s_{p'} = t_{p'}$  from Eq. (72). Next, we rewrite the problem as

$$\begin{cases} y_p + z_p + w_p + s_p + t_p = x_p \pmod{2}, \\ x_p x_q + y_p y_q + z_p z_q + w_p w_q + s_p s_q + t_p t_q = 0 \pmod{2} \end{cases}$$
(76)

Similarly, substituting the first equation into the second,

$$t_p(y_q + z_q + w_q + s_q) + y_p(z_q + x_q + w_q + s_q) + z_p(t_q + y_q + w_q + s_q) + w_p(t_q + y_q + z_q + s_q) + s_p(t_q + y_q + z_q + w_q) = 0.$$
 (77)

Remember we assumed that  $t_{p'} = s_{p'}$ ,  $t_{p'} \neq w_{p'}$ ,  $y_{p'} = z_{p'} = w_{p'}$ , and  $y_i = z_i = w_i = s_i = t_i$  for i < p'. This is exactly the case of solving under the assumption (i). So we conclude the same statement that t = s, two of y, z, w are equal and hence remaining one equals x.

Throughout cases (i) and (ii), we finally conclude that the coefficient of  $|x, y, z\rangle \langle w, s, t|$  is nonzero only when each 3-couples in variable set  $\{x, y, z, w, s, t\}$  must be equal and in such all cases, coefficients  $\mathbb{E}_{|\phi_{\mathbf{A}}^{\mathrm{req}}\rangle \in \mathcal{D}(S_n^{\mathrm{req}})} \left\{ (-1)^{x\mathbf{A}x^T + y\mathbf{A}y^T + z\mathbf{A}z^T + w\mathbf{A}w^T + s\mathbf{A}s^T + t\mathbf{A}t^T} \right\} = 1$ . The proof for RESPOVM is now completed.

Now, we move on to  $\mathcal{S}_n^{\text{eq}}$ , whence

$$\mathbb{E}_{|\phi_{\mathbf{A}}^{\text{eq}}\rangle\in\mathcal{D}(\mathcal{S}_{n}^{\text{eq}})}|\phi_{\mathbf{A}}^{\text{eq}}\rangle\langle\phi_{\mathbf{A}}^{\text{eq}}|^{\otimes 3}$$

$$= \mathbb{E}_{|\phi_{\mathbf{A}}^{\text{eq}}\rangle\in\mathcal{D}(\mathcal{S}_{n}^{\text{eq}})}\frac{1}{8^{n}}\sum_{\boldsymbol{x},\boldsymbol{y},\boldsymbol{z},\boldsymbol{w},\boldsymbol{s},\boldsymbol{t}\in\mathbb{Z}_{2}^{n}}i^{\boldsymbol{x}\boldsymbol{A}\boldsymbol{x}^{T}+\boldsymbol{y}\boldsymbol{A}\boldsymbol{y}^{T}+\boldsymbol{z}\boldsymbol{A}\boldsymbol{z}^{T}-\boldsymbol{w}\boldsymbol{A}\boldsymbol{w}^{T}-\boldsymbol{s}\boldsymbol{A}\boldsymbol{s}^{T}-\boldsymbol{t}\boldsymbol{A}\boldsymbol{t}^{T}}|\boldsymbol{x},\boldsymbol{y},\boldsymbol{z}\rangle\langle\boldsymbol{w},\boldsymbol{s},\boldsymbol{t}|$$

$$= \frac{1}{8^{n}}\sum_{\boldsymbol{x},\boldsymbol{y},\boldsymbol{z},\boldsymbol{w},\boldsymbol{s},\boldsymbol{t}\in\mathbb{Z}_{2}^{n}}\mathbb{E}_{|\phi_{\mathbf{A}}^{\text{eq}}\rangle\in\mathcal{D}(\mathcal{S}_{n}^{\text{eq}})}\left\{i^{\boldsymbol{x}\boldsymbol{A}\boldsymbol{x}^{T}+\boldsymbol{y}\boldsymbol{A}\boldsymbol{y}^{T}+\boldsymbol{z}\boldsymbol{A}\boldsymbol{z}^{T}-\boldsymbol{w}\boldsymbol{A}\boldsymbol{w}^{T}-\boldsymbol{s}\boldsymbol{A}\boldsymbol{s}^{T}-\boldsymbol{t}\boldsymbol{A}\boldsymbol{t}^{T}}\right\}|\boldsymbol{x},\boldsymbol{y},\boldsymbol{z}\rangle\langle\boldsymbol{w},\boldsymbol{s},\boldsymbol{t}|.$$
(78)

By the same argument, for the coefficient not to be 0, the following equation must hold. For all  $p, q \in \mathbb{Z}_2^n$  (p < q),

$$\begin{cases} x_p + y_p + z_p = w_p + s_p + t_p \pmod{4} \\ x_p x_q + y_p y_q + z_p z_q + w_p w_q + s_p s_q + t_p t_q = 0 \pmod{2}. \end{cases}$$
(79)

We add  $w_p + s_p$  for both sides of the first equation of (79), we obtain that

$$\begin{cases} x_p + y_p + z_p + w_p + s_p = t_p \pmod{2} \\ x_p x_q + y_p y_q + z_p z_q + w_p w_q + s_p s_q + t_p t_q = 0 \pmod{2}. \end{cases}$$
(80)

This is equation for  $S_n^{\text{req}}$ -case. Hence we obtain the same statement, each 3-couples in variable set  $\{x, y, z, w, s, t\}$  must be equal. However, in this case, we have a stricter condition, the first equation of Eq. (79). WLOG, we only consider two cases.

(i)  $\boldsymbol{x} = \boldsymbol{y} : 2x_p + z_p = w_p + s_p + t_p \pmod{4} \rightarrow z_p = w_p + s_p + t_p \pmod{2}$ . Hence two variables in  $\{\boldsymbol{z}, \boldsymbol{w}, \boldsymbol{s}, \boldsymbol{t}\}$  are equal each other.

(ii)  $\mathbf{x} = \mathbf{w} : y_p + z_p = s_p + t_p \pmod{4}$ . If  $\mathbf{y} = \mathbf{z}, 2y_p = s_p + t_p \rightarrow \mathbf{y} = \mathbf{z} = \mathbf{s} = \mathbf{t}$ . If  $\mathbf{y} = \mathbf{s}, \mathbf{z} = \mathbf{t}$ . If  $\mathbf{y} = \mathbf{w}$ , all cases are equivalent to previous cases. Therefore for the coefficients to be non-zero, if  $|\mathbf{x}, \mathbf{y}, \mathbf{z}\rangle \langle \mathbf{w}, \mathbf{s}, \mathbf{t}|$  has 2 same variables where each do not locate in the same position(bra and ket) and the other 2 variables in bra (or ket) are equal, remaining variables in ket (or bra) must be equal to previous 2 variables. Finally, in those cases, the coefficient cannot be other values but 1.

Other cases can be managed similarly and are known to have similar effects of (i) or (ii). We thus proved Lem. 3.

# The proof of Lemma 4

First, we note that

$$\sum_{\boldsymbol{x}\in\mathbb{Z}_{2}^{n}}\operatorname{tr}(|\boldsymbol{x}\boldsymbol{x}\boldsymbol{x}\rangle\langle\boldsymbol{x}\boldsymbol{x}\boldsymbol{x}|\left(\sigma\otimes O_{0}\otimes O_{0}\right)) = \sum_{\boldsymbol{x}\in\mathbb{Z}_{2}^{n}}\langle\boldsymbol{x}|\sigma|\boldsymbol{x}\rangle\langle\boldsymbol{x}|O_{0}|\boldsymbol{x}\rangle\langle\boldsymbol{x}|O_{0}|\boldsymbol{x}\rangle\langle\boldsymbol{x}|O_{0}|\boldsymbol{x}\rangle$$

$$\leq \sum_{\boldsymbol{x},\boldsymbol{y}\in\mathbb{Z}_{2}^{n}}\langle\boldsymbol{x}|\sigma|\boldsymbol{x}\rangle\langle\boldsymbol{x}|O_{0}|\boldsymbol{y}\rangle\langle\boldsymbol{y}|O_{0}|\boldsymbol{x}\rangle\leq\operatorname{tr}(O_{0}^{2}). \tag{81}$$

Here, we used the fact that  $\langle \boldsymbol{x}|O_0|\boldsymbol{y}\rangle\langle \boldsymbol{y}|O_0|\boldsymbol{x}\rangle \geq 0$  for  $\forall \boldsymbol{x},\boldsymbol{y}\in\mathbb{Z}_2^n$ . This proves the Eq. (40). Also, we easily note that

$$|xyz\rangle \langle yzx| (\sigma \otimes O_0 \otimes O_0)) = (\operatorname{tr}(O_0))^2 + \operatorname{tr}(O_0^2) + 2\operatorname{tr}(O_0)\operatorname{tr}(\sigma O_0) + 2\operatorname{tr}(\sigma O_0^2)$$

$$\leq (\operatorname{tr}(O_0))^2 + \operatorname{tr}(O_0^2) + 2\operatorname{tr}(O_0)||O_0||_{\infty} + 2||O_0^2||_{\infty} \leq (\operatorname{tr}(O_0))^2 + 3\operatorname{tr}(O_0^2) + 2\operatorname{tr}(O_0)||O_0||_{\infty} \leq 3\operatorname{tr}(O_0^2),$$
(83)

where  $||O||_{\infty} \equiv \max_{|\psi\rangle} \{|\langle \psi | O | \psi \rangle|\}$ . Furthermore, we can consider another case when two variables are the same in ket. Let  $\sigma = \sum_{\lambda} \lambda |\lambda\rangle \langle\lambda|$  be spectral decomposition of  $\sigma$ , hence  $\forall \lambda \geq 0$  and  $\sum_{\lambda} \lambda = 1$ . Then we obtain that

$$\left| \sum_{\boldsymbol{x}, \boldsymbol{y}, \boldsymbol{z} \in \mathbb{Z}_{2}^{n}} \operatorname{tr}(|\boldsymbol{x}\boldsymbol{x}\boldsymbol{y}\rangle \langle \boldsymbol{z}\boldsymbol{z}\boldsymbol{y}| (\sigma \otimes O_{0} \otimes O_{0})) \right| = \left| \sum_{\boldsymbol{x}, \boldsymbol{y}, \boldsymbol{z} \in \mathbb{Z}_{2}^{n}} \langle \boldsymbol{z} | \sigma | \boldsymbol{x}\rangle \langle \boldsymbol{z} | O_{0} | \boldsymbol{x}\rangle \langle \boldsymbol{y} | O_{0} | \boldsymbol{y}\rangle \right| = \left| \operatorname{tr}(O_{0}) \operatorname{tr}(\sigma O_{0}^{T}) \right| \\
\leq \left| \operatorname{tr}(O_{0}) \operatorname{tr}(O_{0}^{T}) \right| = 0 \tag{84}$$

$$\left| \sum_{\boldsymbol{x}, \boldsymbol{y}, \boldsymbol{z} \in \mathbb{Z}_{2}^{n}} \operatorname{tr}(|\boldsymbol{x}\boldsymbol{x}\boldsymbol{y}\rangle \langle \boldsymbol{z}\boldsymbol{y}\boldsymbol{z}| (\sigma \otimes O_{0} \otimes O_{0})) \right| = \left| \sum_{\boldsymbol{x}, \boldsymbol{y}, \boldsymbol{z} \in \mathbb{Z}_{2}^{n}} \langle \boldsymbol{z} | \sigma | \boldsymbol{x}\rangle \langle \boldsymbol{y} | O_{0} | \boldsymbol{x}\rangle \langle \boldsymbol{z} | O_{0} | \boldsymbol{y}\rangle \right| = \left| \operatorname{tr}(\sigma (O_{0}^{T})^{2}) \right| \\
\leq \left| \left| \left( O_{0}^{T} \right)^{2} \right|_{\infty} \leq \operatorname{tr}(\left( O_{0}^{T} \right)^{2}) = \operatorname{tr}(O_{0}^{2}) \tag{85}$$

$$\left| \sum_{\boldsymbol{x}, \boldsymbol{y}, \boldsymbol{z} \in \mathbb{Z}_{2}^{n}} \operatorname{tr}(|\boldsymbol{x}\boldsymbol{x}\boldsymbol{y}\rangle \langle \boldsymbol{y}\boldsymbol{z}\boldsymbol{z}| (\sigma \otimes O_{0} \otimes O_{0})) \right| = \left| \sum_{\boldsymbol{x}, \boldsymbol{y}, \boldsymbol{z} \in \mathbb{Z}_{2}^{n}} \langle \boldsymbol{y} | \sigma | \boldsymbol{x}\rangle \langle \boldsymbol{z} | O_{0} | \boldsymbol{x}\rangle \langle \boldsymbol{z} | O_{0} | \boldsymbol{y}\rangle \right| = \left| \operatorname{tr}(\sigma O_{0}^{T} O_{0}) \right| \\
\leq \left| \left| \left( O_{0}^{T} \right)^{2} \right|_{\infty} \leq \left| \left( O_{0}^{T} \right)^{2} \right| \leq \left| \left( O_{0}^{T} \right)^{2} \right| \\
\leq \left| \left( O_{0}^{T} \right)^{2} \right|_{\infty} \leq \left| \left( O_{0}^{T} \right)^{2} \right| \leq \left| \left( O_{0}^{T} \right)^{2} \right| \leq \left| \left( O_{0}^{T} \right)^{2} \right| \\
\leq \left| \left( O_{0}^{T} \right)^{2} \right|_{\infty} \leq \left| \left( O_{0}^{T} \right)^{2} \right| \leq \left| \left( O_{0}^{T} \right)$$

$$\leq ||(O_0^T)^2||_{\infty} \leq \operatorname{tr}(|(O_0^T)^2) = \operatorname{tr}(O_0^2)$$
(88)
$$\sum_{x,y,z \in T_2^2} \operatorname{tr}(|yxx\rangle \langle yzz| (\sigma \otimes O_0 \otimes O_0))| = |\sum_{x,y,z \in T_2^2} \langle y| \sigma | y\rangle \langle z| O_0 | x\rangle \langle z| O_0 | x\rangle = |\operatorname{tr}(O_0O_0^T)|$$
(89)
$$\sum_{x,y,z \in T_2^2} \operatorname{tr}(|xyx\rangle \langle zzy| (\sigma \otimes O_0 \otimes O_0))| = |\sum_{x,y,z \in T_2^2} \langle z| \sigma | x\rangle \langle z| O_0 | y\rangle \langle y| O_0 | x\rangle \leq \operatorname{tr}(O_0^2)$$
(90)
$$\sum_{x,y,z \in T_2^2} \operatorname{tr}(|xyx\rangle \langle zyz| (\sigma \otimes O_0 \otimes O_0))| = |\sum_{x,y,z \in T_2^2} \langle z| \sigma | x\rangle \langle y| O_0 | y\rangle \langle z| O_0 | x\rangle \leq (\operatorname{tr}(O_0))^2 = 0$$
(91)
$$\sum_{x,y,z \in T_2^2} \operatorname{tr}(|xyx\rangle \langle yzz| (\sigma \otimes O_0 \otimes O_0))| = |\sum_{x,y,z \in T_2^2} \langle y| \sigma | x\rangle \langle z| O_0 | y\rangle \langle z| O_0 | x\rangle \leq ||O_0O_0^T||_{\infty}$$
(92)
$$\sum_{x,y,z \in T_2^2} \operatorname{tr}(|xxy\rangle \langle yyy| (\sigma \otimes O_0 \otimes O_0))| = |\sum_{x,y,z \in T_2^2} \langle y| \sigma | x\rangle \langle y| O_0 | y\rangle \langle z| O_0 | x\rangle \leq ||O_0O_0^T||_{\infty}$$
(92)
$$\leq \sqrt{\sum_{x,y \in T_2^2} |\langle y| \sigma O_0^T | y\rangle \langle y| O_0 | y\rangle \langle z| O_0 | x\rangle} \leq ||O_0O_0^T||_{\infty}$$
(92)
$$\leq \sqrt{\sum_{y \in T_2^2} |\langle y| \sigma O_0^T | y\rangle \langle y| O_0 | y\rangle |} = \sum_{x,x \in T_2^2} \langle z| O_0 | z\rangle \langle z| O_$$

$$\begin{vmatrix} \sum_{x,y \in \mathbb{Z}_{2}^{n}} \operatorname{tr}(|xxy\rangle \langle yxx| (\sigma \otimes O_{0} \otimes O_{0})) \\ = \left| \sum_{x,y \in \mathbb{Z}_{2}^{n}} \langle x| \sigma^{T} | y \rangle \langle x| O_{0} | x \rangle \langle x| O_{0} | y \rangle \\ = \left| \sum_{x,y \in \mathbb{Z}_{2}^{n}} \langle y| \sigma^{T} | x \rangle \langle y| O_{0} | y \rangle \langle y| O_{0} | x \rangle \right| \leq \operatorname{tr}(O_{0}^{2})(\cdot \cdot \cdot \operatorname{Eq.}(93)) \\ = \left| \sum_{x,y \in \mathbb{Z}_{2}^{n}} \operatorname{tr}(|yxx\rangle \langle yyy| (\sigma \otimes O_{0} \otimes O_{0})) \right| = \left| \sum_{x,y \in \mathbb{Z}_{2}^{n}} \langle y| \sigma | y \rangle \langle y| O_{0} | x \rangle \langle x| O_{0}^{T} | y \rangle \right| \\ \leq \sum_{x,y \in \mathbb{Z}_{2}^{n}} \operatorname{tr}(|yxy\rangle \langle yyy| (\sigma \otimes O_{0} \otimes O_{0})) = \left| \sum_{x,y \in \mathbb{Z}_{2}^{n}} \langle y| \sigma | x \rangle \langle y| O_{0} | x \rangle \langle y| O_{0} | x \rangle \right| \leq \operatorname{tr}(O_{0}^{2}) (\cdot \cdot \cdot \operatorname{Eq.}(93)) \\ = \sum_{x,y \in \mathbb{Z}_{2}^{n}} \operatorname{tr}(|yxx\rangle \langle xyy| (\sigma \otimes O_{0} \otimes O_{0})) = \left| \sum_{x,y \in \mathbb{Z}_{2}^{n}} \langle x| \sigma | y \rangle \langle x| O_{0} | x \rangle \langle y| O_{0} | x \rangle \right| \leq \operatorname{tr}(O_{0}^{2}) (\cdot \cdot \cdot \operatorname{Eq.}(93)) \\ = \sum_{x,y \in \mathbb{Z}_{2}^{n}} \operatorname{tr}(|yxx\rangle \langle xxy| (\sigma \otimes O_{0} \otimes O_{0})) = \left| \sum_{x,y \in \mathbb{Z}_{2}^{n}} \langle x| \sigma | y \rangle \langle x| O_{0} | x \rangle \langle x| O_{0} | x \rangle \right| \leq \operatorname{tr}(O_{0}^{2}) (\cdot \cdot \cdot \operatorname{Eq.}(93)) \\ = \sum_{x,y \in \mathbb{Z}_{2}^{n}} \operatorname{tr}(|yxx\rangle \langle xyx| (\sigma \otimes O_{0} \otimes O_{0})) = \left| \sum_{x,y \in \mathbb{Z}_{2}^{n}} \langle x| \sigma | y \rangle \langle y| O_{0} | x \rangle \langle x| O_{0} | x \rangle \right| \leq \operatorname{tr}(O_{0}^{2}) (\cdot \cdot \cdot \operatorname{Eq.}(93)) \\ = \sum_{x,y \in \mathbb{Z}_{2}^{n}} \operatorname{tr}(|xyx\rangle \langle xyx| (\sigma \otimes O_{0} \otimes O_{0})) = \left| \sum_{x,y \in \mathbb{Z}_{2}^{n}} \langle x| \sigma | x \rangle \langle x| O_{0} | x \rangle \langle x| O_{0} | x \rangle \right| \leq \operatorname{tr}(O_{0}^{2}) (\cdot \cdot \cdot \operatorname{Eq.}(93)) \\ = \sum_{x,y \in \mathbb{Z}_{2}^{n}} \operatorname{tr}(|xyx\rangle \langle xyx| (\sigma \otimes O_{0} \otimes O_{0})) = \left| \sum_{x,y \in \mathbb{Z}_{2}^{n}} \langle x| \sigma | x \rangle \langle x| O_{0} | y \rangle \langle x| O_{0} | x \rangle \right| \leq \operatorname{tr}(O_{0}^{2}) (\cdot \cdot \cdot \operatorname{Eq.}(93)) \\ = \sum_{x,y \in \mathbb{Z}_{2}^{n}} \operatorname{tr}(|xyx\rangle \langle xxx| (\sigma \otimes O_{0} \otimes O_{0})) = \left| \sum_{x,y \in \mathbb{Z}_{2}^{n}} \langle x| \sigma | x \rangle \langle x| O_{0} | y \rangle \langle x| O_{0} | x \rangle \right| \leq \operatorname{tr}(O_{0}^{2}) (\cdot \cdot \cdot \operatorname{Eq.}(93)) \\ = \sum_{x,y \in \mathbb{Z}_{2}^{n}} \operatorname{tr}(|xyx\rangle \langle xxx| (\sigma \otimes O_{0} \otimes O_{0})) = \left| \sum_{x,y \in \mathbb{Z}_{2}^{n}} \langle x| \sigma | x \rangle \langle x| O_{0} | y \rangle \langle x| O_{0} | x \rangle \right| \leq \operatorname{tr}(O_{0}^{2}) (\cdot \cdot \cdot \operatorname{Eq.}(93)) \\ = \sum_{x,y \in \mathbb{Z}_{2}^{n}} \operatorname{tr}(|xyx\rangle \langle xxx| (\sigma \otimes O_{0} \otimes O_{0})) = \left| \sum_{x,y \in \mathbb{Z}_{2}^{n}} \langle x| \sigma | x \rangle \langle x| O_{0} | x \rangle \langle x| O_{0} | x \rangle \right| \leq \operatorname{tr}(O_{0}$$

Throughout the above equations, we used the fact that  $\operatorname{tr}(O_0) = 0$ . Also, Eqs. (86), (87), (89), (92), and (97) do not contribute to  $\mathcal{C}^{(i,ii,iv)}$ , and are thus of no consequence to the ESPOVM analysis, for which we can assume  $O_0$  is real and  $O_0^T = O_0$ . So we can easily note that these can be also upper bounded by  $\operatorname{tr}(O_0^2)$ . Note that values of other cases can be calculated from the above-known cases, by re-parametrizing or transpose-conjugating both sides for example. After realizing that other cases are 0 or upper bounded by  $\operatorname{tr}(O_0^2)$ , based on simple trigonometric inequalities, the remaining equations of Lem. 4 other than Eq. (40) may also be proven.

# The proof of Theorem 2 (ii),(iii)

The mean squared error(MSE) is defined by the sample mean value of the squares of the additive error between estimation and target value. If an estimation variance is  $Var(\hat{\sigma})$ , then for a large sampling-copy number N, MSE is bounded by  $\frac{2Var(\hat{\sigma})}{N}$  (Note that sampling trial-number is N/2 that is why we have the

factor 2). Therefore, to make sure that MSE is below of  $\varepsilon > 0$ , we can impose the sufficient condition as  $N > \frac{2 \text{Var}(\hat{\sigma})}{\varepsilon}$ . So, if Thm. 2 (ii) is proved, the asymptotic lines of Figure 2 (a–c) are explained. Now, let us assume that  $2^n \gg 1$ . We take the RESPOVM first. Recall the Eq. (70).

$$\sum_{|\phi_{\mathbf{A}}^{\text{req}}\rangle \in \mathcal{S}_{n}^{\text{req}}} \frac{2^{2n-1}}{|\mathcal{S}_{n}^{\text{req}}|} \left\langle \phi_{\mathbf{A}}^{\text{req}} \right| \rho \left| \phi_{\mathbf{A}}^{\text{req}} \right\rangle \left\langle \phi_{\mathbf{A}}^{\text{req}} \right| O \left| \phi_{\mathbf{A}}^{\text{req}} \right\rangle = \sum_{\boldsymbol{x} \in \mathbb{Z}_{2}^{n}} \left\langle \boldsymbol{x} \right| \rho \left| \boldsymbol{x} \right\rangle \left\langle \boldsymbol{x} \right| O \left| \boldsymbol{x} \right\rangle + \frac{1}{2} \text{tr}(O) + \text{tr}(O\rho). \tag{105}$$

Then we obtain that

$$\mathbb{E}(\hat{\sigma}_{\mathbf{A}}^{\text{req}})^{2} \\
= \left( \operatorname{tr}(\rho\sigma) + \frac{1}{2} \operatorname{tr}(\sigma) - \sum_{\boldsymbol{x} \in \mathbb{Z}_{2}^{n}} \langle \boldsymbol{x} | \rho | \boldsymbol{x} \rangle \langle \boldsymbol{x} | \sigma | \boldsymbol{x} \rangle \right)^{2} \\
= \operatorname{tr}(\sigma\rho)^{2} + \frac{1}{4} + \sum_{\boldsymbol{x}, \boldsymbol{y} \in \mathbb{Z}_{2}^{n}} \langle \boldsymbol{x} | \rho | \boldsymbol{x} \rangle \langle \boldsymbol{y} | \rho | \boldsymbol{y} \rangle \langle \boldsymbol{x} | \sigma | \boldsymbol{x} \rangle \langle \boldsymbol{y} | \sigma | \boldsymbol{y} \rangle + \operatorname{tr}(\sigma\rho) - 2\operatorname{tr}(\sigma\rho) \sum_{\boldsymbol{x} \in \mathbb{Z}_{2}^{n}} \langle \boldsymbol{x} | \rho | \boldsymbol{x} \rangle \langle \boldsymbol{x} | \sigma | \boldsymbol{x} \rangle \\
- \sum_{\boldsymbol{x} \in \mathbb{Z}_{2}^{n}} \langle \boldsymbol{x} | \rho | \boldsymbol{x} \rangle \langle \boldsymbol{x} | \sigma | \boldsymbol{x} \rangle \\
= \frac{1}{4} + \operatorname{tr}((\sigma \otimes \sigma)(\rho \otimes \rho)) + \sum_{\boldsymbol{x}, \boldsymbol{y} \in \mathbb{Z}_{2}^{n}} \operatorname{tr}\left((\rho^{\otimes 2}\sigma^{\otimes 2})(|\boldsymbol{x}\boldsymbol{y}\rangle \langle \boldsymbol{y}\boldsymbol{x}|^{\otimes 2})\right) + \operatorname{tr}(\sigma\rho) \\
- 2\operatorname{tr}(\sigma\rho) \sum_{\boldsymbol{x} \in \mathbb{Z}^{n}} \operatorname{tr}\left((\rho \otimes \sigma)(|\boldsymbol{x}\boldsymbol{x}\rangle \langle \boldsymbol{x}\boldsymbol{x}|)\right). \tag{106}$$

Now, we use the following famous results:

**Lemma 5** ([17]). For a general N-qubit pure state  $\rho = |\phi\rangle\langle\phi|$ , the following identity holds:

$$\int (d\phi) |\phi\rangle \langle \phi| = \frac{1}{2^n} 1, \qquad (107)$$

$$\int (d\phi) |\phi\rangle \langle\phi|^{\otimes 2} = \frac{1}{2^n(2^n+1)} (1+\tau) , \qquad (108)$$

where 1 is identity operator and  $\tau$  is the swap operator between two tensor product parties. The volume measure  $(d\phi)$  refers to the uniform distribution (Haar-measure) of all single-qubit pure states.

From this, when we averaged over all pure input states  $\rho$ , all terms except  $\frac{1}{4}$  are at most the order of  $\frac{1}{2^n}$  for all  $\sigma$ . Hence, when  $2^n \gg 1$ ,

$$\overline{\mathbb{E}(\hat{\sigma}_{\mathbf{A}}^{\mathrm{req}})^{2}}^{\rho,\sigma} \simeq \frac{1}{4}.\tag{109}$$

Next,

$$\mathbb{E}((\hat{\sigma}_{\mathbf{A}}^{\mathrm{req}})^{2}) = 2^{3n-2} \operatorname{tr} \left( \mathbb{E}_{|\phi_{\mathbf{A}}^{\mathrm{req}}\rangle \in \mathcal{D}(\mathcal{S}_{n}^{\mathrm{req}})} |\phi_{\mathbf{A}}^{\mathrm{req}}\rangle \langle \phi_{\mathbf{A}}^{\mathrm{req}}|^{\otimes 3} \rho \otimes \sigma^{\otimes 2} \right)$$
(110)

$$\to \overline{\mathbb{E}((\hat{\sigma}_{\mathbf{A}}^{\text{req}})^2)}^{\rho} = 2^{2n-2} \operatorname{tr} \left( \mathbb{E}_{|\phi_{\mathbf{A}}^{\text{req}}\rangle \in \mathcal{D}(\mathcal{S}_n^{\text{req}})} |\phi_{\mathbf{A}}^{\text{req}}\rangle \langle \phi_{\mathbf{A}}^{\text{req}}|^{\otimes 2} \sigma^{\otimes 2} \right) \text{ ($\cdot :$ Lem. 5$)}. \tag{111}$$

Now, since  $\sigma$  is pure and real, let us rewrite  $\sigma = |\phi\rangle\langle\phi|$  where  $|\phi\rangle = \sum_{\boldsymbol{i}\in\mathbb{Z}_2^n} c_{\boldsymbol{i}} |\boldsymbol{i}\rangle$   $(c_{\boldsymbol{i}}\in\mathbb{R})$ . Then  $|\phi\rangle\langle\phi|^{\otimes 2} = \sum_{\boldsymbol{i},\boldsymbol{j},\boldsymbol{k},\boldsymbol{l}\in\mathbb{Z}_2^n} c_{\boldsymbol{i}} c_{\boldsymbol{j}} c_{\boldsymbol{k}} c_{\boldsymbol{l}} |\boldsymbol{i}\boldsymbol{j}\rangle\langle\boldsymbol{k}\boldsymbol{l}|$ . Since  $\boldsymbol{c}$  lies on hypersphere  $S^{2^n-1}$ , we obtain that from Lem. 1,

$$\overline{\mathbb{E}((\hat{\sigma}_{\mathbf{A}}^{\text{req}})^{2})}^{\rho,\sigma} \qquad (112)$$

$$= \frac{1}{4A} \int_{S^{2^{n}-1}} d^{2^{n}-1} \Omega \cdot \sum_{\boldsymbol{x},\boldsymbol{y} \in \mathbb{Z}_{2}^{n}} (|\boldsymbol{x}\boldsymbol{y}\rangle \langle \boldsymbol{x}\boldsymbol{y}| + |\boldsymbol{x}\boldsymbol{y}\rangle \langle \boldsymbol{y}\boldsymbol{x}| + |\boldsymbol{x}\boldsymbol{x}\rangle \langle \boldsymbol{y}\boldsymbol{y}| - 2|\boldsymbol{x}\boldsymbol{x}\rangle \langle \boldsymbol{x}\boldsymbol{x}|) \sum_{\boldsymbol{i},\boldsymbol{j},\boldsymbol{k},\boldsymbol{l}} c_{\boldsymbol{i}}c_{\boldsymbol{j}}c_{\boldsymbol{k}}c_{\boldsymbol{l}}|\boldsymbol{i}\boldsymbol{j}\rangle \langle \boldsymbol{k}\boldsymbol{l}|$$

$$= \frac{1}{4A} \sum_{\boldsymbol{x},\boldsymbol{y}} \int_{S^{2^{n}-1}} 3c_{\boldsymbol{x}}^{2}c_{\boldsymbol{y}}^{2} - 2c_{\boldsymbol{x}}^{4} d^{2^{n}-1}\Omega, \qquad (113)$$

where A is area of surface of  $S^{2^{n}-1}$ . Note that the sphere is invariant under permutation hence,

$$\overline{\mathbb{E}((\hat{\rho}_{\mathbf{A}}^{\text{req}})^2)}^{\rho,\sigma} = \frac{1}{4A} \left\{ 2^n \int_{S^{2^n-1}} c_1^4 d^{2^n-1}\Omega + 3 \cdot 2^n (2^n - 1) \int_{S^{2^n-1}} c_1^2 c_2^2 d^{2^n-1}\Omega \right\}. \tag{114}$$

We will separately calculate the first and second terms of the right-hand side. First,

$$\int_{S^{2^{n}-1}} c_1^4 d^{2^n-1}\Omega = \oint \cos^4(\phi_1) \sin^{2^n-2}(\phi_1) \sin^{2^n-3}(\phi_2) \cdots \sin(\phi_{2^n-2}) d\phi_1 d\phi_2 d\phi_3 \cdots d\phi_{2^n-1} 
(\text{where } 0 \le \phi_1, \phi_2 \dots, \phi_{2^n-2} \le \pi, \ 0 \le \phi_{2^n-1} \le 2\pi)$$

$$= \oint d^{2^n-1}\Omega \cdot \frac{\int_0^{\pi} \cos^4(\phi_1) \sin^{2^n-2}(\phi_1) d\phi_1}{\int_0^{\pi} \sin^{2^n-2}(\phi_1) d\phi_1} = \frac{A \int_0^{\frac{\pi}{2}} \cos^4(\phi_1) \sin^{2^n-2}(\phi_1) d\phi_1}{\int_0^{\frac{\pi}{2}} \sin^{2^n-2}(\phi_1) d\phi_1}. \tag{115}$$

now we use the formula,

$$\int_0^{\frac{\pi}{2}} \sin^m(\phi) d\phi = \begin{cases} \frac{\pi}{2} \left( \frac{m!}{2^m \left( \left( \frac{m!}{2}! \right) \right)^2} \right) & \text{if } m \text{ is even} \\ \frac{2^{m-1} \left( \left( \frac{m-1}{2} \right)! \right)^2}{m!} & \text{if } m \text{ is odd,} \end{cases}$$
(116)

and the beta function  $\frac{1}{2}B(p,q) = \frac{\Gamma(p)\Gamma(q)}{2\Gamma(p+q)} = \int_0^{\frac{\pi}{2}} \sin^{2p-1}(\phi) \cos^{2q-1}(\phi) d\phi$ , where  $\Gamma(p)$  is gamma function. Then we obtain that with Stirling's formula,

$$\int_{S^{2^{n-1}}} c_1^4 d^{2^n - 1} \Omega$$

$$= \frac{A}{\pi} \cdot \frac{B(\frac{5}{2}, 2^{n-1} - \frac{1}{2})}{\left(\frac{(2^n - 2)!}{2^{(2^n - 2)((2^{n-1} - 1)!)^2}}\right)}$$

$$\simeq \frac{A}{\pi} \Gamma\left(\frac{5}{2}\right) \frac{2^{2^n - 2}}{(2^{n-1} + 1)2^{n-1}} \cdot \sqrt{2\pi e} \cdot \sqrt{\frac{(2^{n-1} - \frac{3}{2})(2^{n-1} - 1)}{2^n - 2}} \cdot \frac{(2^{n-1} - \frac{3}{2})^{2^{n-1} - \frac{3}{2}}(2^{n-1} - 1)^{2^{n-1} - 1}}{(2^n - 2)^{2^n - 2}}$$

$$\simeq \frac{A}{\pi} \Gamma\left(\frac{5}{2}\right) \sqrt{2\pi e} \cdot 2^{2^n - \frac{5n}{2} - 1} \cdot \frac{(2^{n-1} - \frac{3}{2})^{2^{n-1} - \frac{3}{2}}(2^{n-1} - 1)^{2^{n-1} - 1}}{(2^n - 2)^{2^n - 2}}.$$
(117)

Note that

$$\log_2(C) \simeq \left(2^n - \frac{5n}{2} - 1\right) + \left(2^{n-1} - \frac{3}{2}\right)(n-1) + (2^{n-1} - 1)(n-1) - (2^n - 2)n)$$

$$= (-3n + \frac{3}{2})$$

$$\rightarrow \therefore \frac{1}{A} \int_{C^{2^n - 1}} c_1^4 d^{2^n - 1}\Omega \simeq \frac{1}{\pi} \Gamma\left(\frac{5}{2}\right) \sqrt{2\pi e} \cdot 2^{-3n + \frac{3}{2}}.$$
(118)

Let us go to the second term.

$$\int_{S^{2^{n}-1}} \mathbf{c}_{1}^{2} \mathbf{c}_{2}^{2} d^{2^{n}-1} \Omega \tag{120}$$

$$= \oint \cos^{2}(\phi_{1}) \cos^{2}(\phi_{2}) \sin^{2}(\phi_{2}) \sin^{2^{n}-2}(\phi_{1}) \sin^{2^{n}-3}(\phi_{2}) \cdots \sin(\phi_{2^{n}-2}) d\phi_{1} d\phi_{2} d\phi_{3} \cdots d\phi_{2^{n}-1}$$

$$(\text{where } 0 \leq \phi_{1}, \phi_{2}, \dots, \phi_{2^{n}-2} \leq \pi, \quad 0 \leq \phi_{2^{n}-1} \leq 2\pi)$$

$$= \oint d^{2^{n}-1} \Omega \cdot \frac{\int_{0}^{\pi} \cos^{2}(\phi_{1}) \sin^{2^{n}-2}(\phi_{1}) d\phi_{1}}{\int_{0}^{\pi} \sin^{2^{n}-2}(\phi_{1}) d\phi_{1}} \cdot \frac{\int_{0}^{\pi} \cos^{2}(\phi_{2}) \sin^{2^{n}-1}(\phi_{2}) d\phi_{2}}{\int_{0}^{\pi} \sin^{2^{n}-3}(\phi_{2}) d\phi_{2}}$$

$$= \frac{A}{2\pi} \cdot \frac{B(\frac{3}{2}, 2^{n-1} - \frac{1}{2}) B(\frac{3}{2}, 2^{n-1})}{\left(\frac{2^{2^{n}-4}((2^{n}-1-2)!)^{2}}{(2^{n}-3)!}\right) \left(\frac{2^{2^{n}-4}((2^{n}-1-2)!)^{2}}{(2^{n}-3)!}\right)} = \frac{2A}{\pi} \cdot \frac{\Gamma(\frac{3}{2})^{2} (2^{n-1} - \frac{3}{2})! (2^{n-1} - 1)! (2^{n-1} - 1)^{2}}{(2^{n}-2)(2^{n-1})! (2^{n-1} + \frac{1}{2})}$$

$$= \frac{2A}{\pi} \Gamma\left(\frac{3}{2}\right)^2 \frac{(2^{n-1})^2}{(2^n - 2)2^{n-1}(2^{n-1} + \frac{1}{2})(2^{n-1} - \frac{1}{2})} \simeq A \cdot 2^{-2n} \left[ :: \Gamma\left(\frac{3}{2}\right) = \frac{\sqrt{\pi}}{2} \right]. \tag{121}$$

Therefore, substituting the Eq. (117), (118), (109), and (120) into Eq. (114) leads to

$$\overline{\mathrm{Var}(\hat{O}_{\mathbf{A}}^{\mathrm{req}})}^{\rho,\sigma} = \overline{\mathbb{E}((\hat{\sigma}_{\mathbf{A}}^{\mathrm{req}})^2)}^{\rho,\sigma} - \overline{\mathbb{E}(\hat{\sigma}_{\mathbf{A}}^{\mathrm{req}})^2}^{\rho,\sigma} \simeq \frac{1}{2}.$$
 (122)

Next, let us direct our attention to ESPOVM. As we proceed in a similar manner, we may skip most of the steps but note that

$$\sum_{|\phi_{\mathbf{A}}^{\text{req}}\rangle \in \mathcal{S}_{n}^{\text{eq}}} \frac{2^{2n}}{|\mathcal{S}_{n}^{\text{req}}|} \left\langle \phi_{\mathbf{A}}^{\text{req}} \right| \rho \left| \phi_{\mathbf{A}}^{\text{req}} \right\rangle \left\langle \phi_{\mathbf{A}}^{\text{req}} \right| O \left| \phi_{\mathbf{A}}^{\text{req}} \right\rangle = \sum_{\boldsymbol{x} \in \mathbb{Z}_{2}^{n}} \left\langle \boldsymbol{x} \right| \rho \left| \boldsymbol{x} \right\rangle \left\langle \boldsymbol{x} \right| O \left| \boldsymbol{x} \right\rangle + \text{tr}(O) + \text{tr}(O\rho),$$
(123)

and

$$\overline{\mathbb{E}((\hat{\sigma}_{\mathbf{A}}^{\mathrm{eq}})^{2})}^{\rho,\sigma} = \frac{1}{A} \int_{\boldsymbol{c} \in S^{2^{n}-1}} d^{2^{n}-1} \Omega \cdot \sum_{\boldsymbol{x},\boldsymbol{y} \in \mathbb{Z}_{2}^{n}} (|\boldsymbol{x}\boldsymbol{y}\rangle \langle \boldsymbol{x}\boldsymbol{y}| + |\boldsymbol{x}\boldsymbol{y}\rangle \langle \boldsymbol{y}\boldsymbol{x}| - |\boldsymbol{x}\boldsymbol{x}\rangle \langle \boldsymbol{x}\boldsymbol{x}|) \sum_{i,j,k,l} c_{i} c_{j} c_{k} c_{l} |\boldsymbol{i}\boldsymbol{j}\rangle \langle \boldsymbol{k}\boldsymbol{l}|$$

$$= \frac{1}{A} \sum_{\boldsymbol{x},\boldsymbol{y}} \int_{\boldsymbol{c} \in S^{2^{n}-1}} 2c_{\boldsymbol{x}}^{2} c_{\boldsymbol{y}}^{2} - c_{\boldsymbol{x}}^{4} d^{2^{n}-1} \Omega, \tag{124}$$

By the same method with RESPOVM, we can find that

$$\overline{\mathbb{E}((\hat{\sigma}_{\mathbf{A}}^{\mathrm{eq}})^{2})}^{\rho,\sigma} \simeq 2, \text{ and } \overline{\mathbb{E}(\hat{\sigma}_{\mathbf{A}}^{\mathrm{eq}})^{2}}^{\rho,\sigma} \simeq 1, \rightarrow \overline{\mathrm{Var}(\hat{O}_{\mathbf{A}}^{\mathrm{eq}})}^{\rho,\sigma} = \overline{\mathbb{E}((\hat{\sigma}_{\mathbf{A}}^{\mathrm{eq}})^{2})}^{\rho,\sigma} - \overline{\mathbb{E}(\hat{\sigma}_{\mathbf{A}}^{\mathrm{eq}})^{2}}^{\rho,\sigma} \simeq 1.$$
 (125)

Lastly, for both ESPOVM and RESPOVM,

$$\mathbb{E}((\hat{\sigma}^{\text{bin}})^2) = \sum_{\boldsymbol{x}} \langle \boldsymbol{x} | \rho | \boldsymbol{x} \rangle |\langle \boldsymbol{x} | \sigma | \boldsymbol{x} \rangle|^2 = \sum_{\boldsymbol{x}} \operatorname{tr}((\rho \otimes \sigma \otimes \sigma) | \boldsymbol{x} \boldsymbol{x} \boldsymbol{x} \rangle \langle \boldsymbol{x} \boldsymbol{x} \boldsymbol{x} |)$$
(126)

$$\to \overline{\mathbb{E}((\hat{\sigma}^{\text{bin}})^2)}^{\rho} = \frac{1}{2^n} \sum_{\boldsymbol{x}} (\langle \boldsymbol{x} | \, \sigma \, | \boldsymbol{x} \rangle)^2 \simeq 0. \tag{127}$$

Hence, even if we average over real pure states  $\sigma$ , the result will be nearly 0. Lastly, let us consider randomized-Clifford tomography. Then, we can refer to Eq. (S43) of Ref. [9] stating that the estimation variance is equal to the *shadow norm* without maximizing over  $\rho$  and it is,

$$\operatorname{Var}(\hat{\sigma}^{\mathrm{s}}) = \frac{2^{n} + 1}{2^{n} + 2} \left( \operatorname{tr}(\rho) \operatorname{tr}\left( (\sigma - \frac{\mathbb{I}}{2^{n}})^{2} \right) + 2\operatorname{tr}\left( \rho(\sigma - \frac{\mathbb{I}}{2^{n}})^{2} \right) \right) - \left( \operatorname{tr}\left( \rho(\sigma - \frac{\mathbb{I}}{2^{n}}) \right) \right)^{2}. \tag{128}$$

After we average over pure  $\rho$ , by Lem. 5, we the second and last terms are ignored and

$$\overline{\operatorname{Var}(\hat{\sigma}^{\mathrm{s}})}^{\rho,\sigma} \simeq \overline{\operatorname{tr}\left(\sigma^{2} - \frac{2\sigma}{2^{n}} + \frac{\mathbb{I}}{4^{n}}\right)^{\sigma}} \simeq 1, \qquad (129)$$

which settles the proof for Thm. 2 (ii). Note that RESPOVM gives half the average variance than even randomized-Clifford. Since we need two input states for a single sampling trial, the number of states is not improved but we can reduce the total gate count for the whole estimation process. This is because in RESPOVM, half of the input-state copies are used for direct Z-basis measurement.

The proof of Thm. 2 (iii) is much simpler. We start with

$$\overline{\mathbb{E}((\hat{\sigma}_{\mathbf{A}}^{\mathrm{eq}})^{2})}^{\rho} = 2^{2n} tr\left(\mathbb{E}_{|\phi_{\mathbf{A}}^{\mathrm{eq}}\rangle \in \mathcal{D}(\mathcal{S}_{n}^{\mathrm{eq}})} |\phi_{\mathbf{A}}^{\mathrm{eq}}\rangle \langle \phi_{\mathbf{A}}^{\mathrm{eq}}|^{\otimes 2} \sigma^{\otimes 2}\right). \tag{130}$$

By averaging over Haar-random pure state  $\sigma$ , by Lem. 5 and using the fact that  $\operatorname{tr}((\rho \otimes \sigma)\tau) = \operatorname{tr}(\rho\sigma)$ , we conclude that  $\overline{\mathbb{E}((\hat{\sigma}_{\mathbf{A}}^{\operatorname{eq}})^2)}^{\rho,\sigma} \simeq 2$ . Also,  $\overline{\mathbb{E}(\hat{\sigma}_{\mathbf{A}}^{\operatorname{eq}})^2}^{\rho,\sigma} \simeq 1$ , in exactly the same way as with Eq. (123). Hence  $\overline{\operatorname{Var}(\hat{\sigma}_{\mathbf{A}}^{\operatorname{eq}})^2}^{\rho,\sigma} = \overline{\mathbb{E}((\hat{\sigma}_{\mathbf{A}}^{\operatorname{eq}})^2)}^{\rho,\sigma} - \overline{\mathbb{E}(\hat{\sigma}_{\mathbf{A}}^{\operatorname{eq}})^2}^{\rho,\sigma} \simeq 1$ . Furthermore, similar to Eq. (129), the average variance of random Clifford tomography is also 1. The proof is thus completed.

# Informational completeness of ESPOVM+computational basis

In this section, we prove that the ESPOVM+computational basis is informationally complete (IC) so that this POVM can fully extract all density-matrix information of any given input state. Explicitly, the condition for informational completeness of the POVM  $\{\Pi_j\}_{j\in J}$ , where J is an index set and  $\Pi_j>0$  for all  $j\in J$ , necessitates that any quantum state be expressible as a linear combination of the elements  $\Pi_j$ .

We now prove the following lemmas:

**Lemma 6.** For a d-dimensional Hilbert space, a POVM, comprising a set of  $M \ge d^2$  positive-operator elements  $\Pi_i$  that sum to the identity, is IC if the matrix

$$\mathbf{V} = (|\Pi_1\rangle\rangle |\Pi_2\rangle\rangle \cdots |\Pi_M\rangle\rangle) \tag{131}$$

has rank  $d^2$ , and only then. Here  $|\Pi_j\rangle\rangle$  is a basis-dependent superket (vectorization) of  $\Pi_j$ .

*Proof.* Since **V** has rank  $d^2 = \dim(\mathbb{C}^d \otimes \mathbb{C}^d)$  if and only if it spans a set of vectorized quantum states. By reversing the vectorization (which is an injective map), we note that all quantum state can be expressed as a linear combination of  $\{\Pi_i\}$ .

**Lemma 7.** A POVM  $\{\Pi_i\}$  is IC if the frame operator [43]

$$\mathcal{F} \equiv \sum_{j=1}^{M} \frac{|\Pi_{j}\rangle\rangle \langle\langle \Pi_{j}|}{\operatorname{tr}(\Pi_{j})}$$
(132)

is invertible, and only then.

*Proof.* Suppose we have the IC POVM. Clearly from Lem. 6, rank  $\{\mathbf{V}\} = d^2$ , with  $d = 2^n$  in our multiqubit context. Note that  $\mathcal{F} \cong \mathbf{V} \mathbf{\Pi}^{-1} \mathbf{V}^{\dagger}$ , where

$$\mathbf{\Pi} = \begin{pmatrix} \operatorname{tr}(\Pi_1) & 0 & \cdots & 0 \\ 0 & \operatorname{tr}(\Pi_2) & \cdots & 0 \\ \vdots & \vdots & \ddots & \vdots \\ 0 & 0 & \cdots & \operatorname{tr}(\Pi_M) \end{pmatrix} .$$
(133)

Now, we use the fact that for an arbitrary (non-square) complex matrix A,  $\operatorname{rank}\{A^{\dagger}\} = \operatorname{rank}\{A\} = \operatorname{rank}\{A^{\dagger}A\}$  [80]. Then, after setting  $A = \sqrt{\Pi^{-1}}V^{\dagger}$ , we have  $\operatorname{rank}\{\mathcal{F}\} = \operatorname{rank}\{V\sqrt{\Pi^{-1}}\}$ . Since  $\sqrt{\Pi^{-1}}$  is invertible, it is easy to note that  $\operatorname{rank}\{V\sqrt{\Pi^{-1}}\} = \operatorname{rank}\{V\}$ , so that  $\operatorname{rank}\{\mathcal{F}\} = \operatorname{rank}\{V\} = d^2$ . As  $\mathcal{F}$  is  $d^2$  by  $d^2$  matrix, it is therefore invertible.

Conversely, suppose that  $\mathcal{F}^{-1}$  exists. Then  $\operatorname{rank}\{\mathcal{F}\}=d^2$ . Since  $\operatorname{rank}\{\mathcal{F}\}\leq \operatorname{rank}\{\mathbf{V}\}\leq d^2$ , we conclude that  $\operatorname{rank}\{\mathbf{V}\}=d^2$ . By Lem. 6,  $\{\Pi_j\}_{j\in J}$  is IC.

**Proposition 4.** The collection of ESPOVM and computational basis forms an IC measurement. However, ESPOVM itself is not an IC POVM.

*Proof.* First, we calculate the frame operator of the ESPOVM.

$$\mathcal{F}_{\text{es}} = \sum_{|\phi_{\mathbf{A}}^{\text{eq}}\rangle \in \mathcal{S}_n^{\text{eq}}} \frac{2^n}{|\mathcal{S}_n^{\text{eq}}|} |\phi_{\mathbf{A}}^{\text{eq}}\rangle \left( \langle \phi_{\mathbf{A}}^{\text{eq}} | \right)^T \langle \phi_{\mathbf{A}}^{\text{eq}} | \left( \langle \phi_{\mathbf{A}}^{\text{eq}} | \right)^* = 2^n \left( \mathbb{E}_{|\phi_{\mathbf{A}}^{\text{eq}}\rangle \in \mathcal{D}(\mathcal{S}_n^{\text{eq}})} |\phi_{\mathbf{A}}^{\text{eq}}\rangle \langle \phi_{\mathbf{A}}^{\text{eq}} |^{\otimes 2} \right)^{T_2}, \tag{134}$$

where  $T_2$  means partial transpose for the second part. From Lem. 1, we note that

$$\mathcal{F}_{es} = \frac{1}{2^n} \left( 1 + \sum_{\boldsymbol{x}, \boldsymbol{y} \in \mathbb{Z}_2^n} |\boldsymbol{x}\boldsymbol{x}\rangle \langle \boldsymbol{y}\boldsymbol{y}| - \sum_{\boldsymbol{x} \in \mathbb{Z}_2^n} |\boldsymbol{x}\boldsymbol{x}\rangle \langle \boldsymbol{x}\boldsymbol{x}| \right) = \frac{1}{2^n} \left( 1 + \sum_{\boldsymbol{x} \in \mathbb{Z}_2^n} \sum_{\boldsymbol{y} \neq \boldsymbol{x} \in \mathbb{Z}_2^n} |\boldsymbol{x}\boldsymbol{x}\rangle \langle \boldsymbol{y}\boldsymbol{y}| \right). \tag{135}$$

One can show that the operator  $W = \sum_{\boldsymbol{x} \in \mathbb{Z}_2^n} \sum_{\boldsymbol{y} \neq \boldsymbol{x} \in \mathbb{Z}_2^n} |\boldsymbol{x}\boldsymbol{x}\rangle \langle \boldsymbol{y}\boldsymbol{y}|$  has at least one eigenvalue equal to -1 by inspecting its action on  $|\boldsymbol{z}\boldsymbol{z}\rangle$  for any  $\boldsymbol{z} \in \mathbb{Z}_2^n$ ,

$$W|zz\rangle = \sum_{x \neq z \in \mathbb{Z}_2^n} |xx\rangle = \sum_{x \in \mathbb{Z}_2^n} |xx\rangle - |zz\rangle.$$
 (136)

It follows that any ket  $(|z_1, z_1\rangle - |z_2, z_2\rangle)/\sqrt{2}$  with  $z_1, z_2 \in \mathbb{Z}_2^n$  is an eigenket in the "-1"-eigenvalue subspace. As a side note, it is easy to check that the superposition  $|\phi\rangle \equiv \sum_{z\in\mathbb{Z}_2^n} |z,z\rangle \, 2^{-n/2}$  is an eigenket that gives a positive eigenvalue of  $2^n - 1$ ,

$$W \sum_{\boldsymbol{z} \in \mathbb{Z}_2^n} |\boldsymbol{z}\boldsymbol{z}\rangle \, 2^{-n/2} = \sum_{\boldsymbol{x} \in \mathbb{Z}_2^n} |\boldsymbol{x}\boldsymbol{x}\rangle \sum_{\boldsymbol{z} \neq \boldsymbol{x} \in \mathbb{Z}_2^n} 2^{-n/2} = \sum_{\boldsymbol{x} \in \mathbb{Z}_2^n} |\boldsymbol{x}\boldsymbol{x}\rangle \, 2^{-n/2} (2^n - 1) \,. \tag{137}$$

We may then conclude that  $\mathcal{F}_{es}$  has at least one null eigenvalue. Based on Lem. 7, it follows that the ESPOVM is non-IC.

Upon recognizing that  $\sum_{\boldsymbol{x} \in \mathbb{Z}_2^n} |\boldsymbol{x}\boldsymbol{x}\rangle \langle \boldsymbol{x}\boldsymbol{x}|$  is the frame operator  $\mathcal{F}_{\text{comp}}$  for the computational basis, the total frame operator may be written as

$$\mathcal{F} = \mathcal{F}_{es} + \mathcal{F}_{comp} = \frac{1}{2^{n}} \left( 1 + \sum_{\boldsymbol{x}, \boldsymbol{y} \in \mathbb{Z}_{2}^{n}} |\boldsymbol{x}\boldsymbol{x}\rangle \langle \boldsymbol{y}\boldsymbol{y}| - \mathcal{F}_{comp} \right) + \mathcal{F}_{comp}$$

$$= (1 - 2^{n}) \mathcal{F}_{es} + 1 + \sum_{\boldsymbol{x}, \boldsymbol{y} \in \mathbb{Z}_{2}^{n}} |\boldsymbol{x}\boldsymbol{x}\rangle \langle \boldsymbol{y}\boldsymbol{y}|$$

$$= \frac{1}{2^{n}} + |\phi\rangle \langle \phi| + (1 - \frac{1}{2^{n}}) \sum_{\boldsymbol{x} \in \mathbb{Z}_{2}^{n}} |\boldsymbol{x}\boldsymbol{x}\rangle \langle \boldsymbol{x}\boldsymbol{x}| > 0.$$
(138)

Therefore,  $\mathcal{F}$  has full-rank (with all positive eigenvalues) and is invertible. By Lem. 7, ES-POVM+computational basis is IC POVM.

# CNOT—CZ—CNOT decomposition of a CZ circuit

Here, we show the method to transform any CZ circuit into the form CNOT—CZ—CNOT so that we may then ignore the last CNOT section for (R)ESPOVM. This will further improve the gate reduction via the Patel-Markov-Hayes(PMH) construction [52]. Note that a CZ circuit can be defined by a binary-valued quadratic function Q(x) and the mapping

$$CZ: |\mathbf{x}\rangle \mapsto (-1)^{Q(\mathbf{x})} |\mathbf{x}\rangle$$
 (139)

on the computational basis. Now, we rewrite  $Q_{\{1,2,\ldots,k\}}$  as a quadratic function not having  $x_1$  or  $x_2$  or  $\ldots$  or  $x_k$ . We can then express  $Q(\boldsymbol{x})$  as  $c_1x_1L_{\{1\}}(\boldsymbol{x})+Q_{\{1\}}(\boldsymbol{x})$ , where  $c_1\in\{0,1\}$  and  $L_{\{1,2,\ldots,k\}}$  is a linear function not having variables  $x_1$  or  $x_2$  or  $\ldots$  or  $x_k$ . Next, we find the linear transformation  $S_1$  such that maps  $x_{i_1}$  to  $L_{\{1\}}(\boldsymbol{x})$  where  $x_{i_1}$  is a single term contained in  $L_{\{1\}}(\boldsymbol{x})$ , and makes other variables intact. This is invertible transformation and maps  $Q(\boldsymbol{x})$  to  $Q_1(\boldsymbol{x})=c_1x_1x_{i_1}+Q'_{\{1\}}(\boldsymbol{x})$ , where  $Q'_{\{1\}}(\boldsymbol{x})$  is some quadratic polynomial.

The same procedure may then be repeated for  $Q_{\{1\}}^{(1)}(\boldsymbol{x})$  to become  $Q_1(\boldsymbol{x}) = c_1x_1x_{i_1} + c_2x_2x_{i_2} + Q'_{\{1,2\}}(\boldsymbol{x})$ . After n-1 repetitions, we obtain the transformations  $S_1, S_2, \ldots, S_{n-1}$  to map the function  $Q_L(\boldsymbol{x}) \equiv c_1x_1x_{i_1} + c_2x_2x_{i_2} + \ldots + c_{n-1}x_{n-1}x_{i_{n-1}} + L^{(1,2,\ldots,n-1)}(\boldsymbol{x})$ , where  $L^{(1,2,\ldots,n-1)}(\boldsymbol{x})$  is some linear function

From these elements, we can implement the original CZ circuit in a different yet equivalent way. We first implement CNOT-gate mapping  $|x\rangle \mapsto |(S_1S_2\dots S_{n-1})^{-1}(x)\rangle$  and then we utilize the CZ+Z mapping  $|x\rangle \mapsto (-1)^{Q_L(x)}|x\rangle$ , and finally take CNOT gates for  $S_1S_2\dots S_{n-1}$  to send  $|(S_1S_2\dots S_{n-1})^{-1}(x)\rangle$  back to  $|x\rangle$ . If an X-basis measurement is performed after that, there is no need to physically enact the last CNOT section and just, instead, treat it as linear post-processing of the measurement outcome.

# Linear nearest-neighboring (LNN) architecture of CZ circuit [38]

In this section, we explain how to transform the arbitrary CZ circuit to the 2n + 2-depth LNN form, which has only neighboring CNOT gates. Since we used the technique by Ref. [38], we recommend readers who are interested in Clifford circuit synthesis refer to this paper. This section is for introducing only the information of Ref. [38] we need.

The actual circuit we transform is the so-called  $\widehat{CZ}$  circuit. This is defined by CZ circuit followed by qubit-reversal layers, REV:  $|x_1, x_2, \dots, x_n\rangle \mapsto |x_n, x_{n-1}, \dots, x_1\rangle$ . However, the CZ section is equal to CZ-REV-REV and the last REV can be ignored by reversing the measurement outcome if we only do the

non-adaptive measurement. Hence if  $\widehat{\text{CZ}}$  can be transformed to 2n+2-depth LNN architecture, the proof is done.

Now, consider some arbitrary  $\widehat{CZ}$  circuit. We will prove only when n is odd. Proof for even n follows similarly. Suppose we take  $|x_1, x_2, \ldots, x_n\rangle$  as an input. Next, we define two unitaries

$$C_1 \equiv \text{CNOT}_{1\to 2} \text{CNOT}_{3\to 4} \dots \text{CNOT}_{n-2\to n-1} \text{CNOT}_{3\to 2} \text{CNOT}_{5\to 4} \dots \text{CNOT}_{n\to n-1}$$
(140)

$$C_2 \equiv \text{CNOT}_{2\to 1} \text{CNOT}_{4\to 3} \dots \text{CNOT}_{n-1\to n-2} \text{CNOT}_{2\to 3} \text{CNOT}_{4\to 5} \dots \text{CNOT}_{n-1\to n}. \tag{141}$$

and  $C \equiv C_1 C_2$ . Now, let n = 2m + 1. If we operate C to input as  $t \leq m$ -times, the output state is

$$C^{t}|x_{1}, x_{2}, \dots, x_{n}\rangle = |\bigoplus_{i=1}^{n} [Pj(n-3-2(t-1)+i), Pk(2(t-1)+i)]\rangle$$
 (142)

where we defined  $[x_j, x_k](x_j \neq x_k) \equiv x_j \oplus x_{j+1} \oplus \cdots \oplus x_k, [x_j, x_j] \equiv x_j$  and the patterns,

$$Pj \equiv (n-1, n-3, n-3, \dots, 4, 4, 2, 2, 1, 1, 3, 3, \dots, n-2, n-2)$$
(143)

$$Pk \equiv (3, 3, 5, 5, \dots, n, n, n - 1, n - 1, n - 3, n - 3, \dots, 6, 6, 4, 4, 2). \tag{144}$$

Note that both are of length 2n-3. We note that given  $t \leq m$  and  $i \in [n]$ , there's no case when [Pj(n-3-2(t-1)+i), Pk(2(t-1)+i)] is equal with [Pj(n-3-2(t'-1)+i'), Pk(2(t'-1)+i')] for the other  $t' \leq m$  and  $i' \in [n]$ . This is schematically seen in Ref. [38]. Also, the number of tuples obtained during  $t=0,1,\ldots,m$  is  $(m+1)n=\frac{n(n+1)}{2}=_n C_2+n$ . Those facts mean that after we recorded all elements of output ket at each step we operate S, for m-times, we can see all [j,k]  $(j,k \in [n])$ . Note that [j,j] can be seen at the starting point (t=0).

Now, we show that  $C^{m+1}$  is a qubit reversal. After the m-th operation, we operate C one more time and let us calculate the p-th qubit output of the output state, and let p be even. By neighboring property, we just need to sum the  $\{p-1,p,p+1\}$ -th inputs. The result is  $[n-(2\lfloor\frac{p-1}{2}\rfloor+1),n-(2\lfloor\frac{p-2}{2}\rfloor-1)] \oplus [n-(2\lfloor\frac{p}{2}\rfloor+1),n-(2\lfloor\frac{p-1}{2}\rfloor+1)] \oplus [n-(2\lfloor\frac{p+1}{2}\rfloor+1),n-(2\lfloor\frac{p}{2}\rfloor+1)] = n-p+1$ , which is reversal of p. We can also note that the result of odd p is also a reversal. Therefore we conclude that  $S^{m+1}$  is a qubit reversal by a similar method.

Second, we remember that in Sec. 4.3 of "Methods" in the main text, we defined  $y_i = x_1 \oplus x_2 \oplus \ldots \oplus x_i$ . Under this context,  $y_i = [1,i]$  and  $y_j \oplus y_k = [j+1,k]$ . Hence we can achieve  $i^{u_j y_j}$  and  $i^{u_{j,k}(y_j \oplus y_k)}$   $(u_j, u_{j,k} \in \mathbb{Z}_4)$  by inserting phase gate in each sections of C-operated output, or at the starting point. Also, the depth of the LNN architecture is 4(m+1) = 2n+2. The 1-1 mapping  $(t,i) \leftrightarrow [Pj(n-3-2(t-1)+i), Pk(2(t-1)+i)]$  must be recorded in  $\mathcal{O}(n^2)$ -memory before the circuit sampling so that we do not need to be bothered with the time to find the right location of phase gate insertion. A similar manner can be used in the case when n is even but with slightly different  $C_1, C_2$ , and patterns [38]. In conclusion, we can achieve  $\widehat{CZ}$  operation with only neighboring CNOT and phase gates with 2n+2-depth. Lastly, we note that Y-basis measurements can be done by X-basis measurements after phase gates. If we operate these phase operations before the CZ action and transform the CZ circuit to LNN architecture, 2-depth rightmost CNOT gates can be ignored for (R)ESPOVM measurement, but to classical post-processing of the X-basis measurement outcome. Therefore, only 2n depth is needed.